August 2020

Development of Seaweed Biodegradable Nanocomposite Films Reinforced with Cellulose Nanocrystals for Food Packaging

Hansol Doh
Clemson University, hsdoh02@gmail.com

DEVELOPMENT OF SEAWEED BIODEGRADABLE NANOCOMPOSITE FILMS REINFORCED WITH CELLULOSE NANOCRYSTALS FOR FOOD PACKAGING

A Dissertation
Presented to
the Graduate School of
Clemson University

In Partial Fulfillment
of the Requirements for the Degree
Doctor of Philosophy
Food Technology

---

by
Hansol Doh
August 2020

Accepted by:
William S. Whiteside, Ph.D., Committee Chair
Ron Thomas, Ph.D.
Hojae Bae, Ph.D.
Kyle D. Dunno, Ph.D

ABSTRACT

This research studied is about development of seaweed biodegradable nanocomposite films reinforced with cellulose nanocrystals (CNCs) from seaweed biomass and investigating the properties of the films. Study was conducted to isolate CNCs from seaweed biomass and these isolated CNCs are applied to developed seaweed biopolymer films. At last, degradability of these films was evaluated with a weight loss method in soil burial and lake water immersion systems.

CNCs were extracted from seaweed biomass of brown, red, and green by four steps process of depolymerization, bleaching, acid hydrolysis, and mechanical dispersion. Physicochemical and thermal properties were determined for each seaweed group and compared. Among the seaweeds, *Sargassum fluitans* (brown seaweed) was used to isolate CNCs and applied to alginate nanocomposite (Alg/CNCs) films. Alg/CNCs films showed gradual decreasing of water absorption/solubility, water vapor permeability (WVP), oxygen permeability (OP), and light transmittance with increasing addition of CNCs. Also, addition of CNCs enhanced the tensile strength but elongation of Alg/CNCs films did not show the tendency due to its shrinkage. Scanning electron microscopy (SEM) results indicated that CNCs layers can be formed in the alginate polymer matrix, and the Fourier-transform infrared spectroscopy (FTIR) spectra showed the chemical interaction between alginate polymer matrix and CNCs. Thermal stability test with thermogravimetric analysis (TGA) and differential scanning calorimetry (DSC) data suggested the addition of CNCs can improve the thermal properties of Alg/CNCs films.

Seaweed nanocomposite films were also developed with brown seaweeds crude extracts; kombu (*Laminaria japonica*) and sargassum (*Sargassum natans*). Obtained supernatant after acid-base pretreatment was used for film forming solution. Seaweed biopolymer films were formed by casting-evaporation method. CNCs were isolated from residues with acid-base pretreatment and applied to seaweed biopolymer film for developing bionanocomposite film. Kombu nanocomposite film was prepared with 5% CNCs (KNF-5), and sargassum nanocomposite film was formed with 5% and 25% CNCs (SNF-5 and SNF-25, respectively). Without addition of CNCs, kombu film (KF) appeared as a dark brown color and sargassum film (SF) as a light brown color. CNCs did not affect the color of the films. Through the SEM observation, holes and cracks were found in surface and cross section of KF and SF but they were covered up with CNCs. Chemical structure changes indicated the molecular strength was increased when CNCs were added to the KF and SF. Also, higher crystallinity index was obtained after CNCs addition. These changings led to improving not only the physicochemical characteristics but also mechanical, barrier, and thermal properties. Total phenolic contents, DPPH radical scavenging effect, and reducing power assay indicated that kombu film showed higher antioxidant properties than sargassum film but not significantly related to the CNCs addition.

Developed bionanocomposite films were conducted to degradation test for evaluating their biodegradability. It was performed under indoor soil burial and lake water immersion systems for 35 days and degradation rate was determined by weight loss. In both conditions, degradation results varied in the order as followed: Alginate

nanocomposite film (ANF-5) > alginate film (AF) > KNF-5 > SNF-25, SNF-5 > KF > SF. Alginate-based films degraded up to 35% in soil and 53% in lake water for 35 days. In the case of seaweed films, they were eliminated by soil in 28 days and lake water in 7 days. Morphological observation showed wrinkles, pores, and cracks on their surface in the later days of the experiment. Besides, chemical structure changes revealed molecular bonding in polymer matrix diminished at the last stage of the process compared to before the test. Thermal stabilities also decreased due to reduction of the bonding strength after a certain period of days in both soil burial and lake water immersion systems.

DEDICATION

This is all for you, Mom and Dad. And grandmother, great thanks for with your great love, supports, and encouragement.

ACKNOWLEDGMENTS

First and foremost, I would like to thank my major advisor Dr. W. Scott Whiteside for providing me this opportunity, his support, and mentoring throughout my career here at Clemson. You have allowed me to flourish and grow as a researcher, and were always there for support, advice, and encouragement throughout my doctoral studies. I would also like to express my gratitude to all my committee members, Dr. Ron Thomas, Dr. Hojae Bae, and Dr. Kyle D. Dunno. They were always there with open doors to discuss and encourage me every single time not only research question I had. They provided great guidance and structure to work. Also, Dr. Hyun Jin Park, I really appreciate about making all these opportunities. I would also like to extend gratitude to everyone in the Department of Food, Nutrition, and Packaging Sciences at Clemson University, especially to Dr. Duncan Darby, Dr. Kay Cooksey, Dr. Anthony Pometto III, Ms. Patricia Marcondes, for their continued encouragements and advice.

My all family members, 할아버지, 할머니, 현기삼촌, 홍선삼촌, 승완삼촌, 큰외숙모, 둘째외숙모, 막내외숙모, 그리고 대구, 부산, 서울고모, 고모부, 서울 큰아버지, 큰어머니, 대구 큰아버지, 큰어머니, and the other all the senior family members, thank you for your supporting and encouragement. Also, my cousins, 지원이형, 지훈이, 민지, 민호, 예진, 예영, 예현이, 현구형, 현재형, 영주누나, 성훈이형, 영곤이형, thank you so much, I love all of you. And thanks to my best friends in my life. Without your support, encouragement, and love, I have never accomplished my goal. Friends of Korea University 09', 무용이형, 서준이, 경훈이, 경이, 수현이, 솔이, 시은이,

연선누나, Basketball club, *Jangsoo*, 현구형, 승렬이형, 우현이형, 인성이형, 승협이형, 세훈이형, 윤호형, 도형이형, 종성이형, 영규, 강욱이, 동건이, 성연이, 성민이, 세진이, 태규, 장영이, 재용이, 종은이, 석민이, 그리고 모든 멤버들, and the basketball club, *Turnover*, 재원이형, 쩐형, 현구형, 영훈이형, 기태형, 재진이형, 성호형, 재용이형, 태영이형, 민준이형, 현구형, 장엽이형, 수한이형 및 모든 형들, B1 friends, 진영이, 주원이, 영빈이, 성도, 중한이, 빡기, 기현이, 원식이, 인혁이, 유자, 상경이, 호용이, 용준이, high school teachers and friends, 윤성배 선생님, 김광국 선생님, 관주형, 감동, 정석이, 원이, Korea University Biopolymer lab members, 정아누나, 현우, 민혁이형, 빛나, 재경이, 정인이, 종란이, 우정이, 선배, 후배들, and other friends 찬우, 용만이, 창옹, 묵이, 세진이, 진석이, 한솔이, 푯, 재성이, 형근이, 해리누나, 우형이형, 진우형, everyone, I sincerely love you. Also, I cannot express my feelings how to say thank you and I love you to, Steve Skrypec, Ryan Ramey, JB Hayes, Reid Love, Matthew Suffern, Mollye MacNaughton, David Huttod, Mo panin, Katie Maloney, Crossfit Movement and Crossfit Clemson friends, Garner Powell, Jesse Salerno, Jim and Mandy Davison, Audrey, Coaches, and Steven and Alyssa Furst. Especially, Steves (both Skrypec and Furst) and Jesse, I cannot do anything without your support, encouragement, advice, and everything here in the US. I would like to specially say thank you and I will keep in mind that in rest of my lifetime.

Accomplishments like this are never completed and should not be celebrated alone. I would like to share this will all my family and friends who have supported me throughout

all the years. A very special thank you to my parents for believing in this journey and in me.

TABLE OF CONTENTS

Table of Contents (Continued)

Page

Table of Contents (Continued)

Page

LIST OF TABLES

List of Tables (Continued)

Table Page

LIST OF FIGURES

List of Figures (Continued)

Figure Page

List of Figures (Continued)

Figure Page

CHAPTER ONE

INTRODUCTION

The main purposes of food packaging are to protect food products from potential damages, to contain the quality of food products, and to provide consumers with convenience and information such as ingredient and nutrition (Coles et al., 2003). Also, food packaging needs to involve food products not only in a cost-effective way for satisfying industrial requirements but also consumer desires, food safety, and minimizes environmental impact (Marsh & Bugusu, 2007). Traditionally, petrochemical-based plastics such as polyethylene (PE), polypropylene (PP), and polystyrene (PS) have been used as packaging materials due to their good mechanical, barrier, and thermal properties at relatively low cost. However, their application to packaging system needs to be restricted since most petroleum-based materials used for food packaging are non-degradable, representing a serious global environmental problem (Siracusa et al., 2008). Therefore, biopolymer-based materials have been investigated to develop biodegradable film for reducing waste, improving the quality of food packaging materials, and extending shelf life of food products (Tharanathan, 2003).

However, the use of biopolymer-based film has been limited due to the issues related to their poor film performances, processing, such as distortion in low temperature, and high cost to manufacture. For instance, starch has gained attention as a biodegradable thermoplastic polymer, however, due to high water sensitivity and low mechanical properties, the usage of the starch film was restricted in the industry and market (Vaidya & Bhattacharya, 1994). Therefore, the application of nanotechnology to biopolymers has been investigated for new possibilities obtaining desired properties including the mechanical, barrier, thermal, and biodegradation properties as well as the cost efficiency (Sorrentino et al., 2007).

Cellulose is one of the most essential and abundant polymers, which can be obtained from numerous renewable resources. Cellulose forms microfibrils that are composed of amorphous and highly ordered crystalline regions. These amorphous domains can be eliminated by chemical and/or mechanical treatments, releasing the crystalline regions, which have a highly dense and ordered structure. Obtained cellulose nanocrystals (CNCs) through the process have been noticed not only for their remarkable mechanical properties, such as a high specific strength and an elastic modulus, but also for their low-cost for production, biocompatibility, and ease of chemical and mechanical modification. Besides, relatively high crystallinity of CNCs has led to CNCs being used as reinforcing agent for nanocomposite materials. CNCs have also been originated from a lot of other resources including sugarcane bagasse, rice straw, banana peel, and coffee silver skin, but there are few reports on the isolation of CNCs from seaweed biomass.

A seaweed crude extraction would be of interest to develop an environmental-friendly biopolymer-based film for various industrial applications. For instance, seaweed biomass can form films and fibrous structures in solid state due to their linear structure, being considered as having a good backbone biopolymer (Blanco-Pascual et al., 2014). Since seaweed crude extract biopolymer film has been considered as potential environmentally friendly and sustainable alternatives of petroleum-based, non-degradable plastics, it has high possibilities for using as a novel packaging material in the industry. In addition, there are some advantages of using seaweeds for producing CNCs including easy to extract, higher yield, and rapid growth rate compared to land plants (Chen et al., 2016).

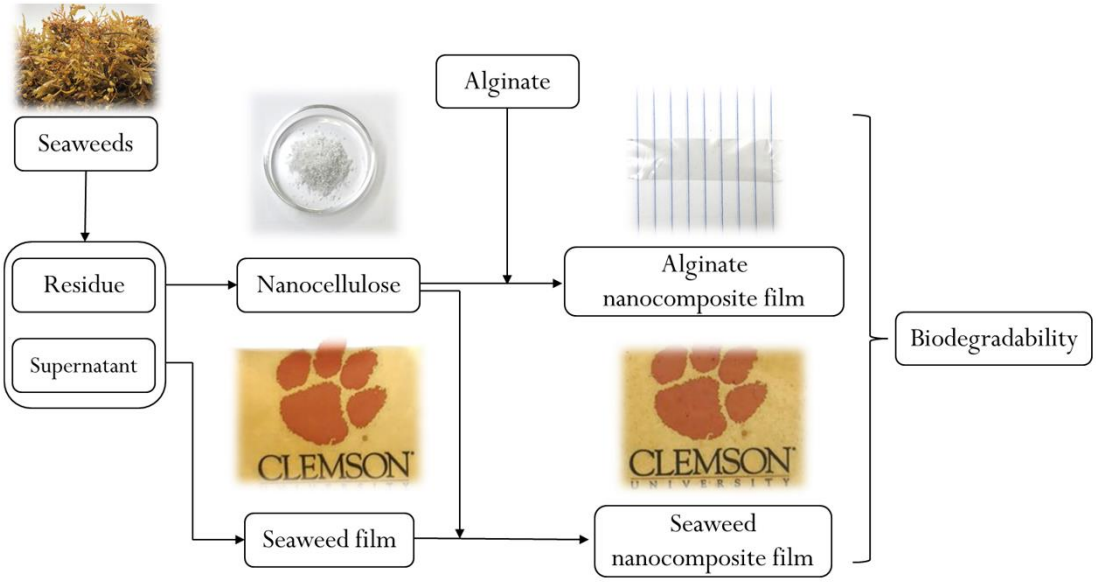

Figure 1.1. Experimental design of this study

This research aims to study successful isolation of CNCs from seaweed biomass and to apply CNCs as a reinforce filler with alginate and seaweed crude extract biopolymer film for preparing bionanocomposite films. Physicochemical, mechanical, barrier, thermal, and antioxidant properties of the film will be investigated and degradation rate will be tested in soil and lake water systems for evaluating their biodegradability.

Reference

Blanco-Pascual, N., Montero, M. P., & Gómez-Guillén, M. C. (2014). Antioxidant film development from unrefined extracts of brown seaweeds Laminaria digitata and Ascophyllum nodosum. Food Hydrocolloids, 37, 100-110.

Chen, Y. W., Lee, H. V., Juan, J. C., & Phang, S.-M. (2016). Production of new cellulose nanomaterial from red algae marine biomass Gelidium elegans. *Carbohydrate polymers, 151*, 1210-1219.

Coles, R., McDowell, D., & Kirwan, M. J. (Eds.). (2003). Food packaging technology (Vol. 5). CRC Press.Marsh, K., & Bugusu, B. (2007). Food packaging—roles, materials, and environmental issues. Journal of food science, 72(3), R39-R55.

Siracusa, V., Rocculi, P., Romani, S., & Dalla Rosa, M. (2008). Biodegradable polymers for food packaging: a review. Trends in Food Science & Technology, 19(12), 634-643.

Sorrentino, A., Gorrasi, G., & Vittoria, V. (2007). Potential perspectives of bionanocomposites for food packaging applications. Trends in Food Science & Technology, 18(2), 84–95.

Tharanathan, R. N. (2003). Biodegradable films and composite coatings: past, present and future. Trends in Food Science & Technology, 14(3), 71–78.

Vaidya, U. R., & Bhattacharya, M. (1994). Properties of blends of starch and synthetic polymers containing anhydride groups. Journal of Applied Polymer Science, 52(5), 617–628.

CHAPTER TWO

REVIEW OF LITERATURE

2.1. Overview of Food Packaging System

Food packaging systems include the process of preparing food products for transportation, distribution, storage, retail, and end-use of consumers. This process should safely deliver food to consumers with optimum cost functions of containment, protection, convenience, and communication (Coles et al., 2003). Since packaging systems protect contents from any possible contamination and spoilage, understanding these necessities can lead to the development of quality packaging (Hill, 1996; Robertson, 2005). To fulfill this goal, numerous factors should be considered, such as the physical environment and characteristics of the packaging material (Hanlon et al., 1996).

Petroleum-based plastics, such as polyethylene terephthalate (PET), polyvinylchloride (PVC), polyethylene (PE), polypropylene (PP), polystyrene (PS), and polyamide (PA), have been typically used as food packaging materials due to not only their good mechanical, barrier, thermal properties but also low cost to produce (Siracusa et al., 2008). However, these petroleum-based packaging materials have caused serious environmental problems, such as the use of non-renewable resources, the energy crisis, global warming, and ecological pollution (Rhim et al., 2013). According to a recent study by Emadian et al., 34 million tons of plastic waste are generated across the world and 93% of it is disposed of in landfills and oceans (Emadian et al., 2017). Although some organizations, such as the European Union (EU), have been trying to reduce plastic waste in various ways; however, developing countries are still dependent on traditional landfilling, which causes severe environmental pollution (Muenmee et al., 2016). There are high correlations between carbon dioxide (CO_2) emissions from these landfills and their contribution global warming (Jain & Tiwari, 2015). For environmental safety

and sustainability, many studies have investigated the development of alternative food packaging materials with biopolymers that can be easily degraded in the environment (Jayaramudu et al., 2013). Recently, biopolymer-based films have been considered as a potential alternative to traditional packaging materials due to their good biodegradability and biocompatibility (Siracusa et al., 2008).

When biopolymer-based and petroleum-based plastics are compared, most parameters, such as renewability, sustainability, gas emission, and fossil fuel usage, are favorable to biopolymer-based plastics in perspective of environmental protection (Table 2.1). Therefore, the applications of these plastics have contributed solutions for altering trends from traditional petroleum-based to biopolymer-based packaging materials.

Table 2.1. Comparison of characteristics of bioplastics and petroleum plastics (Harding et al., 2017).

	Bioplastics	Petroleum plastics
Renewable	Yes or partially	No
Sustainable	Yes	No
Breakdown in the environment	Biodegradable and/or compostable	Some degradable by polymer oxidation
Polymer range	Limited but growing	Extensive
Greenhouse gas emissions	Usually low	Relatively high
Fossil fuel usage	Usually low	Relatively high
Arable land use	Currently low	None

2.2. Biopolymer-based Plastics

Biopolymers consist of two or more monomers connected through covalent bonding and are usually originated from living organisms. Biopolymers can be defined as a polymer of natural origin, which include diverse source materials as wood, cellulose, starch, chitosan, chitin, and so on (Chiellini et al., 2001). Since biopolymer plastics can be defined to consist partly of bio-based raw materials as well as nondegradable biopolymer-based plastics, all biopolymer-based plastics are not included in biodegradable polymers. Figure 2.1 is organized by examples of plastics based on their biodegradability and source.

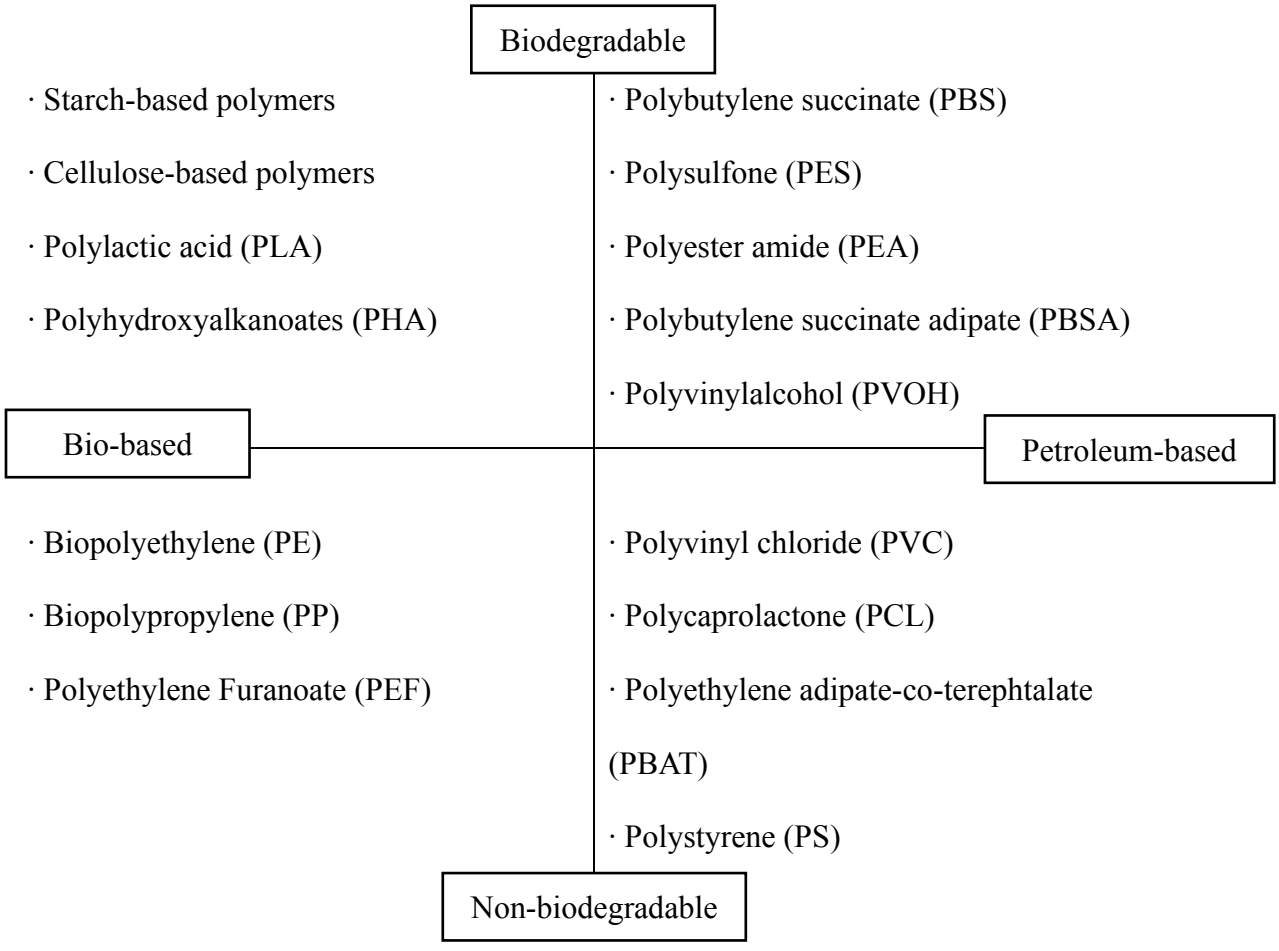

Figure 2.1. Categorization of plastics based on their biodegradability and source.

There are three categories of biopolymers depending on the isolation methods: (1) Biopolymers extracted directly from natural resources including starch, cellulose, and protein, such as gelatin; (2) Biopolymers produced by chemical synthesis from bioderived monomers;

and (3) Biopolymers produced by microorganisms and genetic engineering, such as hydroxy-butyrate and hydroxy-valerate (Cha & Chinnan, 2004). With using these definitions of biopolymers, biopolymer-based plastics can be synthesized through different pathways for manufacture that are suggested in Figure 2.2.

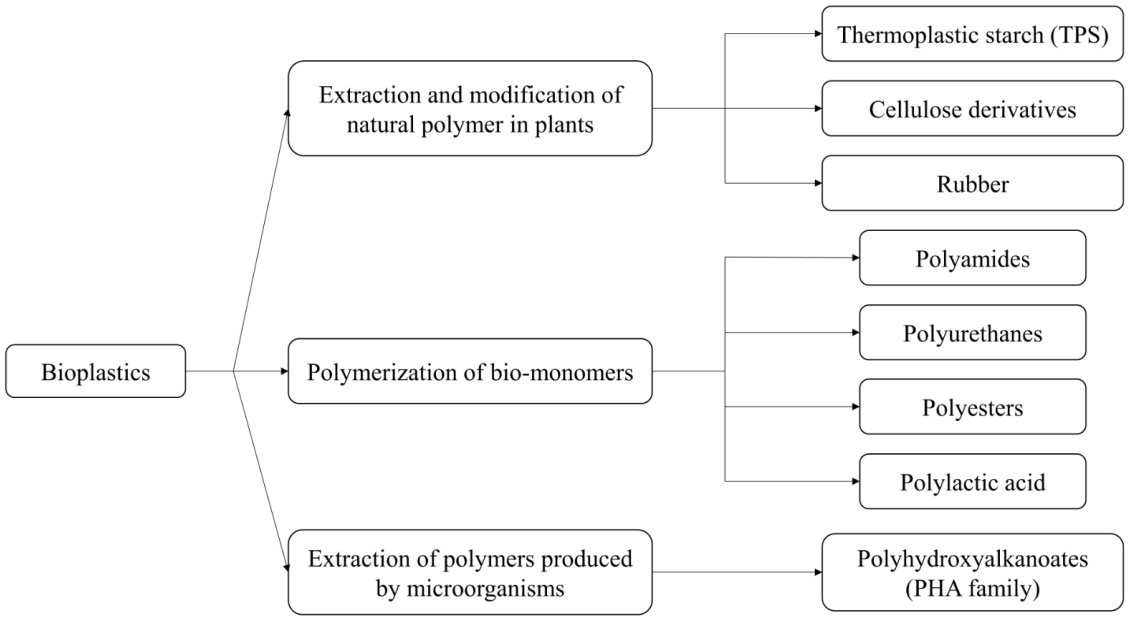

Figure 2.2. Different pathways used to synthesize bioplastics (Rudin & Choi, 2012).

First-generation commercial biopolymer-based plastics were manufactured with starch and polyhydroxyalkanoates (PHAs), which were introduced in the late 1980s and early 1990s. These biopolymers were not successfully established both in the industry and the market due to their uncertain characteristics, economic, and political conditions. However, second-generation biopolymer-based plastics, such as polylactic acid (PLA), improved their properties significantly and could be comparable with traditional petroleum-based plastics. As a result, they had been increasingly competitive in some industrial fields, such as food packaging and utensils. However, these materials had some issues such as high production cost and low production volume at that time (La Rosa, 2016). Therefore, improved second-generation or third-generation biopolymer-based plastics have been recently researched for low

manufacturing cost and high volume of production. Also, these plastics were introduced with the concept of sustainability using renewable sources for manufacturing biodegradable plastics instead of using limited petroleum-based plastics. These biodegradable materials should be more investigated with additional technological improvements, such as mechanical strength, barrier properties, heat resistance, and UV stabilization with low production cost. Global production capacities of bioplastics in 2013 and 2018 are shown in Table 2.2.

Table 2.2. Global production capacities of bioplastics by material type in 2013 and 2018[a] (Aeschelmann & Carus, 2015).

Material type	2013 (%)	2018 (%)
Biobased/Non-biodegradable	**62.4**	**83.3**
Bio-PET30[b]	37.0	74.3
Bio-PE	12.3	3.0
PTT	6.8	1.6
Bio-PA	4.9	1.5
Bio-PVC	-	1.2
Other	1.4[c]	1.7[d]
Biodegradable	**37.6**	**16.7**
PLA	11.4	6.5
Starch blends	11.3	3.1
Polyesters[e]	10.8	5.5
PHA	2.1	1.1
Regenerated cellulose	1.7	-
Other	0.3[f]	0.5[g]
Total	**1.62 million tones**	**6.73 million tones**

[a]Source: European Bioplastics, Institute for Bioplastics and Biocomposites, nova-Institute, 2014.

[b]Biobased content amounts to 30%, increase of volume subject to realization of planned production facilities.

[c]Contains durable starch blends, Bio-PC, Bio-TPE, Bio-PUR (except thermosets).

[d]Contains durable starch blends, Bio-PC, Bio-TPE, Bio-PUR (except thermosets), Bio-PP, PEF

[e]Contains PBAT, PBS, PCL.

[f]Biodegradable cellulose ester.

[g]Contains regenerated cellulose and biodegradable cellulose ester.

As it has been already described, many biopolymer-based plastics have been reported as a material with high potential for altering petroleum-based plastics due to their eco-friendliness and biodegradability (Tang et al., 2012). Nowadays, the application of biopolymer-based plastics in the food industry includes disposable cutlery, drinking cups, salad cups, plates, overwrap and lamination film, straws, stirrers, lids and cups, plates and containers for food dispensed at delicatessen and fast-food establishments (Siracusa et al., 2008). Their physicochemical, mechanical, and barrier properties can be compared to synthetic polymers that are used traditionally in food packaging. However, some biopolymer-based plastics are still not having appropriate properties, such as mechanical and barrier properties, for use as food packaging. Therefore, development and modification approaches for adjusting the properties of biopolymers to the desired application is necessary. A wide variety of approaches have been developed: blending, composite, plasticization, crosslinking, grafting, and etherification.

2.3. Biodegradable Film

The definition of biodegradation film indicates that the substrate must be degraded by microorganisms or related, size-reducing activities from copolymers to oligomers or monomers. These oligomers/monomers can then be used as a source for manufacturing biodegradable film. Biodegradation can be described in three stages (Tosin et al., 2019):

Stage 1: Plastic → monomers/oligomers (depolymerization)

Stage 2: Monomers/oligomers → biomass (uptake and metabolism)

Stage 3: Biomass + O_2 → CO_2 + H_2O (mineralization)

In the depolymerization stage, plastic material is decomposed to monomers and/or oligomers and it is so called the "central dogma" for biodegradation (Kaplan et al., 1993). In the first step, the enzymes and microbes in the liquid phase begin to interact with the constituents of the solid phase of the plastics and it promotes depolymerization of the plastic. At the next stage, these monomers or oligomers are expected to uptake, metabolize, and be turned into biomass. The microbes can be effective at this second stage for obtaining their energy source. Finally, the organic carbon interacts with oxygen and turns into CO_2 and water molecules in early the biodegradation phases through the mineralization stage (Tosin et al., 2019).

Figure 2.3 shows the ideal life cycle of biodegradable film. Overall, biodegradable film should perform not only the traditional functions of packaging materials but also be able to be degraded by microbes and formed into biopolymers for sustainability.

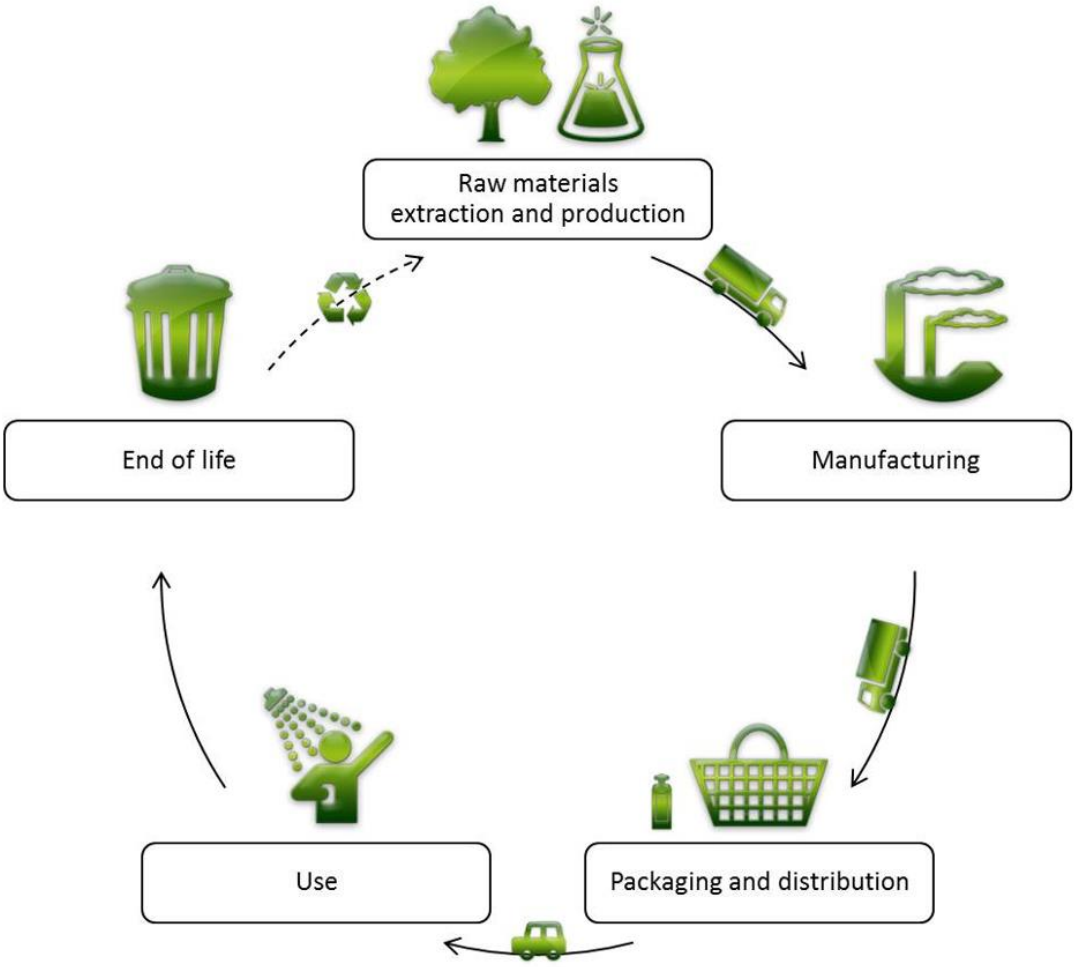

Figure 2.3. Ideal life cycle of biodegradable plastic (Silvia Román, 2013, Credit: sci-env.ch).

A biodegradable film can be formed either from a single polymer or mixture of polymers. Polysaccharides are the most promising polymer in perspective of their cost-effectiveness, accessibility, and ease of handling compared to biopolymers from proteins or lipids. Natural renewable polysaccharides for biodegradable film sources, including cellulose, starch, and chitosan, have been commonly used (Khalil et al., 2017). However, the application to food packaging of biodegradable films from natural sources has some limitations due to its drawbacks, including high water sensitivity and unstable thermal characteristics. To overcome these issues, reinforcement approaches have been performed through blending, composites, plasticization, crosslinking, and grafting. Among these strategies, the concept of a composite film has been noticed with high interests, which is defined as a reinforcement agent added to

the backbone polymer matrix with physicochemical interaction because it leads to the improvement of general properties of films (Miao & Hamad, 2013).

When reinforcement agents are applied to biopolymer-based films, synthetic polymers, such as glass fiber, carbon, or aramid, are considered as the traditional fillers. However, the synthetic reinforcement agents used in composite materials are rarely used recently since they result in environmental problems at their end-of-life disposal due to their poor degradability and the high demand of techniques for recycling of the materials. By changing from synthetic fillers to natural fillers, like cellulose fibers, environmental benefits can be obtained from their biodegradability with similar reinforcement effects as synthetic fillers, while also providing a low cost for recycling (Bhatnagar & Sain, 2005).

As nanotechnology is being applied to the packaging industry, its development has led to a new generation of products with new and improved qualities. The purpose of applying nanotechnology to food packaging systems is to increase the physicochemical properties, shelf-life, and nutrition capacity of the food products as well as communicating with consumers about food quality (Robinson & Morrison, 2010). Nano-sized reinforcement agents for composite films have been developed from natural sources, such as nanoclay, nanocellulose, carbon nanotube, nanocarbon fiber, and montmorillonite (MMT) as a natural nanofiller (Khalil et al., 2017; Saba et al., 2014). For instance, nanoclay and nanocellulose improve the characteristics of nanocomposite films by increasing mechanical strength, stiffness, toughness, barrier properties, and thermal stability. Since nano-sized fillers have higher surface area compared to traditional reinforcing agents, they work more efficiently. The addition of only a small amount of nanomaterials (1–5 wt%) is enough to obtain desirable improvements of composite films (Alexandre & Dubois, 2000). Therefore, investigating nanocomposite film reinforced with a natural filler can be an acceptable method for developing biodegradable film possessing desired properties as well as low cost for production.

2.4. Seaweed Biomass

Seaweed marine biomass is comprised of organisms that usually live attached to rocks or other hard substrata in coastal areas. They grow in a wide range of environments and are abundantly available. Seaweeds have some advantages, such as low cost and ease of cultivation, which can be harvested all year round. Generally, seaweeds are categorized as brown (*Phaeophyta*), red (*Rhodophyta*), and green (*Chlorophyta*) seaweeds (Khalil et al., 2017). These seaweed groups typically have different chemical compositions (Table 2.3).

Table 2.3. Chemical composition of seaweeds (García-Casal et al., 2007).

Components	**Compositions**
Water	80-90%
Carbohydrates	50% dry weight
Proteins	Brown seaweed: 3-15% dry weight Red or Green seaweeds: 10-47% dry weight
Minerals	7-38% dry weight
Lipids	1-3% dry weight

Recently, seaweeds have received much interest and attention in the perspective of application to food, medical engineering, biosensors, and drug delivery systems (Venkatesan et al., 2016). Seaweeds are rich in polysaccharide materials, such as alginate, carrageenan, and agar, and these materials are not only easy to isolate but also inexpensive. The only difference from land plants is that they are harvested from the sea (Daemi et al., 2016). Especially, the high carbohydrate content of seaweed has promoted them to be an industrial source of hydrocolloids (Gade et al., 2013). Table 2.4 shows the various polysaccharides that exist on each type of seaweed. For instance, alginate is usually isolated from brown seaweed, and carrageenan and agar are easy to extract from red seaweed.

Table 2.4. Different polysaccharides content of red, brown, and green seaweed (El-Said & El-Sikaily, 2013).

Polysaccharides	Red seaweed	Brown seaweed	Green seaweed
Agar	○	–	–
Alginate	–	○	–
Carrageenan	○	–	–
Cellulose	○	○	○
Floridean Starch (α-1,4-bindingglucan)	○	–	–
Fucoidan (sulphatedfucose)	–	○	–
Laminarin (β-1,3 glucan)	–	○	–
Mannan	○	–	–
Mannitol	–	○	–
Porphyran	○	–	–
Sargassan	–	○	–
Sulphatedgalactans	○	–	○
Sulphuric acid polysaccharides	–	–	○
Xylans	○	–	○

Since the polysaccharides isolated from the seaweed matrix can form strong interactions, they have advantages for use as precursors for film-forming materials. For instance, Figure 2.4 and 2.5 showed gelling properties that can be used as a backbone of biopolymer films. Film-forming biopolymers isolated from seaweeds are non-toxic, easily degradable in the environment, and biocompatible. Besides, they show a high rigidity and low deformability.

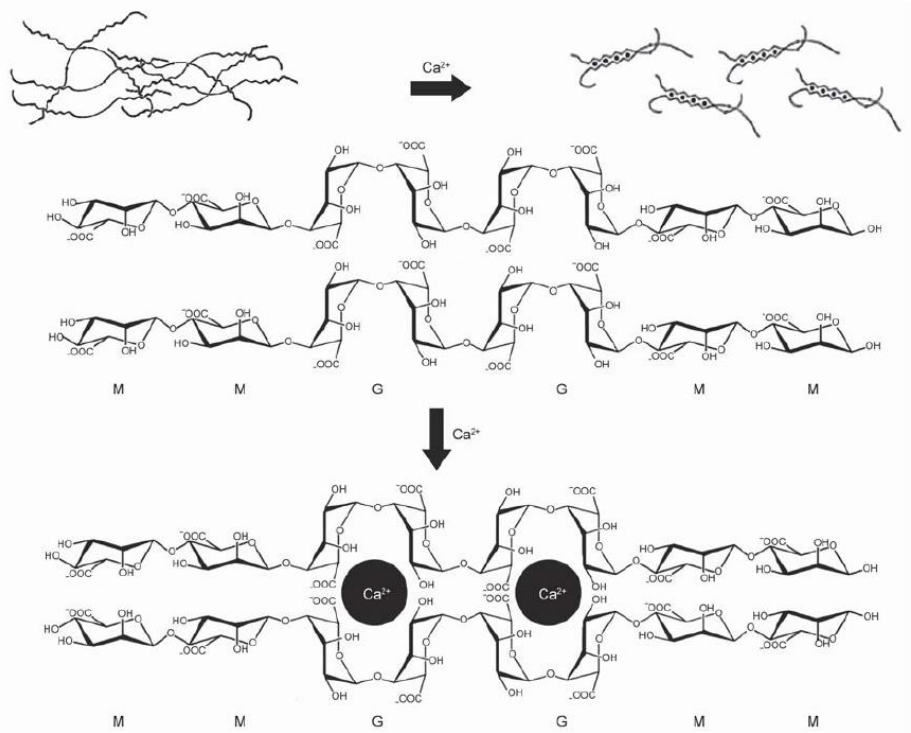

Figure 2.4. Gelling mechanism of calcium cross-linked alginate (Tavassoli-Kafrani et al., 2016).

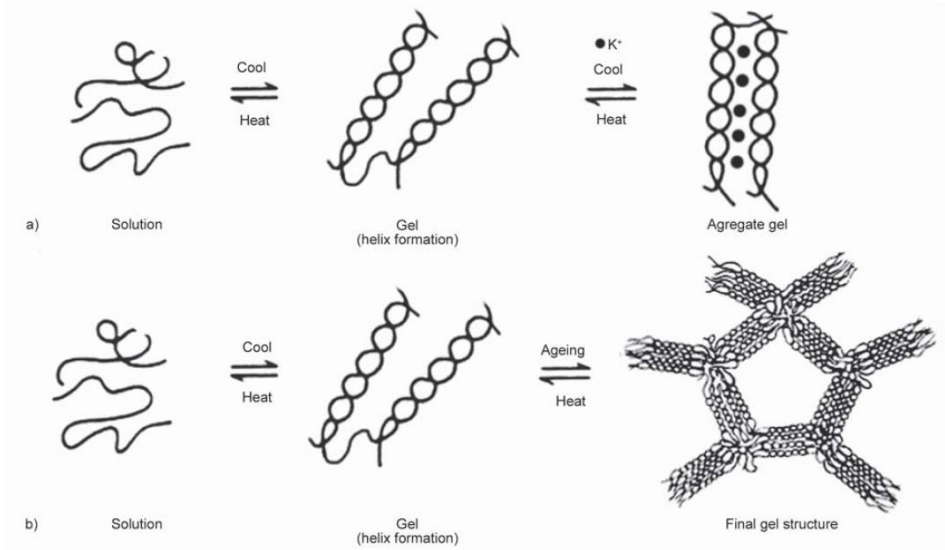

Figure 2.5. Gelling mechanism for (a) carrageenans and (b) agars (Tavassoli-Kafrani, E., Shekarchizadeh, H., & Masoudpour-Behabadi, M., 2016).

However, seaweed films have high water sensitivity, which indicates a poor water resistance due to the hydrophilic nature of seaweeds extracts (Tavassoli-Kafrani et al., 2016).

Therefore, biopolymer films produced from seaweed biomass need to be improved for desired characteristics to be used as a packaging material when they are applied at the industrial scale. Table 2.5 shows the incorporation of various components extracted from seaweed into the polymer matrix for reinforcing performances of seaweed biopolymer film.

Among the potential extractable polysaccharides from seaweed, alginate is one of the most abundant substances in brown seaweed comprising as much as 40% of the dry weight (Gholamipoor et al., 2013). It can be extracted with an alkaline solution from the cell wall of brown seaweed (Gade et al., 2013). Alginate is composed of the monomeric units (1→4)-linked β-D-mannuronic acid (M) and α-L-guluronic acid (G) (Rhim, 2004). The physical characteristics, such as stiffness, can be differed by ratio, source, and chemical structure of two different monomeric units. For instance, the stiffness of the three blocks decreases in the order of GG > MM > MG (Figure 2.6) (Huq et al., 2012). Due to its hydrophilic characteristics, it has been used as a thickening, stabilizing, suspending, gel-producing, and film-forming agent. As a gelling agent, alginate solutions can crosslink with divalent metal cations, such as calcium and magnesium (Figure 2.4).

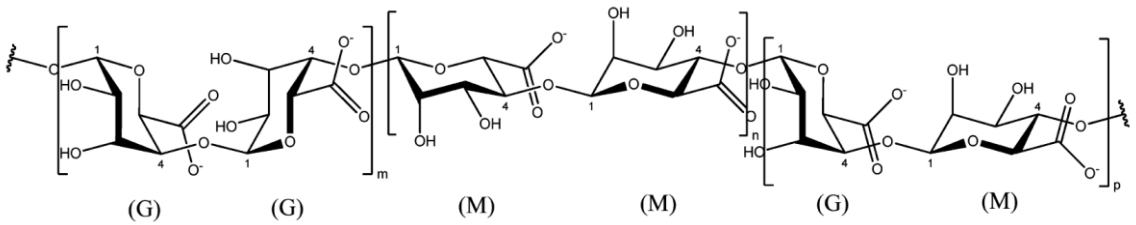

Figure 2.6. Structural units of alginate. Mannuronic acid (M); gluronic acid (G) (Agulhon et al., 2011).

Alginate and alginate-based biopolymer composites have been used not only in food packaging but also in tissue engineering, biomedicine, and pharmaceutical fields due to its non-toxicity, biodegradability, biocompatibility, and gel-forming properties (Abdollahi et al., 2013). Although alginate-based film has a high potential as food packaging, they usually do

not have the desired properties. Therefore, nano-sized cellulose from many sources, which shows different characteristics, has been applied as a reinforcing agent for overcoming this problem. Many studies have developed and investigated alginate nanocomposite film in various ways. As a result, alginate nanocomposite film commonly shows improved film performances including mechanical, barrier, and thermal properties (Deepa et al., 2011; El Miri et al., 2018; Huq et al., 2012). These studies suggest that the reinforced alginate bio-nanocomposite films have potential as a novel biomaterial for food packaging systems.

Table 2.5. The incorporation of components with seaweed extracted polymer (Khalil et al., 2017).

Seaweed	Components/plasticizer added	Film characteristics and improvements
Alginate	Calcium Chloride/glycerin	The film becomes water resistant by immersing alginate film in $CaCl_2$ solutions.
	Apple puree and essential oil	The film exhibits antibacterial activity. No adverse effect of the additives on water vapor & permeability.
	Sago starch and lemongrass oil/glycerol	The film exhibits antibacterial activity. The addition of lemongrass oil and glycerol decrease mechanical properties & increase water vapor permeability.
	Montmorillonite (MMT)	Film with low water solubility & water vapor permeability and high mechanical properties.
	Cinnamon bark oil and soybean oil/glycerol	The addition of these oils improves film microstructure homogeneity, transparency & antibacterial activity, while reduce film mechanical properties & water solubility.
	Kappa- and Iota-carrageenan/glycerol	The addition of K-carrageenan improves moisture barrier & overall tensile properties of film. The addition of I-carrageenan impairs those properties of film.
	Silver nanoparticles/glycerol	The additions of silver particles improve the mechanical strength and water vapor barrier properties of film. This film exhibits a UV screening effect & strong antimicrobial activity.
Kappa-carrageenan	Grapefruit seed extract (GSE)/glycerol	Yellowish tint & great antibacterial activity film. The addition of GSE increases the moisture content, water vapor permeability & surface hydrophilicity, but decreases tensile strength & elastic modulus of film.
	Zataria multiflora essential oil & nanoclay/glycerol	The mechanical, antimicrobial and barrier properties of film are improved.
	Clay mineral & silver particles/glycerol	The nanocomposite film improves on the mechanical & water vapor barrier properties as well as antimicrobial activity.
	Essential oil/glycerol & PEG	The addition of essential oil reduces water vapor permeability, tensile strength, moisture absorption and increases transparency of film.
	Chitin nanofibrils (CNF)	The film shows transparent, strong antibacterial activity and improved mechanical properties.
	Silver nanoparticles (Ag) & PVP/PEG	Addition of nanoparticles exhibit higher thermal stability, strength properties, antimicrobial activity & lower swelling behavior of film.
Agar	Arabinoxylan/glycerol	The addition of arabinoxylan improves moisture barrier efficiency but decreases mechanical properties of film.
	Starch/glycerol	The addition of starch degrades surface resistance to water wetting & mechanical properties of film.
	Silver (Ag) nanoparticles	The film exhibits good mechanical stability, water vapor and gas barrier as well as strong antimicrobial activity.
	Nanoclay/glycerin	Incorporation of clay (up to 10%) increases the tensile strength and decreases the water vapor permeability.
	Grapefruit seed extract (GSE)	The addition of GSE increases the color, UV barrier, moisture content, water solubility & water vapor permeability, but decreases the surface hydrophobicity, tensile strength & elastic modulus of film. The film exhibits distinctive antimicrobial activity.
	Banana powder and Silver (Ag) nanoparticles/glycerol	The addition of banana powder increases the UV light absorption, water vapor barrier property & antioxidant activity, but decreases the mechanical properties of biolayer film. The composite film exhibits distinctive antimicrobial activity & mechanical properties.
	Fish gelatin and TiO_2 nanoparticles	The addition of TiO_2 decreases water vapor permeability and increases tensile strength, UV light barrier property, swelling ratio & moisture content of film.

2.5. Cellulose Nanocrystals

2.5.1. Nanostructured cellulose

Cellulose is the most abundant renewable polymer in nature and is the main component in the cell wall of plants. It is generally found in plant cell walls, such as wood and cotton. It can be also found in various bacterial species and marine products, such as seaweed biomass (algae). Cotton usually has the highest cellulose content at about 90% and that of wood has about 40 – 50%. Other cellulosic fibers, including seaweeds, tunicate, algal, flax, hemp, or ramie have around 70 – 80% of cellulose content (Börjesson & Westman, 2015; Son & Seo, 2015). Cellulose has been extensively used and applied in many industries due to its cost-effectiveness, degradability, and renewable properties. It is also considered as an infinite source that can fulfill the increasing demand for environmental-friendly and biocompatible products (Khalil et al., 2017).

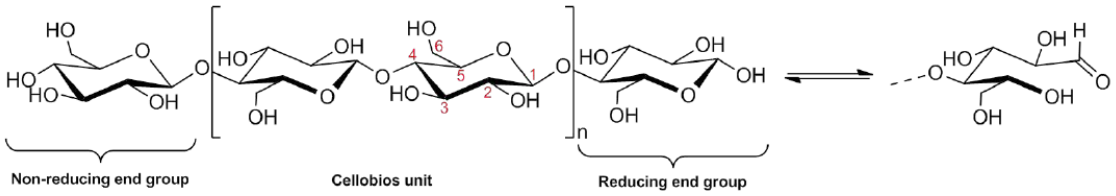

Figure 2.7. The molecular structure of a cellulose polymer (Börjesson & Westman, 2015).

With the development of nanotechnology in recent years, nanostructured cellulose has been hugely noticed in a lot of industrial fields and it has been investigated for many novel possibilities, such as plastics and medical uses. Nanostructured cellulose has various types, which are termed as nanocellulose, cellulose nanocrystals, cellulose nanowhiskers, cellulose nanorods, cellulose nanofibrils, or cellulose nanofibers. These are defined based on the characteristics of the cellulose fiber or crystal, including their size, shape, aspect ratio, and crystallinity. For obtaining nanostructured cellulose, the non-crystalline regions (amorphous regions) need to be removed. Usually, this removal occurs through acid-hydrolyzation and/or

mechanical forces and, as a result, only the crystalline parts will remain in the nano-size range. A schematic representation of how nanocellulose can be obtained from a cellulose fiber is shown in Figure 2.8.

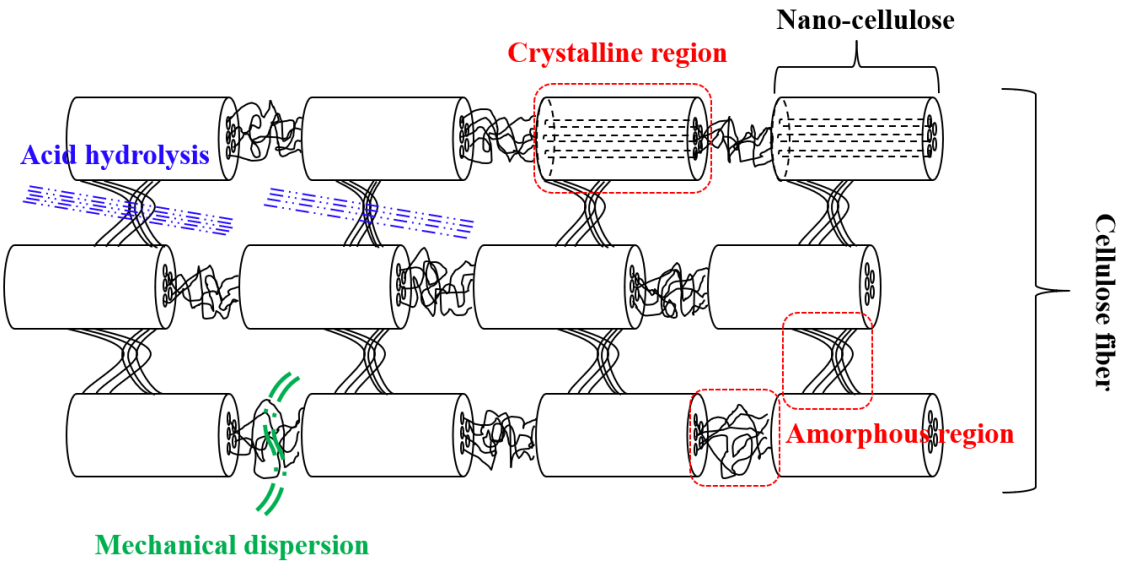

Figure 2.8. Schematic representation of how nanocellulose can be obtained from cellulose fiber.

Nanostructured cellulose has been isolated from various cellulose sources, such as hardwood/softwood pulp (Beck-Candanedo et al., 2005; Revol et al., 1992; Orts et al., 2005), microcrystalline cellulose (MCC) (Bondeson et al., 2006), coffee silver skin (Sung et al., 2017), sisal (de Rodriguez et al., 2006), cotton (El-Sakhawy & Hassan, 2007), wheat/rice straw (Helbert et al., 1996; Lu & Hsieh, 2012), bacterial cellulose (Roman & Winter, 2004), algae (Imai et al., 1998), banana peels (Deepa et al., 2011), sugar beet (Saïd Azizi Samir et al., 2004), and tunicin (Favier et al., 1995; Schroers et al., 2004; Azizi Samir et al., 2004). The source of nanostructured cellulose can affect the structures and morphology as well as physicochemical characteristics. For instance, the aspect ratio and crystallinity are considered as the most important parameters when nanostructured cellulose applied as a reinforcement agent to the polymer matrix (Miao & Hamad, 2013). Also, reaction time, temperature, amplitudes of

sonication, acid concentrations, and numerous factors in the process can affect the characteristics of nanostructured cellulose (Börjesson & Westman, 2015). Among the nanostructured cellulose resources, seaweeds have become more popular as a novel source due to their advantages compared to land plants for manufacturing the nanostructured cellulose: (i) easy to extract, owing to its low content of interfering polysaccharides for cellulose isolation; (ii) contain a high yield of cellulose; and (iii) rapid growth rate compared to other land plant sources (Chen et al., 2016).

One of the main types of nanostructured cellulose are cellulose nanocrystals (CNCs). CNCs are needle-like crystals varied with 2 – 40 nm in width and 10 – 1000 nm in length. They can usually be produced by bleaching (for lignin-rich materials), acid hydrolysis, and mechanical forces, which help remove amorphous regions and obtain the crystalline regions (Jonoobi et al., 2015; Xu et al., 2013). CNCs can be a potential material for nanocomposites in the industry for several reasons. First, CNCs show relatively strong mechanical properties. Since CNCs forms a liquid crystal in concentrated suspensions, they can create a hard, smooth, and tight matrix (Risteen et al, 2017). Besides, due to their thixotropic properties, CNCs can decrease viscosity when they are applied to specific polymer matrix conditions. This can lead to a matrix with higher mechanical properties with for improved mechanical processing (Khoshkava & Kamal, 2014; Wang et al., 2015). At last, CNCs are reactive and compatible with a wide range of solvents and polymer matrices (Mu et al., 2019). Since CNCs have many hydroxyl groups in their chain, CNCs can easily form molecular interaction and can be modified with the reactive surface of the CNCs (Makarem et al., 2018). This characteristic allows the CNCs to bind with a variety of hydrophobic structures (Huq et al., 2014, 2016; Yoo et al., 2017).

Table 2.6. Cellulose source and its length, diameter, and aspect ratio (Börjesson & Westman, 2015; Ferreira et al., 2018).

Cellulose source	Length, L (nm)	Diameter, D (nm)	Aspect ratio, L/D
Wood	100-300	3-5	30-70
Cotton	100-400	7-15	10-20
Algae (*Valonia*)	100 nm to μm	10-20	N/A
Bacterial cellulose	100 nm to μm	5-10	N/A
Tunicate cellulose	100 nm to μm	10-20	67
Sugar beet pulp	210	5	40
Wheat straw	220	5	45
Corn (*Zea mays*)	940 ± 70	6 ± 2	157
Soy Hulls	503 ± 155	4.9 ± 1.1	100
Capim Dourado (*Syngonanthus nitens*)	300 ± 93	4.5 ± 1.1	67
Spruce bark (*Picea abies*)	175 ± 62	2.8 ± 0.8	63
Luffa cylindrica fibers	242 ± 86	5.2 ± 1.3	46.5
Sugarcane bagasse	413 ± 52	10 ± 2.5	41
Agave tequilana	323 ± 113	11 ± 4	28
Acacia mangium	199 ± 22	7.44 ± 1.49	26
Balsa wood (*Ochroma pyramidalis*)	176 ± 68	7.5 ± 2.9	24
Ramie	134 ± 59	10.8 ± 4.5	12

2.5.2. Isolating process of CNCs

CNCs have been considered as a good reinforcement agent in the food packaging industry for improving the mechanical, barrier, thermal, and biodegradation properties of biopolymer-based films because cellulose is widely distributed in natural resources (Natterodt et al., 2017). Also, CNCs can be obtained from waste, and this idea allows CNCs to be one of the most cost-effective materials. It encourages waste to be repurposed to reduce ecological issues, such as global warming and environmental pollution. Recently, acid hydrolysis and mechanical treatment have been combined with other pretreatments, such as depolymerization

with acid-based solution, bleaching, smash after freeze drying, and colloid grinding (Abdallah & Kamal, 2018). Methods for isolating CNCs generally has four steps:

(1) Depolymerization: Removing the constituents except for cellulose, such as pectin, hemicellulose, and lignin with acid, base, or organic solvents.

(2) Bleaching: Especially for lignin-rich materials. This process is an efficient method for eliminating lignin, pectin, and other obstacle components through oxidation.

(3) Acid hydrolysis: For removing amorphous region of obtained cellulose fiber.

(4) Mechanical dispersions: Mechanical treatment, such as a high-pressure homogenization or ultrasonic homogenization, eliminates any possible amorphous regions to obtain the crystalline regions.

Among these steps, acid hydrolysis and mechanical dispersion steps mainly affect the morphological and physicochemical characteristics of nanostructured cellulose. In addition, factors including acid concentration and acid type, amplitudes of sonication, and reaction temperature and time should be highly considered.

2.5.2.1. Acid-hydrolysis

The cellulose fiber will start to degrade with an acid treatment. First, due to its accessibility, reducing end groups and the crystalline surface will break their molecular interactions. The acid will diffuse into the cellulose fiber inside and cleave the glycosidic bonds in the cellulose polymer (Börjesson & Westman, 2015). When an acid hydrolyzation is applied to the cellulose fiber, reaction time, reaction temperature, and acid concentration are considered as the most important factors. If the reaction time is too long, then the acid can also hydrolyze the crystalline part of cellulose, and if the reaction time is too short, then a high degree of polymerization (DP) is obtained due to the amorphous parts of the fibers not degrading effectively (Beck-Candanedo et al., 2005). Besides, the reaction time is related to reaction

temperature. For instance, if the reaction is performed with a high reaction temperature, a short reaction time will be needed. Acid concentration is also an important factor to affect the properties of nanostructured cellulose, such as morphology and crystallinity. The relationship between DP and crystalline size depends on the acid concentration of sulfuric acid, suggested in Figure 2.9.

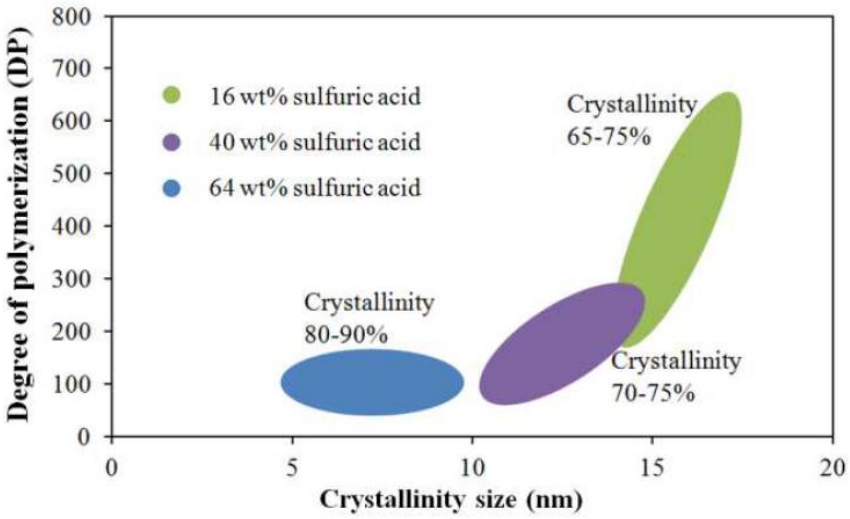

Figure 2.9. Results of degree of polymerization, crystallinity size, and crystallinity with different concentration of sulfuric acid (Börjesson & Westman, 2015).

Sulfuric acid (H_2SO_4) is a common acid for obtaining nanostructured cellulose through acid hydrolysis because nanostructured cellulose from H_2SO_4 can be charged on the surface as shown in Figure 2.10(a). Surface charge on nanostructured cellulose surface is important when forming the stable colloidal dispersions in a polymer matrix. Hydrochloric acid (HCl), hydrobromic acid (HBr), and phosphoric acid (H_3PO_4) have also been used for acid-hydrolysis in isolating nanostructured cellulose. However, HCl and HBr cannot donate any surface charges on nanostructured cellulose. Therefore, it leads to obtain an unstable colloidal dispersion form in polymer composite matrix, as shown in Figure 2.9. (b)&(d). As shown in Figure 2.9. (c)&(e), treated with H_3PO_4 or TEMPO-oxidation, nanostructured cellulose also

showed a charged surface of the nanocrystals. However, considering the industrial process, H_2SO_4 is a more appropriate choice for modification of a charged surface compared to H_3PO_4 due to the yield of nanostructured cellulose and for economic benefit.

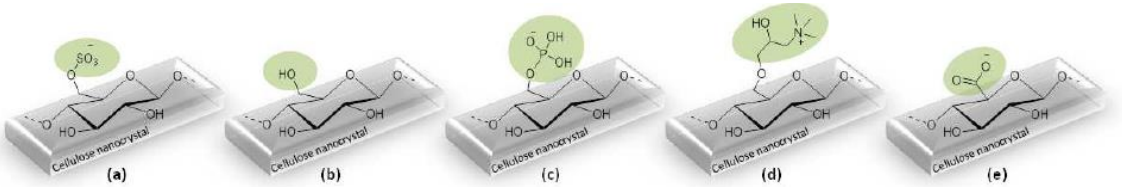

Figure 2.10. Effect of acid to cellulose surface. (a) H_2SO_4; (b) HCl or HBr; (c) H_3PO_4; (d) H_2SO_4 hydrolysis followed by a surface cationization; (e) HCl/HBr hydrolysis followed by a TEMPO-oxidation (Börjesson & Westman, 2015).

2.5.2.2. Mechanical treatment

Cellulose microfibrils are long, threadlike bundles of molecules that are stabilized by hydrogen bonds. Mechanical force can break the inter-fiber bonds between the cellulose molecules and produce the nanostructured cellulose. Amplitude of ultrasonication, number of cycles in high-pressure homogenization, reaction time, and temperature can significantly affect the morphology, crystallinity, and stability of nanostructured cellulose.

Mechanical treatment to cellulose fiber is the process of refining the pulp with homogenization to break the amorphous fiber regions from the crystalline parts to obtain a stable dispersion. With using a high-pressure homogenization process, cellulose fibers are subjected to high-pressure and high shearing forces so a CNFs suspension can be obtained (Opaprakasit et al., 2009). In addition, ultrasonication, for instance, is applied to cleave the aggregation of CNFs to obtain a CNCs suspension (Miao et al., 2013). Pre-treatments with enzymatic or chemical modification can affect the surface of cellulose fibers and help remove

the amorphous region more easily in the isolating process of combining mechanical treatment (Pääkkö et al., 2007; Saito & Isogai, 2004).

Guo et al. investigated the effects of mechanical treatment by ultrasonic homogenization with acid hydrolysis to increase yield and decrease particle size – shorter and narrower size – on the structure of cellulose nanocrystals. In this study, the authors reported that mechanical treatment can break amorphous regions more efficiently than acid hydrolysis because acid hydrolysis usually occurs in the outer cellulose domain (Guo et al., 2016). Ibrahim et al. reported their results using 30, 40, and 50% of acid treatment with 30, 60, and 90 min sonication for isolating nanostructured cellulose. They found nanostructured cellulose shows the highest crystallinity in 40% of acid concentration and 30 min of sonication process. Also, the crystallinity of CNCs decreased when it is treated for over 60 min because a long mechanical force treatment affects the crystalline part (Ibrahim et al., 2015).

2.6. Bionanocomposite Film Reinforced with Cellulose Nanocrystals

2.6.1. Seaweed biopolymer-based nanocomposite film

Seaweed-derived biopolymers, such as alginate, carrageenan, and agar can be used as a backbone in bionanocomposite films (Gade et al., 2013; Sousa et al., 2010). However, since the preparation of biopolymer films derived from seaweed show some undesirable properties, bionanocomposite films reinforced with CNCs have been developed. Nanocomposite films can be a solution for obtaining the desired properties, exploiting their useful properties, and widening their applications in the industrial field (Khalil et al., 2017).

CNCs have been studied with high interests, especially as a reinforcement agent for bionanocomposite film. CNCs have some advantages with their sustainability, mechanical properties, high flexibility, and good thermal properties as well as their safety with ease of handling and ability to produce (Deepa et al., 2011). Bionanocomposite films with CNCs for packaging materials have high strength due to their highly crystalline structure. They can be effectively embedded in the polymer matrix due to their high specific surface area (Miao & Hamad, 2013). It leads to improve the physical, mechanical, barrier, and thermal properties of bionanocomposite films (El Achaby et al., 2018; Neto et al., 2016; Sirviö et al., 2014; Son & Seo, 2015). With an increasing interest of seaweed extracted polymers, the combination of seaweed-derivatives biopolymers and CNCs in composite materials has been investigated in recent years. Nanocomposites reinforced with CNCs can be manufactured with solvent casting, melt mixing, and *in-situ* polymerization, so far. The advantages and disadvantages of the main processing methods are described in Table 2.7.

Table 2.7. Advantages and disadvantages of the main processing methods of CNC-based nanocomposites (Ferreira et al., 2018).

Methods	Advantages	Disadvantages
Solvent casting	Ease of preparation; possibility of forming a three-dimensional CNC network inside a polymer matrix	Use of hazardous solvents (environmental issues); small scale production
Melt mixing	Potential for large-scale or mass production; hazardous solvents are not required	CNCs can degrade during the process; high shear applied during the process does not allow the 3D CNC network to form
In situ polymerization	Formation of a polymer network with CNCs embedded relatively uniform; possibility of covalent bond between CNCs and polymer matrix potential to large scale production	Temperature can degrade CNCs during polymerization; CNCs dispersion in the monomer phase can lead to a low degree of polymerization

2.6.2. General properties of nanocomposites reinforced with CNCs

2.6.2.1. Rheological properties

CNCs can affect the rheological properties of the polymer matrix when acting as a reinforcement agent (Ching et al., 2016). Rheological properties can provide information about the degree of dispersity and interactions between CNCs and the polymer matrix in the film forming solution (Ching et al., 2016; Rubentheren et al., 2015). The rheological properties are usually investigated through their storage modulus (G'), loss modulus (G˝), and complex viscosity (η^*). The relationship between G´ and G˝ is suggested in Table 2.8 and it is used to classify the status of nanocomposite suspension, which indicates a film forming solution.

Table 2.8. Relative value of the storage modulus and loss modulus for classifying polymer-based solutions (Ferreira et al., 2018).

Classification	Relationship between G′ and G″
Dilute solution	$G' > G''^{*}$
Entanglement network system	$G' = G''$
Weak gel	$G' < G''^{**}$
Strong gel	$G' \ll G''^{**}$

* Viscous behavior, ** Elastic behavior

G´ and G˝ usually increase when CNCs are dispersed in the polymer matrix homogeneously due to the filler-matrix load transfer (Mariano et al., 2016). This transfer is influenced by the agglomeration of the nanoparticles increment, which is derived from decreasing G´ and G˝. Therefore, complex viscosity (η^{*}) can be generally increased or decreased with the addition of CNCs in the nanocomposite matrix. This phenomenon is dependent upon the amount of the reinforcement agent added and dispersity in the polymer matrix (Durmus et al., 2007).

Previous studies have commonly reported that only the addition of 3 wt% of CNCs based on the amount of backbone polymer can increase the viscosity of the nanocomposite suspension (Zhang et al., 2016; Mariano et al., 2017). However, Pinheiro et al. investigated CNCs/PBAT nanocomposite and CNCs used in their research showed a decreased viscosity in film forming solution as the concentration of CNCs increased (Pinheiro et al., 2017). Other previous reports observed a peculiar behavior of poly(oxyethylene) (PEO) and CNCs and the complex presented a decreasing viscosity as the addition of the CNCs increased up to 6 wt%. However, the viscosity increased when CNCs added from 6 to 9 wt%. According to this study, the viscosity decreases in the initial addition due to the strong affinity between PEO and CNCs. However, above 6 wt% of CNCs, the PEO chains were adsorbed by the large amount of the

CNCs. Therefore, the lack of free polymer chains available in the suspension led to an increase of viscosity in the polymer matrix (Ben Azouz et al., 2012). The viscosity of nanocomposite suspensions can be also presented differently by the size and volume of the CNCs and the interaction between the backbone polymer matrix and CNCs. Weak interfacial interactions between the backbone polymer matrix and filler can lead to agglomeration due to the difference of polarity.

In addition, film forming methods can affect the rheological properties of nanocomposite films. When the solution casting method was applied with carboxymethyl cellulose (CMC) in a starch matrix, the results showed that viscosity increased and it lead to the increase of mechanical properties (El Miri et al., 2015). Also, Alloin et al. reported that when casting/evaporation and extrusion methods were combined and applied in PEO/CNCs nanocomposite, the strong reinforcing effect of CNCs was presented due to the percolating network between PEO and CNCs. This reinforcing effect of CNCs in the nanocomposites was reduced by extrusion due to the reducing of a percolating network (Alloin et al., 2011).

2.6.2.2. Mechanical properties

The addition of CNCs to a polymer matrix for accomplishing desired mechanical properties of nanocomposite films is important for various industries. For instance, packaging materials are necessary for high tensile strength, elongation, and tear resistance and biomedical materials should be flexible with high elongation properties. In the case of automotive applications, high tensile strength and toughness are needed for their application (Martino et al., 2006; Neto et al., 2015). Some previous studies focused on the theoretical model of the effect of CNCs to nanocomposite materials in mechanical properties. The Halpin-Tsai model and rule of mixture (ROM) model was investigated for proving effect of CNCs to mechanical properties of nanocomposites. Another study researched the Ouali-Takayanagi model to

interpret the mechanical improvement effect in polymer nanocomposites materials reinforced with CNCs (Ferreira et al., 2018). However, most of the studies have reported based on the experimental results for finding a reinforcement effect of CNCs.

Sung et al. prepared PLA/CNCs nanocomposites. When CNCs from coffee silver skin were added in PLA film with 1, 3, and 5 wt%, the tensile strength of PLA film raised 4, 9, and 4%, respectively. On the other hand, elongation at break showed a continuous decrease. Young's modulus increased 15, 22, and 24% when CNCs was added at 1, 3, and 5 wt% (Sung et al., 2017). Huq et al. found that the incorporation of 1, 3, and 5 wt% addition of CNCs raised the tensile strength of alginate films by 14, 25, and 37%, respectively. However, the tensile strength showed a 32% increase with 8 wt% addition of CNCs, which was a lower tensile strength than that of a 5 wt% addition. In the case of elongation at break, it presented a gradual decrease, specifically a 44% decrease with 8 wt% addition of CNCs (Huq et al., 2012). Many studies have observed the opposite trends between tensile strength and elongation at break, which is commonly found in thermoplastic nanocomposites. This behavior mainly resulted from the substantial local stress concentrations in the nanocomposite matrix (Colom et al., 2003). The addition of CNCs up to the theoretical percolation threshold can lead to homogeneous dispersion in the nanocomposite matrix. However, partially organized structures result in CNCs agglomeration due to their tendency to change from a percolated system to a non-percolated system in a nanocomposite matrix. This CNCs agglomeration affects the dissipation of external stress through the interaction of CNCs and polymer matrix. At last, it results in the reduction of the elongation at break.

The overall mechanical enhancement of the nanocomposites reinforced with CNCs can be related to the increased crystallinity of the polymer matrix. A previous study by Sung et al. insisted that the calculated crystallinity of the PLA/CNCs nanocomposite showed a much higher value than that of the PLA film prior to the addition of CNCs. This is because the high

nucleating effect induced by CNCs as the CNCs content increased (Sung et al., 2017). Also, Fortunati et al. formulated the PLA nanocomposites reinforced with CNCs and an increase of 83% in the Young's modulus was found after the addition of 5 wt% of CNCs with an increasing degree of crystallinity (Fortunati et al., 2014). In addition, other factors such as extraction methods, surface modification of CNCs, and preparation methods of the nanocomposite films can affect the mechanical properties of the nanocomposite film (Ferreira et al., 2018).

2.6.2.3. Barrier properties

Barrier properties are one of the most important properties for industrial application, especially for food packaging. Many previous studies have reported an improvement of barrier properties on water vapor, gas molecules, and light for biopolymer-based film after the addition of CNCs (Ferrer et al., 2017; Nair et al., 2014). CNCs act as blocking agents inside of the polymer matrix, leading to a complicated path for water and gas molecules, and even light. Therefore, CNCs/polymer nanocomposite can raise the barrier properties of the material. Figure 2.11 shows the scheme of the tortuous path of water and gas molecules derived from the addition of CNCs. Morphology, orientation, haziness, and homogeneity of the CNCs in the polymer matrix results in a complicated tortuous path, which can improve the barrier properties of the material (Espino-Pérez et al., 2016).

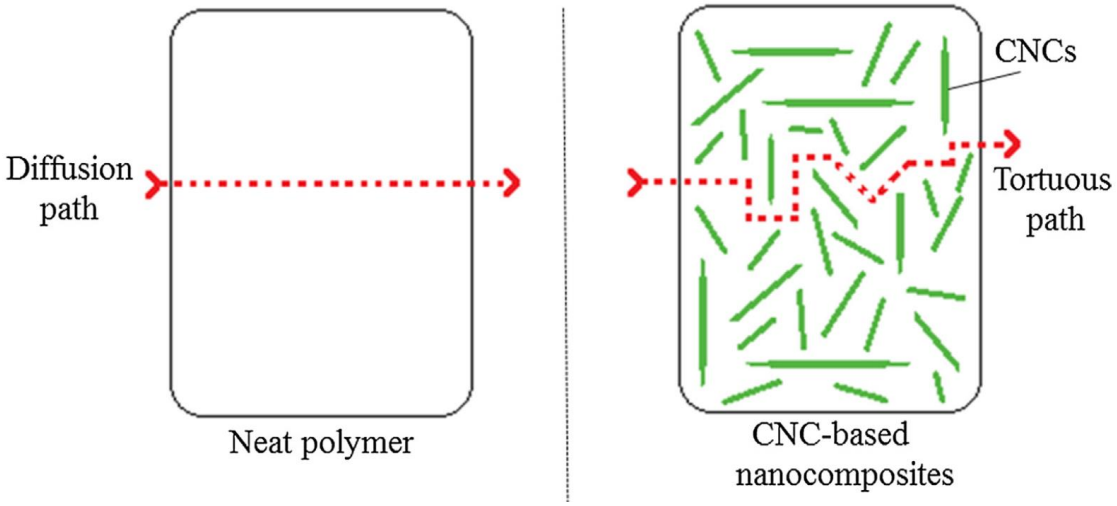

Figure 2.11. Schematic representation of the more tortuous path for water and gas molecules to diffuse due to addition of CNCs (Ferreira et al., 2018).

Some studies explained the reason for improved barrier properties of the nanocomposite is the result of the increased crystallinity due to the addition of CNCs (Charlon et al., 2015). Fortunati et al. and Sung et al. investigated the PLA/CNCs nanocomposite and presented the improvement of barrier properties. They explained this behavior resulted from the increased crystallinity due to the addition of CNCs (Fortunati et al., 2014; Sung et al., 2017). For better understanding of the relationship between barrier properties and crystallinity, Espino-Pérez et al. investigated the PLA/CNCs nanocomposite system with a high D-lactic acid content which cannot crystallize under suggested processing condition as polymer matrix. This experimental design enables to find the reason of increasing barrier properties between the blocking agent effect and the crystallinity of the nanocomposite matrix (Espino-Pérez et al., 2018). This research concluded that the separated dispersion of CNCs can affect the crystallinity of the nanocomposite matrix and led to the limitation of the tortuosity effect on the oxygen barrier properties. However, an improvement of water vapor barrier properties was found after the addition of modified CNCs. From this study, it can be described that the barrier properties of

nanocomposites reinforced with CNCs can be mainly increased from the tortuosity effect caused by CNCs which indicates the change of the structure of the nanocomposite.

2.6.2.4. Thermal properties

For evaluating the thermal properties, glass transition temperature (T_g), melting temperature (T_m), crystallization temperature (T_c), and polymer decomposition temperature (T_d) are determined as important parameters in nanocomposite applications. Biopolymer-based films usually show a lower T_g and T_m compared to the traditional petroleum-based, non-degradable plastics. This causes major issues in perspective of scaling-up to the pilot and industrial scale. Thermal properties have been mainly investigated with differential scanning calorimetry (DSC), thermomechanical analysis (TMA), and thermal gravimetric analysis (TGA). Many studies have already reported that the addition of CNCs can lead to an increase of the T_g, T_m, T_c, and T_d of the bionanocomposite film because CNCs can act as a nucleating agent (Ferreira et al., 2017). Temperatures of T_g, T_m, T_c, and T_d of bionanocomposite can be increased compared to that of the pure polymer due to the nucleating effect of CNCs, however, these can be decreased when CNCs act as an anti-nucleating agent in some polymer matrix (Chen et al., 2017). Therefore, it is important to determine if CNCs can act as a nucleating agent or not by their affecting on the interactions within the nanocomposite matrix. Therefore, the nucleation effect of CNCs should be studied for each system as various factors can affect this nucleation resulting in the thermal properties of the materials.

Some of the other reports have tried to explain the thermal properties of bionanocomposite with the crystallinity. The degree of crystallinity, X_c, of the materials was determined from the equation:

$$X_c = \frac{\Delta H_m}{w\Delta H_{m_0}} \times 100 \qquad \text{(Eq. 1)}$$

where, ΔH_m and ΔH_{m_0} are the enthalpy for the melting process and 100% crystallinity of backbone material, respectively, while w is the weight fraction of backbone polymer matrix in the bionanocomposite (Turner et al., 2004). For instance, Pei et al. prepared PLLA/silylated CNCs nanocomposites by the casting method. The results showed that the X_c of the polymer matrix increased from 14.3% to 30.4% after the addition of 1 wt% CNCs. The authors concluded that an enhanced CNC-polymer interaction could be obtained and thermal stabilities were increased. However, the authors observed that this increasing rate was not found with unmodified CNCs. Thus, the authors described that the reason for this phenomenon is surface modification with silica which resulted in enhanced crystallization and good dispersion in the polymer matrix (Pei et al., 2010).

Other studies have insisted that it is difficult to find significant differences of thermal properties after the addition of CNCs since parameters including T_g, T_m, T_d, and T_{cc} have a complex phenomenon including many factors, such as intermolecular interactions, molecular weight, chain flexibility, and crosslinking density (Chaichi et al., 2017; Krishnamachari et al., 2009). Also, thermal properties should be considered during the film forming process which can be affected by various factors, including cooling conditions, degree of dispersion, processing method, chemical structure, structure of the filler, and so on (Šupová et al., 2011).

2.6.2.5. Biodegradation properties

Biodegradation properties have been noticed as an important requirement for the packaging industry in recent years. Since biopolymer-based materials can become an excellent alternative to traditional, petroleum-based, and non-degradable materials in solving the ecological problems, such as landfills and global warming, many studies have investigated the biodegradation properties (Al Hosni et al., 2019; Stamou & Antizar-Ladislao, 2016).

Previous studies have revealed that biodegradation properties can be improved with the addition of CNCs in the bionanocomposite polymer matrix (Pinheiro et al., 2017; Garcia-Garcia et al., 2018). During the degradation process, the backbone of the polymer matrix can be degraded through non-enzymatic and enzymatic degradation (Shah et al., 2008). In non-enzymatic degradation, such as thermal degradation and chemical hydrolysis, the degradation rate of the polymer is significantly increased by water. Water molecules can lead to hydrolysis of nanocomposite chains between backbone polymer and CNCs because most of the interactions between those are hydrophilic, such as hydrogen bonds. Therefore, these hydrophilic properties of molecular interactions in the nanocomposite matrix has led to enhanced degradation of the matrix with the addition of CNCs. In the case of enzymatic degradation, the activities of microorganisms, including aerobic/anaerobic bacteria and fungi in the natural environment, induce the biodegradation because these microorganisms can consume the CNCs as a source of the energy. Once the nanocomposite has a crack due to the activities of microorganisms, degradation process can be promoted by the surrounding environment (Emadian et al., 2017).

However, the biodegradation rate is not always enhanced with the addition of CNCs. For instance, modification of CNCs surface can change this behavior because it renders nanocomposite matrix decreased of their hydrophilicity (Brand et al., 2017). For instance, Pinheiro et al. prepared PBAT/CNCs nanocomposites and this study reported the incorporation of modified CNCs prevented biodegradation due to the hydrophobicity of the modified CNCs (Pinheiro et al., 2017). Also, other studies insisted that crystallinity, crystal size, and aspect ratio should be considered in the degradation process because crystalline regions are hydrophobic (El-Hadi et al., 2002; Arrieta et al., 2015).

Ecotoxicological effects are also important when biodegradability testing of the polymer matrix is performed. Few studies have focused on this issue, however, some

investigations have reported in perspective of cytotoxicity, phytotoxicity, genotoxicity, and mutagenicity of the polymer matrix (Palsikowski et al., 2018). Mark and Rydz et al. studied the effect of polycaprolactone (PCL), polybutylene succinate (PBS), and polyhydroxybutyrate (PHB) to soil when their biodegradation test was performed, and they concluded these materials are non-toxic in soil (Mark, 2007; Rydz et al., 2015). However, under the circumstances with increasing interests of bionanocomposite film reinforced with CNCs, the research of their biodegradability and the toxicity in the environment should be investigated.

2.7. Potential Application in Industry and Perspective

CNCs have been studied as a reinforcement agent due to its biodegradability, availability, high crystallinity, and ability to enhance film properties of bionanocomposites. For instance, the physicochemical, rheological, mechanical, barrier, thermal, and biodegradation properties of nanocomposites are improved after the addition of CNCs. CNCs can affect the viscosity of the polymer matrix due to its size, free volume in matrix, percolating network, processing method of the nanocomposites, dispersion, and interfacial interaction between CNCs and the polymer matrix. Many previous reports have noticed that the nucleation effect of CNCs can increase the crystallinity of the nanocomposite. The increased crystallinity has been related to the improvement of mechanical properties of the nanocomposite. Also, high dispersion ability and strong interaction between CNCs and the polymer matrix contributes to the dissipated energy from external stresses, which reinforces the mechanical properties of the nanocomposites. The addition of CNCs to the polymer matrix results in a more tortuous path than normal and this phenomenon helps to improve the barrier properties against water vapor and gas molecules.

With increasing interests in nanocomposite materials reinforced with CNCs, these materials have been presented as a potential for use in not only the packaging industry but also for different fields, such as electronics applications, semi structural applications, and so on. However, there are several challenges, for instance, in development of processing these technologies for the industrial scale. As previously mentioned, the processing method is important because many factors can determine their final properties and performance. Further studies are needed to focus on the investigation of CNCs-based nanocomposites for industrial scale manufacturing and altering non-biodegradable polymers to environmental-friendly materials.

2.8. Research Objectives

1. Physicochemical Characteristics of Cellulose Nanocrystals (CNCs) Isolated From Seaweed Biomass

    a. Isolating CNCs successfully from seaweed biomass; brown, red, and green seaweed.

    b. Morphological observation, physicochemical, and thermal properties of cellulose nanocrystals will be determined and compared.

2. Development of Alginate Nanocomposite Film Reinforced with Cellulose Nanocrystals Isolated from *Sargassum fluitans*

    a. Applying CNCs to alginate (biopolymer) matrix and developing alginate nanocomposite film successfully.

    b. Characterization of alginate nanocomposite films with morphology observation, physicochemical properties, and thermodynamics.

    c. Evaluate CNCs were successfully acted as a reinforcing agent in alginate nanocomposite films.

3. Preparation of Novel Seaweed Nanocomposite Film Reinforced with Cellulose Nanocrystals from Brown Seaweeds

    a. Formulating seaweed biopolymer film successfully and developing seaweed nanocomposite film reinforced with CNCs.

    b. Investigating characteristics of seaweed nanocomposite film and evaluating antioxidant properties.

4. Effect of cellulose nanocrystals to biodegradability test with alginate and seaweed nanocomposite films

    a. Determine the effect of cellulose nanocrystals to degradability of nanocomposite film in soil and lake water system.

    b. Evaluate morphological, physicochemical, and thermal properties after biodegradation test.

2.9. References

Abdallah, W., & Kamal, M. R. (2018). Influence of process variables on physical characteristics of spray freeze dried cellulose nanocrystals. Cellulose, 25(10), 5711-5730.

Abdollahi, M., Alboofetileh, M., Rezaei, M., & Behrooz, R. (2013). Comparing physico-mechanical and thermal properties of alginate nanocomposite films reinforced with organic and/or inorganic nanofillers. Food Hydrocolloids, 32(2), 416-424.

Aeschelmann, F., & Carus, M. (2015). Biobased building blocks and polymers in the world: capacities, production, and applications–status quo and trends towards 2020. Industrial Biotechnology, 11(3), 154-159.

Agulhon, P., Robitzer, M., David, L., & Quignard, F. (2011). Structural regime identification in ionotropic alginate gels: influence of the cation nature and alginate structure. Biomacromolecules, 13(1), 215-220.

Al Hosni, A. S., Pittman, J. K., & Robson, G. D. (2019). Microbial degradation of four biodegradable polymers in soil and compost demonstrating polycaprolactone as an ideal compostable plastic. Waste Management, 97, 105-114.

Alexandre, M., & Dubois, P. (2000). Polymer-layered silicate nanocomposites: preparation, properties and uses of a new class of materials. Materials Science and Engineering: R: Reports, 28(1-2), 1-63.

Alloin, F., D'aprea, A., Dufresne, A., El Kissi, N., & Bossard, F. (2011). Poly (oxyethylene) and ramie whiskers based nanocomposites: influence of processing: extrusion and casting/evaporation. Cellulose, 18(4), 957-973.

Arrieta, M. P., Fortunati, E., Dominici, F., López, J., & Kenny, J. M. (2015). Bionanocomposite films based on plasticized PLA–PHB/cellulose nanocrystal blends. Carbohydrate Polymers, 121, 265-275.

Ashraf, M. A., Batool, S., Ahmad, M., Sarfraz, M., & Noor, W. S. A. W. M. (2016). Biopolymers as biofilters and biobarriers. In Biopolymers and Biotech Admixtures for Eco-Efficient Construction Materials (pp. 387-420). Woodhead Publishing.

Azizi Samir, M. A. S., Alloin, F., Sanchez, J. Y., El Kissi, N., & Dufresne, A. (2004). Preparation of cellulose whiskers reinforced nanocomposites from an organic medium suspension. Macromolecules, 37(4), 1386-1393.

Beck-Candanedo, S., Roman, M., & Gray, D. G. (2005). Effect of reaction conditions on the properties and behavior of wood cellulose nanocrystal suspensions. Biomacromolecules, 6(2), 1048-1054.

Ben Azouz, K., Ramires, E. C., Van den Fonteyne, W., El Kissi, N., & Dufresne, A. (2012). Simple method for the melt extrusion of a cellulose nanocrystal reinforced hydrophobic polymer. ACS Macro Letters, 1(1), 236-240.

Bhatnagar, A., & Sain, M. (2005). Processing of cellulose nanofiber-reinforced composites. Journal of Reinforced Plastics and Composites, 24(12), 1259-1268.

Bondeson, D., Mathew, A., & Oksman, K. (2006). Optimization of the isolation of nanocrystals from microcrystalline cellulose by acid hydrolysis. Cellulose, 13(2), 171.

Börjesson, M., & Westman, G. (2015). Crystalline nanocellulose—preparation, modification, and properties. Cellulose-fundamental aspects and current trends, 159-191.

Brand, J., Pecastaings, G., & Sèbe, G. (2017). A versatile method for the surface tailoring of cellulose nanocrystal building blocks by acylation with functional vinyl esters. Carbohydrate polymers, 169, 189-197.

Cha, D. S., & Chinnan, M. S. (2004). Biopolymer-based antimicrobial packaging: a review. Critical reviews in food science and nutrition, 44(4), 223-237.

Chaichi, M., Hashemi, M., Badii, F., & Mohammadi, A. (2017). Preparation and characterization of a novel bionanocomposite edible film based on pectin and crystalline nanocellulose. Carbohydrate polymers, 157, 167-175.

Charlon, S., Follain, N., Chappey, C., Dargent, E., Soulestin, J., Sclavons, M., & Marais, S. (2015). Improvement of barrier properties of bio-based polyester nanocomposite membranes by water-assisted extrusion. Journal of Membrane Science, 496, 185-198.

Chen, J., Wu, D., Tam, K. C., Pan, K., & Zheng, Z. (2017). Effect of surface modification of cellulose nanocrystal on nonisothermal crystallization of poly (β-hydroxybutyrate) composites. Carbohydrate polymers, 157, 1821-1829.

Chen, Y. W., Lee, H. V., Juan, J. C., & Phang, S. M. (2016). Production of new cellulose nanomaterial from red algae marine biomass Gelidium elegans. Carbohydrate polymers, 151, 1210-1219.

Ching, Y. C., Ali, M. E., Abdullah, L. C., Choo, K. W., Kuan, Y. C., Julaihi, S. J., ... & Liou, N. S. (2016). Rheological properties of cellulose nanocrystal-embedded polymer composites: A review. Cellulose, 23(2), 1011-1030.

Coles, R., McDowell, D., & Kirwan, M. J. (Eds.). (2003). Food packaging technology (Vol. 5). CRC Press.

Colom, X., Carrasco, F., Pages, P., & Canavate, J. (2003). Effects of different treatments on the interface of HDPE/lignocellulosic fiber composites. Composites Science and technology, 63(2), 161-169.

Daemi, H., Rajabi-Zeleti, S., Sardon, H., Barikani, M., Khademhosseini, A., & Baharvand, H. (2016). A robust super-tough biodegradable elastomer engineered by supramolecular ionic interactions. Biomaterials, 84, 54-63.

de Rodriguez, N. L. G., Thielemans, W., & Dufresne, A. (2006). Sisal cellulose whiskers reinforced polyvinyl acetate nanocomposites. Cellulose, 13(3), 261-270.

Deepa, B., Abraham, E., Cherian, B. M., Bismarck, A., Blaker, J. J., Pothan, L. A., & Kottaisamy, M. (2011). Structure, morphology and thermal characteristics of banana nano fibers obtained by steam explosion. Bioresource Technology, 102(2), 1988-1997.

Durmus, A., Kasgoz, A., & Macosko, C. W. (2007). Linear low density polyethylene (LLDPE)/clay nanocomposites. Part I: Structural characterization and quantifying clay dispersion by melt rheology. Polymer, 48(15), 4492-4502.

El Achaby, M., Kassab, Z., Aboulkas, A., Gaillard, C., & Barakat, A. (2018). Reuse of red algae waste for the production of cellulose nanocrystals and its application in polymer nanocomposites. International journal of biological macromolecules, 106, 681-691.

El Miri, N., Abdelouahdi, K., Barakat, A., Zahouily, M., Fihri, A., Solhy, A., & El Achaby, M. (2015). Bio-nanocomposite films reinforced with cellulose nanocrystals: Rheology of film-forming solutions, transparency, water vapor barrier and tensile properties of films. Carbohydrate Polymers, 129, 156-167.

El Miri, N., Aziz, F., Aboulkas, A., El Bouchti, M., Ben Youcef, H., & El Achaby, M. (2018). Effect of plasticizers on physicochemical properties of cellulose nanocrystals filled alginate bionanocomposite films. Advances in Polymer Technology, 37(8), 3171-3185.

El-Hadi, A., Schnabel, R., Straube, E., Müller, G., & Henning, S. (2002). Correlation between degree of crystallinity, morphology, glass temperature, mechanical properties and biodegradation of poly (3-hydroxyalkanoate) PHAs and their blends. Polymer testing, 21(6), 665-674.

El-Said, G. F., & El-Sikaily, A. (2013). Chemical composition of some seaweed from Mediterranean Sea coast, Egypt. Environmental monitoring and assessment, 185(7), 6089-6099.

El-Sakhawy, M., & Hassan, M. L. (2007). Physical and mechanical properties of microcrystalline cellulose prepared from agricultural residues. Carbohydrate polymers, 67(1), 1-10.

Emadian, S. M., Onay, T. T., & Demirel, B. (2017). Biodegradation of bioplastics in natural environments. Waste management, 59, 526-536.

Espino-Pérez, E., Bras, J., Almeida, G., Plessis, C., Belgacem, N., Perré, P., & Domenek, S. (2018). Designed cellulose nanocrystal surface properties for improving barrier properties in polylactide nanocomposites. Carbohydrate polymers, 183, 267-277.

Espino-Pérez, E., Bras, J., Almeida, G., Relkin, P., Belgacem, N., Plessis, C., & Domenek, S. (2016). Cellulose nanocrystal surface functionalization for the controlled sorption of water and organic vapours. Cellulose, 23(5), 2955-2970.

Favier, V., Canova, G. R., Cavaillé, J. Y., Chanzy, H., Dufresne, A., & Gauthier, C. (1995). Nanocomposite materials from latex and cellulose whiskers. Polymers for Advanced Technologies, 6(5), 351-355.

Ferreira, F. V., Dufresne, A., Pinheiro, I. F., Souza, D. H. S., Gouveia, R. F., Mei, L. H. I., & Lona, L. M. F. (2018). How do cellulose nanocrystals affect the overall properties of biodegradable polymer nanocomposites: a comprehensive review. European Polymer Journal, 108, 274-285.

Ferreira, F. V., Franceschi, W., Menezes, B. R. C., Brito, F. S., Lozano, K., Coutinho, A. R., ... & Thim, G. P. (2017). Dodecylamine functionalization of carbon nanotubes to improve dispersion, thermal and mechanical properties of polyethylene based nanocomposites. Applied Surface Science, 410, 267-277.

Ferrer, A., Pal, L., & Hubbe, M. (2017). Nanocellulose in packaging: Advances in barrier layer technologies. Industrial Crops and Products, 95, 574-582.

Fortunati, E., Luzi, F., Puglia, D., Dominici, F., Santulli, C., Kenny, J. M., & Torre, L. (2014). Investigation of thermo-mechanical, chemical and degradative properties of PLA-limonene films reinforced with cellulose nanocrystals extracted from Phormium tenax leaves. European Polymer Journal, 56, 77-91.

Gade, R., Tulasi, M. S., & Bhai, V. A. (2013). Seaweeds: a novel biomaterial. International Journal of Pharmacy and Pharmaceutical Sciences, 5(2), 975-1491.

García-Casal, M. N., Pereira, A. C., Leets, I., Ramírez, J., & Quiroga, M. F. (2007). High iron content and bioavailability in humans from four species of marine algae. The Journal of Nutrition, 137(12), 2691-2695.

Garcia-Garcia, D., Lopez-Martinez, J., Balart, R., Strömberg, E., & Moriana, R. (2018). Reinforcing capability of cellulose nanocrystals obtained from pine cones in a biodegradable poly (3-hydroxybutyrate)/poly (ε-caprolactone)(PHB/PCL) thermoplastic blend. European Polymer Journal, 104, 10-18.

Gholamipoor, S., Ghanavati, Y. N., Oromiehie, A. R., & Mohammadi, M. (2013). Extraction and Characterization of Alginat from Sargassum angustifolium collected from northern coasts of Persian Gulf, Bushehr. International Sympo-sium on Advances in Science and Technology., Iran.

Guo, J., Guo, X., Wang, S., & Yin, Y. (2016). Effects of ultrasonic treatment during acid hydrolysis on the yield, particle size and structure of cellulose nanocrystals. Carbohydrate polymers, 135, 248-255.

Hanlon, J. F., Kelsey, R. J., & Forcinio, H. (1998). Handbook of package engineering. CRC press.

Harding, K. G., Gounden, T., & Pretorius, S. (2017). “Biodegradable” plastics: a myth of marketing?. Procedia Manufacturing, 7, 106-110.

Helbert, W., Cavaille, J. Y., & Dufresne, A. (1996). Thermoplastic nanocomposites filled with wheat straw cellulose whiskers. Part I: processing and mechanical behavior. Polymer composites, 17(4), 604-611.

Hill, R. P. (1996). The Total Package: The Evolution and Secret Meanings of Boxes, Bottles, Cans, and Tubes.

Huq, T., Riedl, B., Bouchard, J., Salmieri, S., & Lacroix, M. (2014). Microencapsulation of nisin in alginate-cellulose nanocrystal (CNC) microbeads for prolonged efficacy against Listeria monocytogenes. Cellulose, 21(6), 4309-4321.

Huq, T., Salmieri, S., Khan, A., Khan, R. A., Le Tien, C., Riedl, B., & Lacroix, M. (2012). Nanocrystalline cellulose (NCC) reinforced alginate based biodegradable nanocomposite film. Carbohydrate polymers, 90(4), 1757-1763.

Huq, T., Vu, K. D., Riedl, B., Bouchard, J., Han, J., & Lacroix, M. (2016). Development of probiotic tablet using alginate, pectin, and cellulose nanocrystals as excipients. Cellulose, 23(3), 1967-1978.

Ibrahim, I. K., Hussin, S. M., & Al-Obaidi, Y. (2015). Extraction of cellulose nano crystalline from cotton by ultrasonic and its morphological and structural characterization. Int. J. Mater. Chem. Phys, 1, 99-109.

Imai, T., Boisset, C., Samejima, M., Igarashi, K., & Sugiyama, J. (1998). Unidirectional processive action of cellobiohydrolase Cel7A on Valonia cellulose microcrystals. FEBS letters, 432(3), 113-116.

Jain, R., & Tiwari, A. (2015). Biosynthesis of planet friendly bioplastics using renewable carbon source. Journal of Environmental Health Science and Engineering, 13(1), 11.

Jayaramudu, J., Reddy, G. S. M., Varaprasad, K., Sadiku, E. R., Ray, S. S., & Rajulu, A. V. (2013). Preparation and properties of biodegradable films from Sterculia urens short fiber/cellulose green composites. Carbohydrate polymers, 93(2), 622-627.

Jonoobi, M., Oladi, R., Davoudpour, Y., Oksman, K., Dufresne, A., Hamzeh, Y., & Davoodi, R. (2015). Different preparation methods and properties of nanostructured cellulose from various natural resources and residues: a review. Cellulose, 22(2), 935-969.

Kaplan, D. L., Mayer, J. M., Ball, D., McCassie, J., Allen, A. L., & Stenhouse, P. (1993). Fundamentals of biodegradable polymers. Biodegradable polymers and packaging, 8(5), 1-42.

Khalil, H. P. S., Tye, Y. Y., Saurabh, C. K., Leh, C. P., Lai, T. K., Chong, E. W. N., ... & Syakir, M. I. (2017). Biodegradable polymer films from seaweed polysaccharides: A review on cellulose as a reinforcement material. Express Polymer Letters, 11(4).

Khoshkava, V., & Kamal, M. R. (2014). Effect of cellulose nanocrystals (CNC) particle morphology on dispersion and rheological and mechanical properties of polypropylene/CNC nanocomposites. ACS applied materials & interfaces, 6(11), 8146-8157.

Krishnamachari, P., Zhang, J., Yan, J., Shahbazi, A., Uitenham, L., & Lou, J. (2009). Thermal characterization of biodegradable poly (lactic acid)/clay nanocomposites. In Proceedings of the 2007 National Conference on Environmental Science and Technology (pp. 219-225). Springer, New York, NY.

La Rosa, A. D. (2016). Life cycle assessment of biopolymers. In Biopolymers and Biotech Admixtures for Eco-Efficient Construction Materials (pp. 57-78). Woodhead Publishing.

Lu, P., & Hsieh, Y. L. (2012). Preparation and characterization of cellulose nanocrystals from rice straw. Carbohydrate Polymers, 87(1), 564-573.

Makarem, M., Lee, C. M., Sawada, D., O'Neill, H. M., & Kim, S. H. (2018). Distinguishing surface versus bulk hydroxyl groups of cellulose nanocrystals using vibrational sum

frequency generation spectroscopy. The journal of physical chemistry letters, 9(1), 70-75.

Mariano, M., El Kissi, N., & Dufresne, A. (2016). Structural reorganization of CNC in injection-molded CNC/PBAT materials under thermal annealing. Langmuir, 32(39), 10093-10103.

Mariano, M., Pilate, F., de Oliveira, F. B., Khelifa, F., Dubois, P., Raquez, J. M., & Dufresne, A. (2017). Preparation of cellulose nanocrystal-reinforced poly (lactic acid) nanocomposites through noncovalent modification with PLLA-based surfactants. ACS omega, 2(6), 2678-2688.

Mark, J. E. (Ed.). (2007). Physical properties of polymers handbook (Vol. 1076, p. 825). New York: Springer.

Martino, V., Ruseckaite, R., & Jiménez, A. (2006). Thermal and mechanical characterization of plasticized poly (L-lactide-co-D, L-lactide) films for food packaging. Journal of Thermal Analysis and Calorimetry, 86(3), 707-712.

Miao, C., & Hamad, W. Y. (2013). Cellulose reinforced polymer composites and nanocomposites: a critical review. Cellulose, 20(5), 2221-2262.

Mu, R., Hong, X., Ni, Y., Li, Y., Pang, J., Wang, Q., ... & Zheng, Y. (2019). Recent trends and applications of cellulose nanocrystals in food industry. Trends in Food Science & Technology.

Muenmee, S., Chiemchaisri, W., & Chiemchaisri, C. (2016). Enhancement of biodegradation of plastic wastes via methane oxidation in semi-aerobic landfill. International Biodeterioration & Biodegradation, 113, 244-255.

Nair, S. S., Zhu, J. Y., Deng, Y., & Ragauskas, A. J. (2014). High performance green barriers based on nanocellulose. Sustainable Chemical Processes, 2(1), 23.

Natterodt, J. C., Petri-Fink, A., Weder, C., & Zoppe, J. O. (2017). Cellulose nanocrystals: Surface modification, applications and opportunities at interfaces. CHIMIA International Journal for Chemistry, 71(6), 376-383.

Neto, D. M., Coër, J., Oliveira, M. C., Alves, J. L., Manach, P. Y., & Menezes, L. F. (2016). Numerical analysis on the elastic deformation of the tools in sheet metal forming processes. International Journal of Solids and Structures, 100, 270-285.

Neto, W. A. R., de Paula, A. C. C., Martins, T. M., Goes, A. M., Averous, L., Schlatter, G., & Bretas, R. E. S. (2015). Poly (butylene adipate-co-terephthalate)/hydroxyapatite composite structures for bone tissue recovery. Polymer Degradation and Stability, 120, 61-69.

Opaprakasit, M., Petchsuk, A., Opaprakasit, P., & Chongprakobkit, S. (2009). Effects of synthesis conditions on chemical structures and physical properties of copolyesters from lactic acid, ethylene glycol and dimethyl terephthalate. Express Polymer Letters, 3(7), 458-468.

Orts, W. J., Shey, J., Imam, S. H., Glenn, G. M., Guttman, M. E., & Revol, J. F. (2005). Application of cellulose microfibrils in polymer nanocomposites. Journal of Polymers and the Environment, 13(4), 301-306.

Pääkkö, M., Ankerfors, M., Kosonen, H., Nykänen, A., Ahola, S., Österberg, M., ... & Lindström, T. (2007). Enzymatic hydrolysis combined with mechanical shearing and high-pressure homogenization for nanoscale cellulose fibrils and strong gels. Biomacromolecules, 8(6), 1934-1941.

Palsikowski, P. A., Roberto, M. M., Sommaggio, L. R., Souza, P. M., Morales, A. R., & Marin-Morales, M. A. (2018). Ecotoxicity evaluation of the biodegradable polymers PLA, PBAT and its blends using allium cepa as test organism. Journal of Polymers and the Environment, 26(3), 938-945.

Pei, A., Zhou, Q., & Berglund, L. A. (2010). Functionalized cellulose nanocrystals as biobased nucleation agents in poly (l-lactide) (PLLA)–Crystallization and mechanical property effects. Composites Science and Technology, 70(5), 815-821.

Pinheiro, I. F., Ferreira, F. V., Souza, D. H. S., Gouveia, R. F., Lona, L. M. F., Morales, A. R., & Mei, L. H. I. (2017). Mechanical, rheological and degradation properties of PBAT nanocomposites reinforced by functionalized cellulose nanocrystals. European Polymer Journal, 97, 356-365.

Pinheiro, I. F., Ferreira, F. V., Souza, D. H. S., Gouveia, R. F., Lona, L. M. F., Morales, A. R., & Mei, L. H. I. (2017). Mechanical, rheological and degradation properties of PBAT nanocomposites reinforced by functionalized cellulose nanocrystals. European Polymer Journal, 97, 356-365.

Revol, J. F., Bradford, H., Giasson, J., Marchessault, R. H., & Gray, D. G. (1992). Helicoidal self-ordering of cellulose microfibrils in aqueous suspension. International journal of biological macromolecules, 14(3), 170-172.

Rhim, J. W. (2004). Physical and mechanical properties of water resistant sodium alginate films. LWT-Food science and technology, 37(3), 323-330.

Rhim, J. W., Park, H. M., & Ha, C. S. (2013). Bio-nanocomposites for food packaging applications. Progress in polymer science, 38(10-11), 1629-1652.

Risteen, B. E., Blake, A., McBride, M. A., Rosu, C., Park, J. O., Srinivasarao, M., ... & Reichmanis, E. (2017). Enhanced alignment of water-soluble polythiophene using cellulose nanocrystals as a liquid crystal template. Biomacromolecules, 18(5), 1556-1562.

Robertson, G. L. (2005). Food packaging: principles and practice. CRC press.

Robinson, D. K. R., & Morrison, M. J. (2010). Nanotechnologies for food packaging: Reporting the science and technology research trends: Report for the Observatory NANO. Phytotherapy Res, 15, 476-480.

Roman, M., & Winter, W. T. (2004). Effect of sulfate groups from sulfuric acid hydrolysis on the thermal degradation behavior of bacterial cellulose. Biomacromolecules, 5(5), 1671-1677.

Rubentheren, V., Ward, T. A., Chee, C. Y., & Nair, P. (2015). Physical and chemical reinforcement of chitosan film using nanocrystalline cellulose and tannic acid. Cellulose, 22(4), 2529-2541.

Rudin, A., & Choi, P. (2012). The elements of polymer science and engineering. Academic press.

Rydz, J., Sikorska, W., Kyulavska, M., & Christova, D. (2015). Polyester-based (bio) degradable polymers as environmentally friendly materials for sustainable development. International journal of molecular sciences, 16(1), 564-596.

Saba, N., Tahir, P., & Jawaid, M. (2014). A review on potentiality of nano filler/natural fiber filled polymer hybrid composites. Polymers, 6(8), 2247-2273.

Saïd Azizi Samir, M. A., Alloin, F., Paillet, M., & Dufresne, A. (2004). Tangling effect in fibrillated cellulose reinforced nanocomposites. Macromolecules, 37(11), 4313-4316.

Saito, T., & Isogai, A. (2004). TEMPO-mediated oxidation of native cellulose. The effect of oxidation conditions on chemical and crystal structures of the water-insoluble fractions. Biomacromolecules, 5(5), 1983-1989.

Schroers, M., Kokil, A., & Weder, C. (2004). Solid polymer electrolytes based on nanocomposites of ethylene oxide–epichlorohydrin copolymers and cellulose whiskers. Journal of Applied Polymer Science, 93(6), 2883-2888.

Shah, A. A., Hasan, F., Hameed, A., & Ahmed, S. (2008). Biological degradation of plastics: a comprehensive review. Biotechnology advances, 26(3), 246-265.

Silvia Román, 2013, 'Are we really prepared for bioplastics?', https://mappingignorance.org/2013/02/27/are-we-really-prepared-for-bioplastics/, Credit: sci-env.ch

Siracusa, V., Rocculi, P., Romani, S., & Dalla Rosa, M. (2008). Biodegradable polymers for food packaging: a review. Trends in Food Science & Technology, 19(12), 634-643.

Sirviö, J. A., Kolehmainen, A., Liimatainen, H., Niinimäki, J., & Hormi, O. E. (2014). Biocomposite cellulose-alginate films: Promising packaging materials. Food chemistry, 151, 343-351.

Son, H. N., & Seo, Y. B. (2015). Physical and bio-composite properties of nanocrystalline cellulose from wood, cotton linters, cattail, and red algae. Cellulose, 22(3), 1789-1798.

Sousa, A. M., Alves, V. D., Morais, S., Delerue-Matos, C., & Gonçalves, M. P. (2010). Agar extraction from integrated multitrophic aquacultured Gracilaria vermiculophylla: evaluation of a microwave-assisted process using response surface methodology. Bioresource technology, 101(9), 3258-3267.

Stamou, I., & Antizar-Ladislao, B. (2016). A life cycle assessment of the use of compost from contaminated biodegradable municipal solid waste with silver and titanium dioxide nanoparticles. Journal of Cleaner Production, 135, 884-891.

Sung, S. H., Chang, Y., & Han, J. (2017). Development of polylactic acid nanocomposite films reinforced with cellulose nanocrystals derived from coffee silverskin. Carbohydrate polymers, 169, 495-503.

Šupová, M., Martynková, G. S., & Barabaszová, K. (2011). Effect of nanofillers dispersion in polymer matrices: a review. Science of advanced materials, 3(1), 1-25.

Tang, X. Z., Kumar, P., Alavi, S., & Sandeep, K. P. (2012). Recent advances in biopolymers and biopolymer-based nanocomposites for food packaging materials. Critical reviews in food science and nutrition, 52(5), 426-442.

Tavassoli-Kafrani, E., Shekarchizadeh, H., & Masoudpour-Behabadi, M. (2016). Development of edible films and coatings from alginates and carrageenans. Carbohydrate polymers, 137, 360-374.

Tosin, M., Pischedda, A., & Degli-Innocenti, F. (2019). Biodegradation kinetics in soil of a multi-constituent biodegradable plastic. Polymer Degradation and Stability.

Turner, J. F. I. I., Riga, A., O'Connor, A., Zhang, J., & Collis, J. (2004). Characterization of drawn and undrawn poly-L-lactide films by differential scanning calorimetry. Journal of Thermal Analysis and Calorimetry, 75(1), 257-268.

Venkatesan, J., Anil, S., Kim, S. K., & Shim, M. S. (2016). Seaweed polysaccharide-based nanoparticles: preparation and applications for drug delivery. Polymers, 8(2), 30.

Wang, F., Drzal, L. T., Qin, Y., & Huang, Z. (2015). Multifunctional graphene nanoplatelets/cellulose nanocrystals composite paper. Composites Part B: Engineering, 79, 521-529.

Xu, X., Liu, F., Jiang, L., Zhu, J. Y., Haagenson, D., & Wiesenborn, D. P. (2013). Cellulose nanocrystals vs. cellulose nanofibrils: a comparative study on their microstructures and effects as polymer reinforcing agents. ACS applied materials & interfaces, 5(8), 2999-3009.

Yoo, Y., Martinez, C., & Youngblood, J. P. (2017). Synthesis and characterization of microencapsulated phase change materials with poly (urea−urethane) shells containing cellulose nanocrystals. ACS applied materials & interfaces, 9(37), 31763-31776.

Zhang, X., Ma, P., & Zhang, Y. (2016). Structure and properties of surface-acetylated cellulose nanocrystal/poly (butylene adipate-co-terephthalate) composites. Polymer Bulletin, 73(7), 2073-2085.

CHAPTER THREE

Physicochemical characteristics of cellulose nanocrystals isolated from seaweed biomass

Abstract

Cellulose nanocrystals (CNCs) were successfully isolated from marine biomass of brown, red, and green seaweeds by a four-step process of de-polymerization, bleaching, acid hydrolysis, and mechanical dispersion. Chemical composition, yield, and density were determined for each seaweed group and compared to other cellulose sources. Morphological analysis was performed by transmission electronic microscopy (TEM) and showed that CNCs from seaweed showed rod shape particles 21 – 248 nm length and 4.8 – 41 nm width. The obtained aspect ratio was varied from 2.5 to 15. Fourier transform infrared spectroscopy (FTIR) analysis was performed to investigate chemical structure of CNCs from seaweeds, which revealed obtained crystalline cellulosic from the extraction process. X-ray diffraction (XRD) data showed the main crystalline structure of CNCs was cellulose I in all cases. The crystalline index increased about 21.5% going from cellulose to CNCs. The thermal properties of untreated seaweeds, extracted cellulose, and CNCs were compared by thermogravimetric analysis (TGA). The onset thermal decomposition (T_{on}) increased in all cases and weight loss changes significantly decreased during the extraction process except *Sargassum fluitans*, indicating the thermal stability of CNCs.

3.1. Introduction

Cellulose is the one of the most abundant biopolymers in nature and the main component in the cell wall of plants (Börjesson & Westman, 2015). It is widely used for various industrial applications due to its low cost, renewability, environmental benefits, and good mechanical properties (El Achaby, Kassab, Aboulkas, Gaillard, & Barakat, 2018). In addition, with the development of nano technology in industrial fields, there is increasing interest in nano-sized cellulose (Beck-Candanedo, Roman, & Gray, 2005; Bondeson, Mathew, & Oksman, 2006). Cellulose nanocrystals (CNCs) have been investgated in the fields of biomedical engineering, wastewater treatment, energy and electronics sector, and food packaging or additives to polymer matrices (Grishkewich, Mohammed, Tang, & Tam, 2017; Serpa et al., 2016).

Traditionally, CNCs have been extracted from wood and pulse (Börjesson et al., 2015; Serpa et al., 2016). More recently, there have been attempts to isolate CNCs from a variety of other resources, such as sugar cane (Mandal & Chakrabarty, 2011), rice straw (Lu & Hsieh, 2012), coconut and rice husk (Johar, Ahmad, & Dufresne, 2012; Rosa et al., 2010), coffee skin (Sung, Chang, & Han, 2017), and banana peel (Tibolla, Pelissari, & Menegalli, 2014). Among the resources, macroalgae (seaweeds) of marine biomass has become more popular as a potential source for CNCs production due to its several advantages (Chen, Lee, Juan, & Phang, 2016). Compared to land plants, the advantages of using seaweeds for producing CNCs are: (i) easy of extraction due to a low content of other polysaccharides interfering with cellulose isolation; (ii) seaweeds contain a relatively higher yield of stored carbohydrates; (iii) rapid growth reduces harvest time compared to other sources (Chen et al., 2016).

Chemical industries have used brown and red seaweed for extracting alginate and agar since the 1980s (Armisen & Galatas, 1987; Bixler & Porse, 2011). In addition, seaweeds have

recently been produced and consumed as a healthy food in western countries (Doh & Park, 2018; Romarís–Hortas et al., 2011). Extraction processes for seaweeds in industrial fields results in much waste. For overcoming this issue, some recent researchers have explored the use of this waste to isolate nanocellulose (Chen et al., 2016; Liu, Li, Xie, & Deng, 2017). Even though it has been recognized that each seaweed group has different components and substances, no study has tried to compare the characteristics of CNCs from groups and species (Rioux, Beaulieu, & Turgeon, 2017). Therefore, CNCs were extracted, characterized, and compared from various kinds of seaweeds in this study.

Various methods have been used for producing CNCs, but processes usually included three steps: (1) pretreatment, (2) bleaching, (3) acid hydrolysis (Börjesson et al., 2015; Chen et al., 2016; Liu et al., 2017; Sung et al., 2017; Tibolla et al., 2014). The characteristics of CNCs could be changed not only by process conditions but are also dependent on the sources (Rosa et al., 2010). For instance, reaction temperature, time, and type of acid can change the crystallinity and the morphology of CNCs including rod, sphere, and needle shape. These shapes were an important factor in CNCs because it related to the inter/intra-molecular hydrogen bond, as well as crystallinity of CNCs depending on the source (El Achaby et al., 2018; Grishkewich et al., 2017; Tang, Sisler, Grishkewich, & Tam, 2017; Tonoli et al., 2012). Thus, it is more desireable to compare the characteristics of CNCs from each group of seaweeds extracted by the same controlled conditions.

In this study, representative seaweeds of each group, kombu (*Laminaria japonica*) and sargassum (*Sargassum fluitans*) as a brown seaweed, dulse (*Palmaria palmata*) and nori (*Porhyra umbilicalis*) as a red seaweed, and sea lettuce (*Ulva lactuca*) and spirulina (*Arthrospira maxima*) as a green seaweed were selected to produce CNCs. The physicochemical properties, structural changes, and thermal dynamics of CNCs from seaweeds

were determined by investigating chemical functional groups (FTIR), crystallinity (XRD), morphology studies (TEM), and thermal stability (TGA), systematically.

3.2. Materials and methods

3.2.1. Seaweeds collection and preparation

Representative seaweed of each group was collected from local markets. Seaweed species were determined by common names and places where harvested with the exception of sargassum (*Sargassum fluitans*), which obtained from the Florida seashore (Rioux et al., 2017). The brown seaweed group had kombu (*Laminaria japonica*) and sargassum (*Sargassum fluitans*) and the red seaweed group had dulse (*Palmaria palmata*) and nori (*Porphyra umbilicalis*). Sea lettuce (*Ulva lactuca*) and spirulina (*Arthrospira maxima*) were selected as the green seaweed group. Each seaweed was pulverized and stored in a powder form.

3.2.2. Isolating cellulose nanocrystals (CNCs) from seaweeds

Isolating cellulonse nanocrystals (CNCs) was accomplished with a four-step process; (1) de-polymerization, (2) bleaching, (3) acid hydrolysis, and (4) mechanical dispersion. These processes were performed with slight modification and applied to each seaweed group for the first time (Feng et al., 2015; Huq et al., 2012; Liu et al., 2017; Sung et al., 2017).

De-polymerization of each seaweed group was carried out by acid-base pretreatment. Dried seaweed powders were immersed in 0.2 M hydrogen chloride solution in a 1:10 (w/v) proportion with magnetic stirring for 2 h at 30˚C. Then, these colloidal suspensions were washed with distilled water by centrifugation until pH 7.0 ± 0.2 was achieved. After that, colloidal suspensions were soaked in a 1:60 proportion (w/v) with distilled water and pH 10.5 ± 0.5 was achieved with 4% sodium hydroxide solution for 3 h at 75˚C. Then, colloidal

suspensions were centrifuged at 15,000 *g* for 10 min. The supernatant was discarded and precipitates were dried for 3 days at 65˚C in dry oven.

In the second step, the dried residues were bleached to extract cellulose from each seaweed group. Dried residues were stirred with 5% potassium hydorixde for 3 h to remove residual polysaccharide barriers. Then, residues were washed for three times and treated with an excess amount of 6-10% sodium hypochlorite (g/10 mL ratio solid to liquid). After the treatment, pH was adjusted to 5.0 with glacial acetic acid. Samples were reacted for 2 h with magnetic stirring at 75˚C. After the first bleaching step, 30% active hydrogen peroxide was used for the second bleaching step at 80˚C for 70 min (g/5 mL ratio solid to liquid). After these two bleaching steps, the suspension was centrifuged at 22,000 *g* or 10 min to obtain cellulose after removing the supernatant.

After, the bleaching steps, acid hydrolysis was conducted to produce CNCs from the extracted cellulose. The acid hydrolysis method was performed at 45˚C for 30 min with 51% sulfuric acid (ratio of solid and liquid is 1:15, w/w) under constant stirring. After hydrolysis, the suspension was diluted with 100 mL of ice distilled water to stop the reaction for 15 min. The sample was then centrifuged for 25 min at 15,000 *g* several times to remove excess sulfuric acid. After removing supernatant, the residues were collected and the pH was adjusted to 7.0 ± 0.2 with 4% sodium hydroxide solution.

In the last step, the suspensions were homogenized using an ultrasonicator (Q500 sonicator, Qsonica, USA) for 15 min at 30% amplitude and finally lyophilized to obtain powdered CNCs.

3.2.3. Characterization of CNCs from seaweeds

3.2.3.1. Chemical composition, yield, and density

Chemical composition, yield, and density were determined for comparing characteristics of CNCs from each seaweed. Chemical compositions of each seaweed were obtained from previous studies, which included carbohydrates, proteins, lipids, and ash content of each seaweed. Yield of CNCs was determined by below equation:

$$\text{Yield (\%)} = \frac{Weight\ of\ obtained\ CNCs}{Weight\ of\ seaweeds} \times 100 \qquad \text{(Eq. 2)}$$

Density of seaweeds and CNCs were measured using a balance and volumetric beaker. All data are shown in Table 3.1.

3.2.3.2. Morphology of CNCs

To analyze the morphological properties of the CNCs, 0.2 - 0.5% (w/v) of CNCs suspension was prepared and a drop of the suspension was deposited on a carbon-coated copper grid. After drying overnight, grids were observed using a high resolution transmission electron microscope (TEM, H-9500; Hitachi, USA), operating at an accelerating voltage of 20 kV. Image J software (National Institute of Health, Bethesda, MD., USA) was used for analyzing CNCs particle length and width. For obtaining aspect ratio (L/d, where L is the length and d is the width), 50 measurements were analyzed.

3.2.3.3. Fourier transform infrared spectrometry (FTIR) analysis

The FTIR spectra of cellulose and CNCs from each seaweed were examined in the infrared range of 4000 – 500 cm^{-1} using an FTIR spectrometer (Nicolet iS10, Thermo Fisher Scientific, USA). The spectra were collected from 128 scans at a resolution of 4 cm^{-1} for each sample.

3.2.3.4. X-ray diffraction (XRD)

Crystallinity was determined by X-ray diffraction with an X-ray diffractometer (Rigaku Ultima IV, Tokyo, Japan) at a scanning rate of 2˚/min from 5˚ to 40˚ with Cu K_α radiation (λ = 1.5418 Å) using a voltage and current of 40 kV and 40 mA, respectively. The crystallinity index of the sample was calculated by the Segal method (Segal, Creely, Martin Jr, & Conrad, 1959) using the following equation:

$$\text{Crystallinity index (\%)} = \frac{I_{200} - I_{am}}{I_{200}} \times 100 \qquad \text{(Eq. 3)}$$

where, I_{200} is the maximum intensity at plane and I_{am} is the minimum intensity at the valley between planes.

3.2.3.5. Thermal properties

Thermal properties of the CNCs were measured using a thermogravimetric analysis by a thermal gravimetric analyzer (TGA) (Model 2950, TA, USA) All samples were weighed about 2 – 10 mg and heated from 30 to 600˚C under nitrogen atmosphere with the aluminum pan. Heating rate was 10˚C min^{-1}.

3.2.4. Statistical analysis

All data are presented as mean ± standard deviation. The data were analyzed using the analysis of variance (ANOVA) method. The ANOVA statistical analyses with Duncan's multiple comparison tests at a significance level of $p \leq 0.05$ were applied to the results using the Statistical Package for the Social Sciences software (SPSS, Version 20.0, SPSS Inc., Chicago, IL, USA).

3.3. Results and discussion

3.3.1. Chemical composition, yield, and density analysis

Chemical composition of seaweeds has been previously established (Table 3.1). Seaweeds typically contain carbohydrate up to 50%, lipid 1 – 5%, proteins 10 – 47%, minerals 8 – 40%, and phenolic compounds up to 25%. However, it has been observed that the chemical composition of seaweeds is quite different even though they are included in the same group (brown, red, and green). Previous studies have reported the chemical composition can vary according to not only the species but also season and location of harvest (Beaulieu, Sirois, & Tamigneaux, 2016; Cardoso, Pereira, Seca, Pinto, & Silva, 2015). Seaweeds typically have a lower content of carbohydrate and polysaccharides such as hemicellulose, lignin, and ash compared to land plants. Lignocellulosic parts can interfere with extraction of crystalline cellulose from seaweeds, but the relatively low content of hemicellulose and lignin make it easier to extract crystalline cellulose from seaweeds compared to the other CNCs sources. Chen et al., (2016) studied red algae, *Gelidium amansii*, and proved that hemicellulose, lignin, and ash content decreased through alkali-treating, bleaching, and acid hydrolyzing. On the other hand, α-cellulose content which determined the crystallinity of CNCs increased through the process (Chen et al., 2016).

Brown seaweeds showed the highest yields among the three groups (26.1 ± 1.2% of kombu and 25.8 ± 0.9% of sargassum, respectively). The red seaweed group had slightly lower yield (13.3 ± 2.4% of dulse and 17.4 ± 1.8% of nori, respectively) than the green seaweed group (16.3 ± 4.3% of sea lettuce and 20.3 ± 3.5% of spirulina, respectively), but there were no significant differences between red and green seaweeds. Both groups showed a lower yield compared to brown seaweeds. Compared to other CNCs sources such as hardwood (20%), softwood (20.5%), and cattail fibers (17%), yields from seaweeds are quite similar of around 20% (Son & Seo, 2015). Rice straw cellulose yield was 16.9% (Jiang & Hsieh, 2013; Zhou, Fu, Zheng, & Zhan, 2012) and the red seaweed group, *Gelidium amansii* showed 15.5% yield (Chen et al., 2016). Some studies also tried to calculate the yield from micro-cellulose which

is an intermediate product in the isolation process. In this study, all samples had about 42 – 51% yield except nori, which was 34.5 ± 2.4%. These yields agree with previous reports. According to the study of Liu et al. (2017), extracted CNCs from kelp (*Laminaria japonica*; brown seaweed) waste was 49.3 ± 1.4% yield from micro-cellulose and that of *Gelidium amansii* (red seaweed) was 52.1% yield (Chen et al., 2016).

In addition, based on the data of density, yield might be related to density and not carbohydrate content. As density increased, higher yields were obtained (R^2 = 0.9543). The brown seaweed group had the highest density of all the groups. Even though there were no significant differences between red and green seaweeds, the trend of average yield showed the possibility that density could affect the yield of CNCs isolation.

3.3.2. Characterization of CNCs from seaweeds

3.3.2.1. Morphology

It was proven that CNCs could be isolated as a nano-sized form from seaweeds (Fig. 3.1). All CNCs were rod shaped and these results are supported by previous studies with kelp waste (*Laminaria japonica*) and red algae marine biomass (*Gelidium elegans*) (Chen et al., 2016; Liu et al., 2017). Some aggregates were observed in all cases. These aggregates emerged due to freeze drying for sample preparation which resulted in strong intermolecular hydrogen bond formations among particles (Agustin, Ahmmad, Alonzo, & Patriana, 2014). The average length and width of the CNCs are shown in Table 3.2. In the case of kombu, range of length and width were 239.43 ± 38.57 nm and 22.45 ± 6.51 nm, respectively. Compared to the results from a previous study, the size of CNCs produced with the same source (*Laminaria japonica*) is quite similar with this study (Liu et al., 2017). Even though sargassum belongs to the brown seaweed group like kombu, the length and width of sargassum CNCs differed greatly from those of kombu (length and width of sargassum were 43.72 ± 7.44 nm and 8.81 ± 1.58 nm,

respectively). On the other hand, the red seaweed group including dulse (*Palmaria palmata*) and nori (*Porphyra umbilicalis*) was 64.23 ± 9.59 nm and 27.60 ± 5.83 nm of length and 17.38 ± 3.44 nm and 10.89 ± 3.07 nm of width, respectively. Similar with the brown seaweed group, they have significant differences in size. Compared to a previous study which used the same red seaweed group, *Gelidium elegans*, length was much shorter (Chen et al., 2016). However, the green seaweed group showed similar size. Sea lettuce (*Ulva Lactuca*) had 53.18 ± 8.48 nm of length and 17.30 ± 3.54 nm of width and those of spirulina (*Arthrospira maxima*) was 50.55 ± 5.73 nm and 14.91 ± 2.93 nm, respectively. The length of CNCs from this study was shorter than shown from other previous studies due to ultrasonication treatment during CNC production (Chen et al., 2016; El Achaby et al., 2018; Liu et al., 2017).

The aspect ratio of each seaweed is shown in Table 3.2. This parameter is one of the most important factors to packaging systems because it is expected that the higher the aspect ratio, the higher reinforcement capacity in the case of applying composite materials, assuming aggregation does not occur (Deepa et al., 2011; Landry, Alemdar, & Blanchet, 2011). Round-shaped crystal particles have a comparatively low aspect ratio (≈ 1), while fibrils can have a high aspect ratio due to their long length compared to short width (Börjesson et al., 2015). Typical aspect ratio for CNCs were varied from 1 to 100 and the results of this study showed the aspect ratio as about 2 – 15 (Börjesson et al., 2015; Miao & Hamad, 2013). Brown seaweed group, especially kombu, showed higher aspect ratio than other two groups. On the other hand, red and green seaweed groups showed similar aspect ratio with 2 – 3. The different types of cellulose sources showed different structures and aspect ratio. Acid hydrolysis or catalyst could change the length because some amorphous region could remain even though cellulose was treated with acids (Miao & Hamad, 2013). The result of other studies showed brown algae, *Laminaria japonica*, had an aspect ratio of 35, and red algae, *Gelidium elegans*, had an aspect ratio of 25 (Chem et al., 2016; Liu et al., 2017). This is because CNCs had much longer length

than CNCs used in this study. The aspect ratio of other resources from coffee silver skin, cotton, rice husk, and wood showed 9, 10.7, 10-15, and 24, respectively (Son et al., 2015; Sung et al., 2017).

3.3.2.2. Chemical structure analysis

Chemical structure changes of extracted cellulose and CNCs from seaweeds were analyzed with FTIR, and the spectra are shown in Fig. 3.2 (a) and (b), respectively. Although the spectra of cellulose and CNCs showed similar chemical structures in all cases, there were large differences between cellulose and CNCs in each seaweed. Transmittance signal at 1440, 1160, and 898 cm^{-1} indicated that CNCs were primarily in the form of cellulose I structure and all spectra showed related peak in those signals (Chen et al., 2016; El Achaby et al., 2018; Liu et al., 2017; Sung et al., 2017). Peaks near 890 cm^{-1} in cellulose were eliminated in CNCs. These peaks were due to the β-glycosidic linkages between anhydroglucose rings in the cellulose and it represents the glycosidic $^4C_1$ ring conformation (Chirayil et al., 2014; Hamid, Zain, Das, & Centi, 2016). Therefore, this disappearance of these peaks means amorphous regions in extracted cellulose were removed in CNCs. In addition, peaks between 996 and 1160 cm^{-1} of CNCs did not exist in the cellulose spectra. The spectra in this region was assigned to the C-C ring structure of cellulose. Peaks were appeared clearly due to reduction in amorphous regions in polysaccharide matrix by acid hydrolysis (Chirayil et al., 2014). In the same way, peaks around 890 – 1100 cm^{-1} (C-O stretching vibration) indicated that more cellulose content was exposed by removing non-cellulosic polysaccharides (Hamid et al., 2016; Saelee, Yingkamhaeng, Nimchua, & Sukyai, 2016). These results also agree previous studies suggesting that the peak at 1050 cm^{-1} indicated the C-O-C pyranose ring in cellulose (Yahya, Lee, & Hamid, 2015). The intensity of the peaks gradually increased from untreated seaweed to CNCs as the cellulose content of the treated cellulose increased during the pretreatment. On

the other hands, peaks at around 996 cm^{-1} were related to the structure of cellulose II which represented β-glycosidic linkages between glucose units in cellulose. Therefore, it can be said that the structure of cellulose II was significantly enhanced in CNCs compared to extracted cellulose. Also, peaks between 1440 – 1557 cm^{-1} from extracted cellulose were weakened in the spectra of CNCs. Peaks around 1530 cm^{-1} were assigned to the C=C stretching from aromatic hydrocarbons of lignin. Therefore, these weakened peaks showed that lignin was reduced through the processes (Chen et al., 2016). This explanation was also supported by other research. Sung et al. insisted that the absorption peaks at around between 1427 cm^{-1} and 1507 cm^{-1} were associated with the aromatic C=C in plane symmetrical stretching vibration of aromatic rings present in lignin, and these peaks diminished throughout the process (Sung et al., 2017). Wide bands at around 1730 cm^{-1} indicated the vibration of the acetyl groups and ester linkages in hemicellulose and lignin, and peaks at around 1620 – 1650 cm^{-1} described the aromatic rings of lignin and absorption of water which were observed in cellulosic parts. As the chemical process progressed, weakening of those bands in extracted cellulose was clearly verified and they were not observed in CNCs spectra. These phenomena happened because of the elimination of hemicellulose and lignin (Chirayil et al., 2014). Bands at around 3000 – 3400 cm^{-1} in extracted cellulose were also weakened in spectra of CNCs. These broad bands included the hydroxyl group which indicated O-H stretching vibration between 3000 and 3600 cm^{-1}. The O-H stretching vibration reduced in CNCs spectra after the chemical processes of extracted cellulose because water molecular were formed and evaporated during acid hydrolysis and freeze drying. Therefore, based on the discussion and analysis above, the results of FTIR indicate that the chemical processes conduced in the present study could effectively remove the amorphous regions composed of lignin and hemicellulose, which resulted in the increase of crystallinity of the CNCs.

3.3.2.3. Crystallinity analysis

The XRD patterns of extracted cellulose and CNCs from seaweeds are shown in Fig. 3.3. Crystalline patterns of CNCs were similar to each other and tended to increase in crystallinity after acid hydrolysis (Chen et al., 2016; Son et al., 2015; Sung et al., 2017). According to previous studies, peaks at 2θ = 18˚, 22˚, and 34˚ represent the typical cellulose I structure (Chen et al., 2016; Liu et al., 2017; Mandal et al., 2011; Park, Baker, Himmel, Parilla, & Johnson, 2010; Son et al., 2015; Sung et al., 2017). The sharpest peak of the CNCs describes higher crystallinity compared with extracted cellulose (Park et al., 2010; Rosa et al., 2010). Beside these peaks, the other common peaks were deserved at 2θ = 25˚ and 2θ = 34˚ which represented trimethylcellulose and native cellulose, respectively. Most of the peaks are included in the cellulose group (Park et al., 2010). A few peaks which were not included in cellulose peaks were observed in all cases due to the impurities originating from nature which could be generally formed and found in the sea biomass (Bettaieb et al., 2015).

The crystallinity index of extracted cellulose ranged from 58 – 79% (Table 3). This agrees with previous research because crystallinity degree of isolated cellulose from natural sources is usually considered to be about 41.4 – 71.5% (Hall, Bansal, Lee, Realff, & Bommarius, 2010; Park, Johnson, Ishizawa, Parilla, & Davis, 2009; Son et al., 2015). In the case of the crystallinity index of CNCs, kombu showed 98.89 ± 0.24% which was the highest. Sargassum, dulse, nori, and spirulina showed 83.06 ± 8.14%, 84.91 ± 4.66%, 87.54 ± 0.85%, and 89.71 ± 3.20% crytstallinity index, respectively. In the case of sea lettue, crystallinity index was 66.97 ± 3.89% which is the lowest. Although some differences of crystallinity index were obtained from each seaweed, all of the seaweeds showed enough crystallinity index for increasing mechanical and barrier properties when they are applied in films or plastics as a filler. Overall, the calculated crystallinity index for CNCs from seaweeds showed increments of about 21.5% compared with extracted cellulose. These results could be explained by the acid

hydrolysis step. As mentioned with respect to the FTIR analysis, most non-cellulosic parts were removed by acid hydrolysis. This is because hydronium ions (H_3O^+) penetrated into the polysaccharides components and amorphous regions of extracted cellulose from seaweeds (Chen et al., 2016; de Souza Lima & Borsali, 2004; Sung et al., 2017). This penetration resulted to hydrolytic cleaved of the β-1,4-glycosidic linkages within the cellulose chains and led to the release of individual crystalline segments (Tan, Hamid, & Lai, 2015).

3.3.2.4. Thermal properties

Fig. 3.4 shows the thermogravimetric (TGA) curves of the untreated seaweeds, extracted cellulose, and cellulose nanocrystals (CNCs). Since moisture bounded or chemisorbed on seaweed surface evaporated, weight loss was observed around 100˚C (Chandra, George, & Narayanankutty, 2016). As observed in the FTIR study, the presence of absorved water was also detected by a peak at 1640 cm^{-1} which indicated water intermolecular hydrogen bonding (Chen et al., 2016). The onset thermal decomposition (T_{on}) increased from untreated to CNCs in all cases and weight loss changes significantly decreased during the process except for sargassum. These phenomena could have happened due to the increase of thermal stability of CNCs. There are two reasons. First, CNCs in all seaweeds showed more dense and compact structures after successive elimination of amorphous parts in the seaweeds matrix (Chandra et al., 2016). As data already have shown in Table 3.3, Fig. 3.2, and 3.3, CNCs chemical structure changed throughout the whole process and crystallinity increased by more than 20% compared to the extracted cellulose in all cases. Crystalline domains of CNCs was attributed to rearrangement of molecular structure by removing amorphous regions. Therefore, CNCs showed the highest thermal stability among analyzed samples. Second, the the impurities in seaweeds matrix can initiate the heating process in the furnace of the TGA instrument because impurities have more active sites than CNCs (Chirayil et al., 2014). Several previous

studies have similar trends for sea algae biomass (Chen et al., 2016; Muradov et al., 2015). Weight change tendency of sargassum was different from other seaweeds. This is because CNCs from sargassum showed ionic association around molecules. Amorphous regions of CNCs from sargassum might provide for enhanced interchain spaces thus showing dramatic weight decrease compared to other CNCs (Mandal et al., 2011). In addition, acid hydrolysis with surfuric acid led to thermal stability reduction of CNCs due to the active sulfate groups. According to the thermogravimetric data from previous research, the thermal stability of CNCs were less than extracted cellulose from its source (Mandal et al., 2011). The authors described that the decrease of T_{on} was affected by the drastic reduction of molecular weight and the increase of sulfated amorphous regions (Liu et al., 2017; Mandal et al., 2011). In this study, however, 4% sodium hydroxide solution was used during seaweed treatment which was a different method compared with previous studies and diminished the effect of active sulfate groups. Thus, it was found that thermal stability would increase in all cases through the isolating process.

3.4. Conclusions

In the present study, CNCs were successfully isolated from marine biomass of each seaweed group through de-polymerization, bleaching, acid hydrolysis, and mechanical dispersion processes. The physicochemical characterization data showed that length and width could be different depended on the species of seaweeds, not on the group. The parameter, aspect ratio, which indicated the possibility for increasing mechanical properties when applied to films varied from about 2.79 to 10.49. FTIR analysis showed amorphous parts would decrease during the process. In addition, these data indicated crystalline parts of CNCs could have more crystallinity than extracted cellulose. Crystalline index increased in all cases from extracted

cellulose (about 61.01 – 75.76%) to CNCs (66.97 – 98.89%). Thermogravimetric analysis indicated that thermal stability of all seaweed samples increased through the processes. Compared to traditional CNCs sources, CNCs from seaweeds showed easy access, relatively higher crystallinity, and better thermal stability. When comparing CNCs from each seaweed, there were no significant differences because they had all good range in aspect ratio, crystallinity, and thermal stability for use as a filler in packaging system. Thus, the results of this study suggest that CNCs from seaweeds have the potential to be used for reinforcing agents for increasing mechanical properties of polymer materials for food packaging.

3.5. References

Agustin, M. B., Ahmmad, B., Alonzo, S. M. M., & Patriana, F. M. (2014). Bioplastic based on starch and cellulose nanocrystals from rice straw. *Journal of Reinforced Plastics and Composites, 33*(24), 2205-2213.

Armisen, R., & Galatas, F. (1987). Production, properties and uses of agar. *Production and utilization of products from commercial seaweeds. FAO Fish. Tech. Pap, 288*, 1-57.

Beaulieu, L., Sirois, M., & Tamigneaux, É. (2016). Evaluation of the in vitro biological activity of protein hydrolysates of the edible red alga, Palmaria palmata (dulse) harvested from the Gaspe coast and cultivated in tanks. *Journal of applied Phycology, 28*(5), 3101-3115.

Beck-Candanedo, S., Roman, M., & Gray, D. G. (2005). Effect of reaction conditions on the properties and behavior of wood cellulose nanocrystal suspensions. *Biomacromolecules, 6*(2), 1048-1054.

Bettaieb, F., Khiari, R., Hassan, M. L., Belgacem, M. N., Bras, J., Dufresne, A., & Mhenni, M. F. (2015). Preparation and characterization of new cellulose nanocrystals from marine

biomass Posidoniaoceanica. *Industrial Crops and Products, 72*, 175-182.

Bixler, H. J., & Porse, H. (2011). A decade of change in the seaweed hydrocolloids industry. *Journal of applied Phycology, 23*(3), 321-335.

Bondeson, D., Mathew, A., & Oksman, K. (2006). Optimization of the isolation of nanocrystals from microcrystalline cellulose by acid hydrolysis. *Cellulose, 13*(2), 171.

Börjesson, M., & Westman, G. (2015). Crystalline nanocellulose—preparation, modification, and properties. In *Cellulose-fundamental aspects and current trends*: IntechOpen.

Cardoso, S., Pereira, O., Seca, A., Pinto, D., & Silva, A. (2015). Seaweeds as preventive agents for cardiovascular diseases: From nutrients to functional foods. *Marine Drugs, 13*(11), 6838-6865.

Chandra, J., George, N., & Narayanankutty, S. K. (2016). Isolation and characterization of cellulose nanofibrils from arecanut husk fibre. *Carbohydrate polymers, 142*, 158-166.

Chen, Y. W., Lee, H. V., Juan, J. C., & Phang, S.-M. (2016). Production of new cellulose nanomaterial from red algae marine biomass Gelidium elegans. *Carbohydrate polymers, 151*, 1210-1219.

Chirayil, C. J., Joy, J., Mathew, L., Mozetic, M., Koetz, J., & Thomas, S. (2014). Isolation and characterization of cellulose nanofibrils from Helicteres isora plant. *Industrial Crops and Products, 59*, 27-34.

de Souza Lima, M. M., & Borsali, R. (2004). Rodlike cellulose microcrystals: structure, properties, and applications. *Macromolecular rapid communications, 25*(7), 771-787.

Deepa, B., Abraham, E., Cherian, B. M., Bismarck, A., Blaker, J. J., Pothan, L. A., Leao, A. L., De Souza, S. F., & Kottaisamy, M. (2011). Structure, morphology and thermal characteristics of banana nano fibers obtained by steam explosion. *Bioresource Technology, 102*(2), 1988-1997.

Doh, H. S., & Park, H. J. (2018). Speciation of Bio-Available Iodine in Abalone (Haliotis discus

hannai) by High-Performance Liquid Chromatography Hyphenated with Inductively Coupled Plasma-Mass Spectrometry Using an In Vitro Method. *Journal of food science, 83*(6), 1579-1587.

El Achaby, M., Kassab, Z., Aboulkas, A., Gaillard, C., & Barakat, A. (2018). Reuse of red algae waste for the production of cellulose nanocrystals and its application in polymer nanocomposites. *International journal of biological macromolecules, 106*, 681-691.

Feng, X., Meng, X., Zhao, J., Miao, M., Shi, L., Zhang, S., & Fang, J. (2015). Extraction and preparation of cellulose nanocrystals from dealginate kelp residue: structures and morphological characterization. *Cellulose, 22*(3), 1763-1772.

Grishkewich, N., Mohammed, N., Tang, J., & Tam, K. C. (2017). Recent advances in the application of cellulose nanocrystals. *Current opinion in colloid & interface science, 29*, 32-45.

Hall, M., Bansal, P., Lee, J. H., Realff, M. J., & Bommarius, A. S. (2010). Cellulose crystallinity–a key predictor of the enzymatic hydrolysis rate. *The FEBS journal, 277*(6), 1571-1582.

Hamid, S. B. A., Zain, S. K., Das, R., & Centi, G. (2016). Synergic effect of tungstophosphoric acid and sonication for rapid synthesis of crystalline nanocellulose. *Carbohydrate polymers, 138*, 349-355.

Han, T. U., Kim, Y.-M., Siddiqui, M. Z., Lee, T., Watanabe, A., Teramae, N., Kim, S., & Park, Y.-K. (2018). Non-isothermal pyrolysis properties of Laminaria japonica. *Journal of analytical and applied pyrolysis, 130*, 277-284.

Huq, T., Salmieri, S., Khan, A., Khan, R. A., Le Tien, C., Riedl, B., Fraschini, C., Bouchard, J., Uribe-Calderon, J., & Kamal, M. R. (2012). Nanocrystalline cellulose (NCC) reinforced alginate based biodegradable nanocomposite film. *Carbohydrate polymers, 90*(4), 1757-1763.

Jiang, F., & Hsieh, Y.-L. (2013). Chemically and mechanically isolated nanocellulose and their self-assembled structures. *Carbohydrate polymers, 95*(1), 32-40.

Johar, N., Ahmad, I., & Dufresne, A. (2012). Extraction, preparation and characterization of cellulose fibres and nanocrystals from rice husk. *Industrial Crops and Products, 37*(1), 93-99.

Landry, V., Alemdar, A., & Blanchet, P. (2011). Nanocrystalline cellulose: morphological, physical, and mechanical properties. *Forest products journal, 61*(2), 104-112.

Liu, Z., Li, X., Xie, W., & Deng, H. (2017). Extraction, isolation and characterization of nanocrystalline cellulose from industrial kelp (Laminaria japonica) waste. *Carbohydrate polymers, 173*, 353-359.

Lu, P., & Hsieh, Y.-L. (2012). Preparation and characterization of cellulose nanocrystals from rice straw. *Carbohydrate polymers, 87*(1), 564-573.

Mandal, A., & Chakrabarty, D. (2011). Isolation of nanocellulose from waste sugarcane bagasse (SCB) and its characterization. *Carbohydrate polymers, 86*(3), 1291-1299.

Miao, C., & Hamad, W. Y. (2013). Cellulose reinforced polymer composites and nanocomposites: a critical review. *Cellulose, 20*(5), 2221-2262.

Montalvo, G. E. B., Thomaz-Soccol, V., Vandenberghe, L. P., Carvalho, J. C., Faulds, C. B., Bertrand, E., Prado, M. R., Bonatto, S. J., & Soccol, C. R. (2019). Arthrospira maxima OF15 biomass cultivation at laboratory and pilot scale from sugarcane vinasse for potential biological new peptides production. *Bioresource Technology, 273*, 103-113.

Muradov, N., Taha, M., Miranda, A. F., Wrede, D., Kadali, K., Gujar, A., Stevenson, T., Ball, A. S., & Mouradov, A. (2015). Fungal-assisted algal flocculation: application in wastewater treatment and biofuel production. *Biotechnology for biofuels, 8*(1), 24.

Park, S., Baker, J. O., Himmel, M. E., Parilla, P. A., & Johnson, D. K. (2010). Cellulose crystallinity index: measurement techniques and their impact on interpreting cellulase

performance. *Biotechnology for biofuels, 3*(1), 10.

Park, S., Johnson, D. K., Ishizawa, C. I., Parilla, P. A., & Davis, M. F. (2009). Measuring the crystallinity index of cellulose by solid state 13 C nuclear magnetic resonance. *Cellulose, 16*(4), 641-647.

Postma, P., Cerezo-Chinarro, O., Akkerman, R., Olivieri, G., Wijffels, R. H., Brandenburg, W., & Eppink, M. H. (2018). Biorefinery of the macroalgae Ulva lactuca: extraction of proteins and carbohydrates by mild disintegration. *Journal of applied Phycology*, 1-13.

Rioux, L.-E., Beaulieu, L., & Turgeon, S. L. (2017). Seaweeds: A traditional ingredients for new gastronomic sensation. *Food Hydrocolloids, 68*, 255-265.

Romarí –Hortas, V., Garcí -Sartal, C., del Carmen Barciela-Alonso, M., Domínguez-González, R., Moreda-Piñeiro, A., & Bermejo-Barrera, P. (2011). Bioavailability study using an in-vitro method of iodine and bromine in edible seaweed. *Food Chemistry, 124*(4), 1747-1752.

Rosa, M., Medeiros, E., Malmonge, J., Gregorski, K., Wood, D., Mattoso, L., Glenn, G., Orts, W., & Imam, S. (2010). Cellulose nanowhiskers from coconut husk fibers: Effect of preparation conditions on their thermal and morphological behavior. *Carbohydrate polymers, 81*(1), 83-92.

Saelee, K., Yingkamhaeng, N., Nimchua, T., & Sukyai, P. (2016). An environmentally friendly xylanase-assisted pretreatment for cellulose nanofibrils isolation from sugarcane bagasse by high-pressure homogenization. *Industrial Crops and Products, 82*, 149-160.

Segal, L., Creely, J., Martin Jr, A., & Conrad, C. (1959). An empirical method for estimating the degree of crystallinity of native cellulose using the X-ray diffractometer. *Textile Research Journal, 29*(10), 786-794.

Serpa, A., Velásquez-Cock, J., Gañán, P., Castro, C., Vélez, L., & Zuluaga, R. (2016). Vegetable nanocellulose in food science: A review. *Food Hydrocolloids, 57*, 178-186.

Son, H. N., & Seo, Y. B. (2015). Physical and bio-composite properties of nanocrystalline cellulose from wood, cotton linters, cattail, and red algae. *Cellulose, 22*(3), 1789-1798.

Sung, S. H., Chang, Y., & Han, J. (2017). Development of polylactic acid nanocomposite films reinforced with cellulose nanocrystals derived from coffee silverskin. *Carbohydrate polymers, 169*, 495-503.

Suwal, S., Perreault, V., Marciniak, A., Tamigneaux, É., Deslandes, É., Bazinet, L., Jacques, H., Beaulieu, L., & Doyen, A. (2019). Effects of high hydrostatic pressure and polysaccharidases on the extraction of antioxidant compounds from red macroalgae, Palmaria palmata and Solieria chordalis. *Journal of Food Engineering, 252*, 53-59.

Tan, X. Y., Hamid, S. B. A., & Lai, C. W. (2015). Preparation of high crystallinity cellulose nanocrystals (CNCs) by ionic liquid solvolysis. *Biomass and Bioenergy, 81*, 584-591.

Tang, J., Sisler, J., Grishkewich, N., & Tam, K. C. (2017). Functionalization of cellulose nanocrystals for advanced applications. *Journal of colloid and interface science, 494*, 397-409.

Tapia-Martinez, J., Hernández-Cruz, K., Franco-Colín, M., Mateo-Cid, L. E., Mendoza-Gonzalez, C., Blas-Valdivia, V., & Cano-Europa, E. (2019). Safety evaluation and antiobesogenic effect of Sargassum liebmannii J. Agardh (Fucales: Phaeophyceae) in rodents. *Journal of applied Phycology*, 1-11.

Tibolla, H., Pelissari, F. M., & Menegalli, F. C. (2014). Cellulose nanofibers produced from banana peel by chemical and enzymatic treatment. *LWT-Food Science and Technology, 59*(2), 1311-1318.

Tonoli, G., Teixeira, E., Corrêa, A., Marconcini, J., Caixeta, L., Pereira-da-Silva, M., & Mattoso, L. (2012). Cellulose micro/nanofibres from Eucalyptus kraft pulp: preparation and properties. *Carbohydrate polymers, 89*(1), 80-88.

Venkatraman, K. L., & Mehta, A. (2019). Health Benefits and Pharmacological Effects of

Porphyra Species. *Plant Foods for Human Nutrition, 74*(1), 10-17.

Yahya, M. B., Lee, H. V., & Hamid, S. B. A. (2015). Preparation of nanocellulose via transition metal salt-catalyzed hydrolysis pathway. *BioResources, 10*(4), 7627-7639.

Zhou, Y., Fu, S., Zheng, L., & Zhan, H. (2012). Effect of nanocellulose isolation techniques on the formation of reinforced poly (vinyl alcohol) nanocomposite films. *Express Polymer Letters, 6*(10).

Table 3.1. Chemical composition, yield, and density of seaweeds

Group	Sample	Species	Composition (%)				Reference	Yield (%)	Density (g/100 mL)
			Carbohydrates	Proteins	Lipids	Ash			
Brown	Kombu	*Laminaria japonica*	45.2	7.4	1.1	14.4	(Han et al., 2018)	26.1 ± 1.2^{a}	62.1
	Sargassum	*Sargassum fluitans*	48.7	23.9	5.0	11.7	(Tapia-Martinez et al., 2019)	25.8 ± 0.9^{a}	57.7
Red	Dulse	*Palmaria plamata*	60.1	10.2	0.8	21.1	(Suwal et al., 2019)	13.3 ± 2.4^{c}	40.6
	Nori	*Porphyra umbilicalis*	44.4	24-47	2-3	7-20	(Venkatraman & Mehta, 2019)	17.4 ± 1.8^{bc}	47.2
Green	Sea lettuce	*Ulva lactuca*	45.8	12.3	-	21.9	(Postma et al., 2018)	16.3 ± 4.3^{bc}	43.6
	Spirulina	*Arthrospira maxima*	10.7	57.0	11.2	5.7	(Montalvo et al., 2019)	20.3 ± 3.5^{ab}	53.8

(1) Data are mean ± S.D.
(2) Mean values with different letters within a column are significantly different ($p < 0.05$) by ANOVA with Duncan's multiple comparison test, n=3.

Table 3.2. Dimensions and aspect ratio of cellulose nanocrystals from each seaweed.

Group	Sample	Species	Length (nm)	Width (nm)	Aspect ratio
Brown	Kombu	*Laminaria japonica*	239.43 ± 38.57^{a}	22.45 ± 6.51^{a}	11.50 ± 3.66^{a}
	Sargassum	*Sargassum fluitans*	43.72 ± 7.44^{c}	8.81 ± 1.58^{c}	5.05 ± 0.92^{b}
Red	Dulse	*Palmaria plamata*	64.23 ± 9.59^{b}	17.38 ± 3.44^{ab}	3.85 ± 1.02^{b}
	Nori	*Porphyra umbilicalis*	27.60 ± 5.83^{cd}	10.89 ± 3.07^{bc}	2.79 ± 1.13^{bc}
Green	Sea lettuce	*Ulva lactuca*	53.18 ± 8.48^{bc}	17.30 ± 3.54^{ab}	3.16 ± 0.62^{bc}
	Spirulina	*Arthrospira maxima*	50.55 ± 5.73^{bc}	14.91 ± 2.93^{ab}	3.51 ± 0.79^{bc}

(1) Data are mean ± S.D.
(2) Mean values with different letters within a column are significantly different ($p < 0.05$) by ANOVA with Duncan's multiple comparison test, n=3.

Table 3.3. Crystallinity index of extracted cellulose and cellulose nanocrystals from seaweeds.

Group	Sample	Species	Crystallinity (%)	
			Cellulose	Cellulose nanocrystals
Brown	Kombu	*Laminaria japonica*	75.76 ± 3.18[a]	98.89 ± 0.24[a]
	Sargassum	*Sargassum fluitans*	65.59 ± 2.67[b]	83.06 ± 8.14[b]
Red	Dulse	*Palmaria plamata*	61.01 ± 2.70[b]	84.91 ± 4.66[c]
	Nori	*Porphyra umbilicalis*	65.97 ± 2.18[b]	87.54 ± 0.85[c]
Green	Sea lettuce	*Ulva lactuca*	46.74 ± 5.13[c]	66.97 ± 3.89[d]
	Spirulina	*Arthrospira maxima*	67.24 ± 3.21[b]	89.71 ± 3.20[b]

(1) Data are mean ± S.D

(2) Mean values with different letters within a column are significantly different ($p < 0.05$) by ANOVA with Duncan's multiple comparison test, n=3.

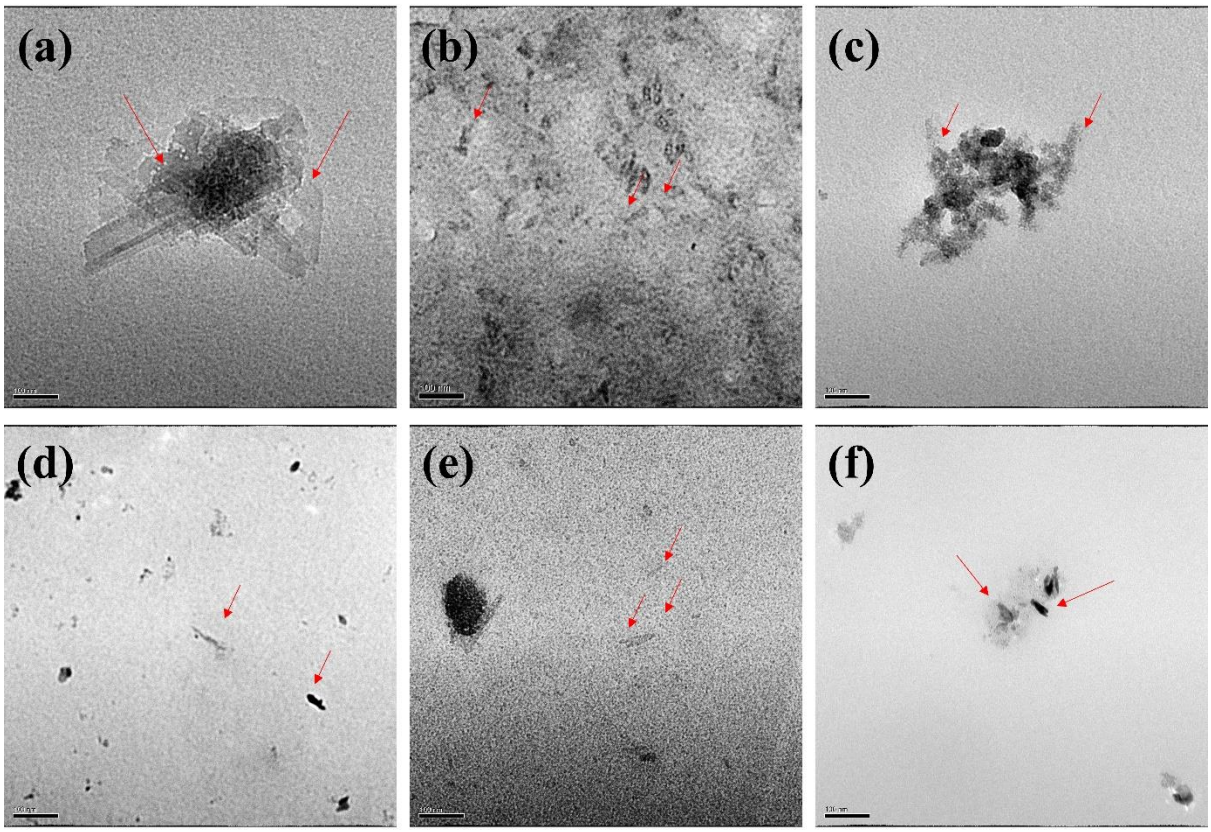

Figure 3.1. TEM images of CNCs of kombu, (a); sargassum, (b); dulse, (c); nori, (d); sea lettuce, (e); and spirulina, (f).

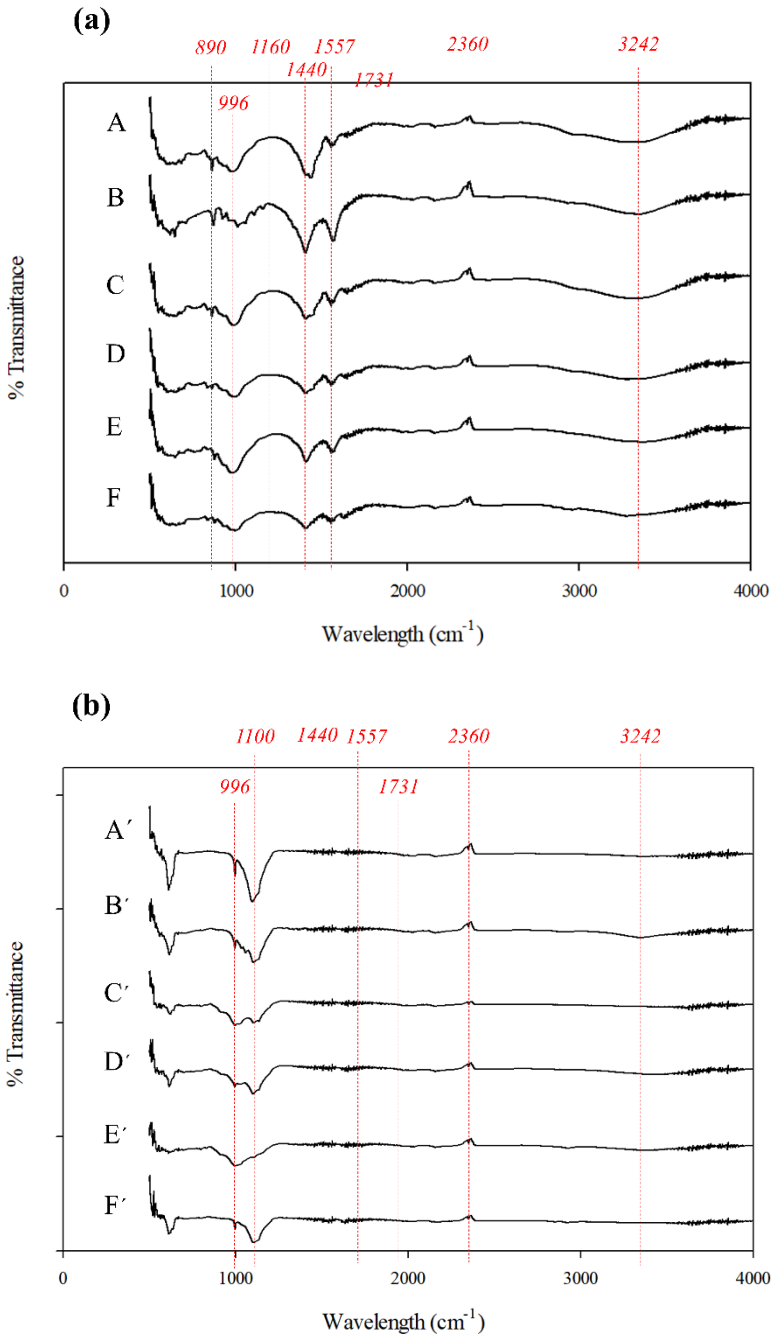

Figure 3.2. FTIR spectra of extracted cellulose, (a) and cellulose nanocrystals, (b). (A)-(F) in each graph indicated, kombu, (A); sargassum, (B); dulse, (C); nori, (D); sea lettuce, (E); and spirulina, (F).

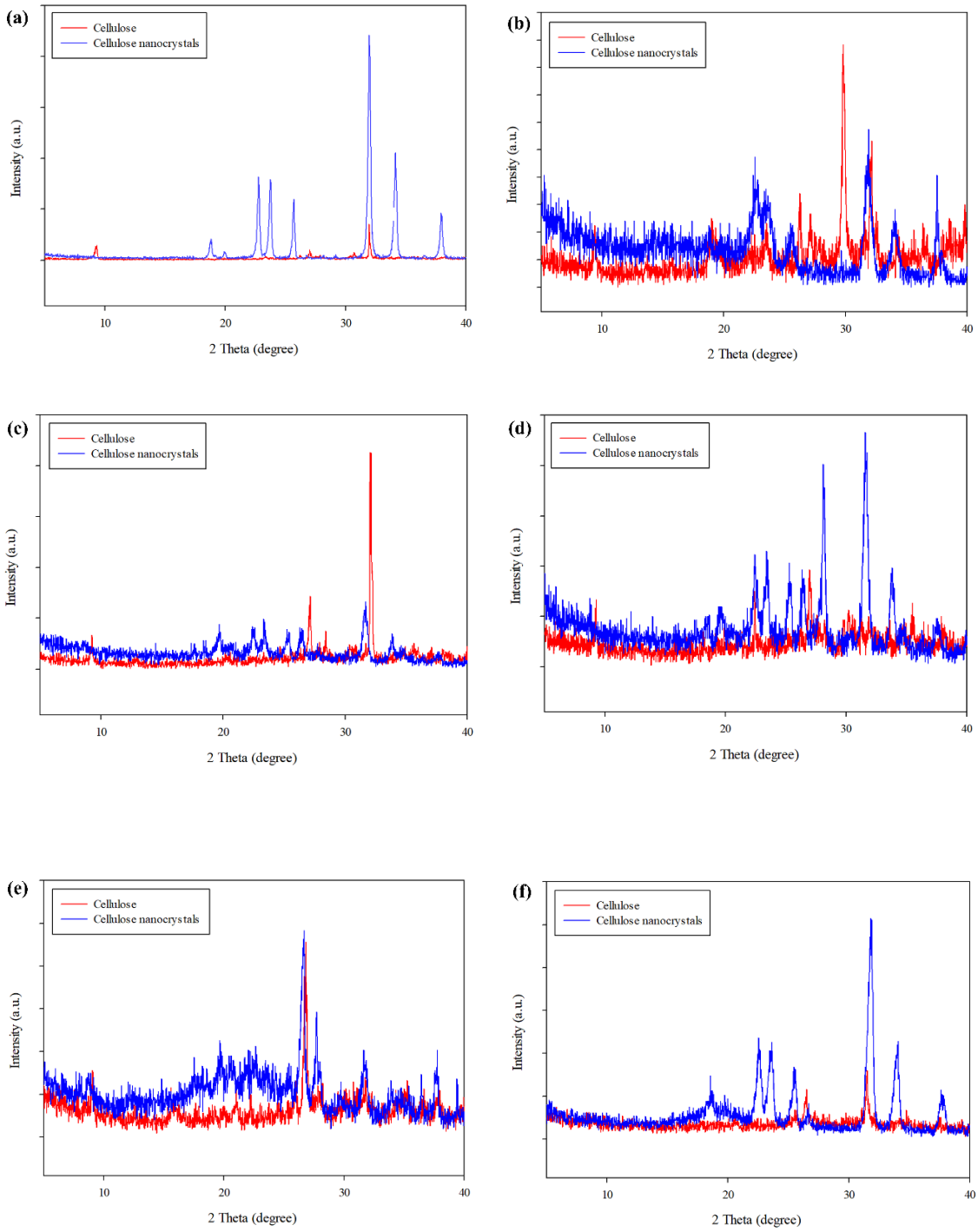

Figure 3.3. X-ray diffraction patterns of kombu extracted cellulose and CNCs, (a); sargassum extracted cellulose and CNCs, (b); dulse extracted cellulose and CNCs, (c); nori extracted cellulose and CNCs, (d); sea lettuce extracted cellulose and CNCs, (e); and spirulina extracted cellulose and CNCs, (f).

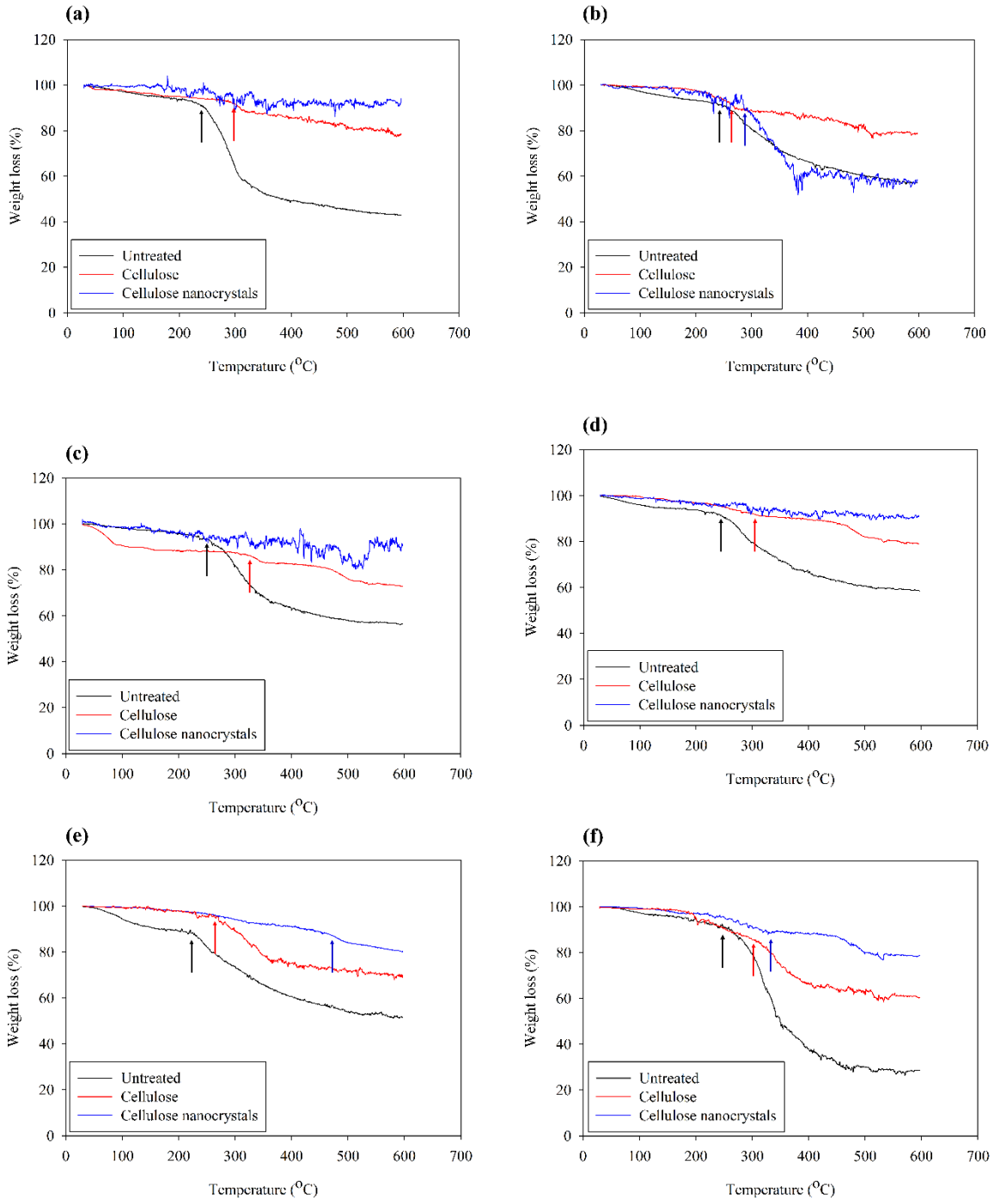

Figure 3.4. Thermogravimetric analysis of untreated, extracted cellulose, and CNCs: kombu, (a); sargassum, (b); dulse, (c); nori, (d); sea lettuce, (e); and spirulina, (f).

CHAPTER FOUR

Development of alginate nanocomposite film reinforced with cellulose nanocrystals isolated from *Sargassum fluitans*

Abstract

Alginate nanocomposite (Alg/CNCs) films reinforced with cellulose nanocrystals (CNCs) isolated from *Sargassum fluitans*. *Sargassum* spp. have been treated as waste in the North Atlantic Ocean. CNCs were isolated by acid hydrolysis and mechanical treatment and used as reinforcing agents to obtain Alg/CNCs film by addition at different concentrations (1%, 3%, 5%, and 10%). Morphological, mechanical, and barrier properties of the bio-nanocomposites were analyzed. CNCs layers can be observed in the alginate polymer matrix by scanning electron microscopy (SEM) observation and addition of 1%, 3%, and 5% (w/w) CNCs enhanced the tensile strength of Alg/CNCs film. Water vapor, oxygen permeability, and light transmittance decreased gradually with increasing addition of CNCs. Chemical interaction between CNCs and alginate was analyzed with FTIR. TGA and DSC data suggested the addition of CNCs can improve the thermal properties of Alg/CNCs films. Therefore, Alg/CNCs films can potentially be used for food packaging systems with enhanced properties.

4.1. Introduction

Sargassum spp. have recently caused both environmental issues and economic losses in the Caribbean and West Africa including the North Atlantic Ocean. The number of inundations of *Sargassum* spp. has led to economic disruption to tourism, aquaculture, and traditional fisheries in the Caribbean and West Africa including the North Atlantic sea. Also, fast-growing of this seaweed species threatens coastal ecosystems by using up oxygen and nutrient overload in the ocean (Milledge & Harvey, 2016). Therefore, environmental organizations have tried to establish removal techniques and guidelines for *Sargassum* spp. (Milledge & Harvey, 2016; Doyle & Franks, 2015). One solution is using *Sargassum* spp. as a commercial product for food. However, there is little evidence that *Sargassum* spp. can be used as food products. Some investigations of *Sargassum* spp. have concluded that they have high contents of arsenic, which precludes using it as a food product (Cao et al., 2014). Another approach has been discovered for using them as a biomaterial. *Sargassum* spp. is categorized as a brown seaweed, which is considered as an alternative and renewable source of producing biomaterials for food packaging material. Brown seaweeds are known for their rich source of biopolymers, such as alginate and fucoidan. Therefore, *Sargassum* spp. can be used as a good source of biopolymers (Blanco-Pascual et al., 2014). Despite their great potential as a biomaterial, *Sargassum* spp. has still been considered as a waste in this region.

With increasing interests in nanotechnology, cellulose nanocrystals (CNCs) have typically been isolated from land plants, such as wood and pulp, with mechanical and chemical treatments (Habibi et al., 2010; Rosa et al., 2010). These isolated CNCs have been applied to biopolymer films because they can be used as a reinforcing agent since CNCs have some advantages including remarkable mechanical properties, such as a high specific strength and elastic modulus, biocompatibility, renewable properties, high aspect ratio and crystallinity,

ease of chemical and mechanical modification, and cost-effectiveness (Sung et al., 2017). These isolated CNCs have been applied to biopolymer films because they can be used as a reinforcing agent. Therefore, recent studies focused on developing biopolymer nanocomposite film by using CNCs for overcoming obstacles, such as poor mechanical properties of biopolymer film, found in food packaging (Chaichi et al., 2017; Sung et al., 2017; Wang et al., 2017). CNCs from various sources include coffee silver skin, sugarcane bagasse, rice straw, coconut husk, banana peel, and grape skin have been incorporated for developing new biopolymer nanocomposites with improved physical and mechanical characteristics (Abdollahi et al., 2013b; George, J. 2012; Huq et al., 2012; Sung et al., 2017; Zhou et al., 2013). Recently, seaweeds have been recognized as a new source of CNCs and they have been isolated from various seaweeds successfully (Doh et al., 2020). Compared to traditional sources of CNCs, CNCs from seaweeds have some advantages: (i) easy to remove natural barriers; (ii) relatively higher yield of stored carbohydrates; (iii) rapid growth for harvesting in shorter periods of time compared to other sources (Chen et al., 2016). In addition, these CNCs also offer many advantages compared to inorganic reinforcement agents because they have relatively easy process-ability, high filling contents, and cost-effectiveness (Abdollahi et al., 2013b). Among the *Sargassum* spp., *Sargassum fluitans* was selected as a CNCs source because it is a major species in the North Atlantic Ocean (Milledge & Harvey, 2016).

Alginate has been investigated for numerous years and used in the food and pharmaceutical industry because of its eco-friendly and cost-effective characteristics. Also, there has been a major focus for manufacturing biopolymer-based packaging systems using alginate (Benavides et al., 2012; Pranoto et al., 2005). However, these biopolymer films have some issues including mechanical, barrier, and thermal properties compared to petroleum-based packaging film (Chaichi et al., 2017; Sirviö et al., 2014; Wang et al., 2017). Since CNCs can increase these properties by acting as a filler in a polymer nanocomposite matrix, these

poor properties can be improved (Habibi et al., 2010; Huq et al., 2012; Sung et al., 2017). Even though there have been many studies that focused on developing biopolymer-nanocomposite films, alginate films enhanced by CNCs isolated from *Sargassum fluitans* has not yet been attempted.

Thus, the objectives of this study were (1) to isolate and characterize CNCs successfully from *Sargassum fluitans*, (2) to produce alginate nanocomposite (Alg/CNCs) films reinforced with CNCs from *Sargassum fluitans* and, (3) to investigate physicochemical, barrier, and thermodynamic properties of Alg/CNCs films which can be potentially applied in food packaging systems.

4.2. Materials and methods

4.2.1. Materials

Sodium alginate (alginic acid sodium salt from brown algae, Mannurocid acid (M) : Guluronic acid (G) = 1:3) was supplied by VWR international, LLC (Atlanta, GA, USA). Calcium chloride used as a crosslinking agent for sodium alginate and glycerol for plasticizer were purchased by Fisher Scientific Company L.L.C, (Hampton, NH, USA).

4.2.2. Seaweeds collection and preparation

Sargassum fluitans from the North Atlantic shore was obtained from Carolina Biological Supply Company (Burlington, NC, USA). Samples were washed with running tap water several times and dried. Dried seaweed was pulverized with a commercial blender for homogenization and stored in a drying oven at 35˚C.

4.2.3. Isolation of cellulose nanocrystals from Sargassum fluitans

CNCs were isolated following a previous report by Doh et al. (Doh et al., 2020). *Sargassum fluitans* powders were immersed in 0.2 M hydrochloric acid in a 1:10 (w/v) proportion with stirring for 2 h at 30˚C. After washing with distilled water until an achieved pH 7.0, washed colloids were soaked in a 1:60 proportion (w/v) with distilled water and adjusted to pH 10.5 with 4% sodium hydroxide. The suspension was then subjected to continuous stirring for 3 h at 75˚C. After stirring, suspensions were centrifuged with 15,000 *g* for 10 min and the supernatant was discarded and precipitates were dried for 3 days at 65˚C in a drying oven. Dried residues were stirred with 5% potassium hydroxide for 3 h, and the residues were washed with distilled water and treated with excess amounts of 6 – 10% (w/v) sodium hypochlorite. After the pH was adjusted to 5.0 by glacial acetic acid, samples were stirred for 2 h with magnetic stirring at 75˚C. 30% active hydrogen peroxide was used for another bleaching at 80˚C for 70 min. Cellulose could be obtained after removing the supernatant. With the obtained cellulose, acid hydrolysis was performed at 45˚C for 30 min with 51% sulfuric acid under constant stirring for removing amorphous regions. Then, the suspension was diluted with ice water to stop the reaction and the sample was centrifuged to remove excess sulfuric acid. After washing with distilled water until achieving a pH around 7.0, the suspensions were homogenized with an ultrasonicator for 15 min. These CNCs suspensions were freeze-dried to obtain a powdered form of CNCs.

4.2.4. Film preparation

Sodium alginate (3%, w/v) was dissolved in distilled water. Glycerol was added at 30% (w/w, based on the sodium alginate) as a plasticizer. 1, 3, 5, and 10% (w/w, based on the solid material) of CNCs from *sargassum fluitans* were added and homogenized with an ultrasonicator for 10 min at 25% amplitude. Films were then cast by pouring into Petri dishes with 90 mm inner diameter and oven dried at 35˚C. Then, the films were detached from the

Petri dishes and soaked in 1% calcium chloride solution for 30 min for crosslinking. Films were washed several times with distilled water to remove the excess calcium chloride present on the surface of the films. These films were dried at 35˚C with a 3 – 5 N on the film to prevent critical shrinkage of the films. Alginate films without CNCs were used as control.

4.2.5. Characterization of cellulose nanocrystals

4.2.5.1. Size distribution, zeta potential, and polydispersity index

Particle size distribution, zeta potential, and polydispersity index (PdI) were measured by a Malvern Zetasizer Nano-Z (Malvern Instruments, Worcestershire, UK). Measurement parameters were set as follows: refractive index, 1.470; absorption, 0.100; dispersant (distilled water) refractive index, 1.330.

4.2.5.2. Morphology of CNCs

To analyze the morphological properties of the CNCs, 0.005% (w/v) of CNCs suspension was prepared and a drop of the suspension was deposited on a carbon-coated copper grid. After drying, the grids were observed using a transmission electron microscope (TEM, Titan 80–300; FEI, Hillsboro, OR, USA), operating at an accelerating voltage of 120 kV. Image J software was used for analyzing the CNC particles with 50 measurements (National Institute of Health, Bethesda, MD, USA).

4.2.5.3. Fourier transform infrared spectrometry (FTIR) analysis

The FTIR spectra of CNCs particles were recorded in the infrared range of 4000 – 600 cm^{-1} using an FTIR spectrometer (Nicolet iS10, Thermo Fisher Scientific, USA). The spectra were collected in 128 scans at a resolution of 4 cm^{-1}.

4.2.5.4. X-ray diffraction (XRD)

Crystallinity was determined by X-ray diffraction with an X-ray diffractometer (Rigaku Ultima IV, Tokyo, Japan) at a scanning rate of 5˚/min from 5˚ to 45˚ with Cu K_α radiation (λ = 1.5418 Å) using a voltage and current of 40 kV and 40 mA, respectively. The crystallinity index of the sample was calculated by the Segal method (Segal et al., 1959) using the following equation:

$$\text{Crystallinity index (\%)} = \frac{I_{200} - I_{am}}{I_{200}} \times 100 \qquad \text{(Eq. 4)}$$

where, I_{200} is the maximum intensity at the plane and I_{am} is the minimum intensity at the valley between planes.

4.2.6. Characterization of alginate-CNCs nanocomposite film

4.2.6.1. Morphology

The morphological properties of the Alg/CNCs films were evaluated with their cross-section and surface by using an emission scanning electron microscope S4800 (SEM; Hitach High Technologies America, Inc., USA) operated with a voltage of 5.0 kV. The samples were coated with a platinum layer under a vacuum for 60 sec.

4.2.6.2. Viscosity, thickness, and moisture content

The viscosity of the film-forming solution was estimated by a Paar Physica MCR 302 stress-controlled rheometer (Anton Paar, Graz, Austria). The thickness of every film was determined using a device with 0.001 mm accuracy. Measurements were performed at five different locations with five repetitions per film. Moisture content of the films was estimated by HR73-P Halogen Moisture Analyzer (Muttler Toledo, Ohio, USA).

4.2.6.3. Water absorption and solubility

The water absorption and water solubility of the films was determined gravimetrically. 20 mm × 20 mm of film samples were held in a drying oven at 95˚C for a day to obtain a constant weight. Then, each film sample was immersed in 30 mL of distilled water and stored in 25˚C for 24 hr. The film samples were weighed after removing the water on the surface with a filter paper. Subsequently, the residual film samples were dried to a constant weight at 80˚C. The water absorption and water solubility of the films are calculated as follows:

$$\text{Water absorption (\%)} = \frac{W_2 - W_1}{W_1} \times 100 \qquad \text{(Eq. 5)}$$

$$\text{Water solubility (\%)} = \frac{W_1 - W_3}{W_1} \times 100 \qquad \text{(Eq. 6)}$$

where, W_1 and W_2 are the weights of the film sample before and after immersion, respectively. W_3 is the weight of the final dried film sample. Five repetitions were performed for each film sample.

4.2.6.4. Water vapor permeability (WVP) and oxygen permeability (OP)

To determine water vapor permeability (WVP), water vapor transmission rate (WVTR) was determined with a Mocon Permatran 3/33 Model G (Mocon Inc., Minneapolis, MN, USA) in accordance with ASTM F1249-13. The tests were conducted at 23˚C and 90% RH condition. WVP was estimated according to the following equation:

$$WVP = \frac{WVTR \times l}{\Delta p} \qquad \text{(Eq. 7)}$$

where l corresponds to film thickness and Δp is the partial pressure difference across the films.

Oxygen permeability (OP) was calculated from oxygen transmission rate (OTR) obtained using an oxygen permeation analyzer (OX-TRAN Model 2/21; Mocon Inc., Minneapolis, MN, USA) according to ASTM D3985-17 at 23˚C and 100% RH. The OP was calculated by following equation:

$$OP = \frac{OTR \times l}{\Delta p} \qquad \text{(Eq. 8)}$$

where l is the thickness of the film, and Δp is the difference between oxygen partial pressure across the film ($\Delta p = p_1 - p_2$, where p_1 is the oxygen partial pressure at 23˚C, p_2 is equal to zero on the detector side).

4.2.6.5. Mechanical properties

Tensile strength (TS) and elongation at break (EB) were investigated using a universal testing machine (5900 Series, Instron Engineering Co, USA) according to ASTM D882-02. Each sample was prepared with the dimensions of 10 × 70 mm and placed between grip heads of the testing machine. The initial grip separation was set at 10 mm and cross head speed was 50 mm/min. EB were estimated as the maximum extension of the film before its breaking. Five specimens were tested for each sample.

4.2.6.6. Color and light transmittance

The color of the film samples was determined using a HunterLab MiniScan EZ (Hunter Associate Laboratory, Inc., Virginia, USA). L (lightness), a (redness), and b (yellowness) of the films were measured. Measurements were carried out on a white standard plate (L^* = 93.54, a^* = -0.71, and b^* = 3.36) were used as a background. The measurements were performed five times for each sample. The total color difference (ΔE) and whiteness index (WI) are calculated as follow:

$$\Delta E = \sqrt{(L^* - L)^2 + (a^* - a)^2 + (b^* - b)^2} \qquad \text{(Eq. 9)}$$

$$\text{WI} = 100 - \sqrt{(100 - L)^2 + a^2 + b^2} \qquad \text{(Eq. 10)}$$

where, L, a, and b are the color parameter values of the film sample.

The light transparency of the films was determined by Genesys 10S UV-VIS Spectrophotometer (Thermo Fisher Scientific, Waltham, WA, USA) at selected wavelengths of 190, 300, 360, and 600 nm. After specimen (30 mm × 10 mm) were placed on a quartz cell, absorbance was determined. The absorbance value was used to calculate the percentages of light transmission.

4.2.6.7. Thermal properties analysis

Thermal properties of the films were measured using a thermo gravimetric analysis (TGA) and differential scanning calorimeter (DSC; TA Instruments Inc., New Castle, USA). TGA experiments were performed under nitrogen atmosphere. The weight of samples ranged 3 – 5 mg were placed on an aluminum pan. Scanning range was from 30 to 600˚C and heating rate was 10˚C/min. In the case of DSC, about 5 mg of samples were sealed in an aluminum pan and aluminum lid under nitrogen atmosphere. Samples were first heated from 30˚C to 250˚C at a heating rate of 10˚C/min and held for 5 min and then cooled down to 25˚C at the same rate. Second heating was performed under the same conditions. The glass transition temperature (T_g), melting temperature (T_m), decomposition temperature (T_d), and the enthalpy of melting (ΔH_m) of the samples were obtained from the DSC thermograms.

4.2.7. Statistical analysis

All data are presented as mean ± standard deviation. The data were analyzed using the analysis of variance (ANOVA) method. The ANOVA statistical analyses with Duncan's multiple comparison tests at a significance level of $p \leq 0.05$ were applied to the results using the Statistical Package for the Social Sciences software (SPSS, Version 20.0, SPSS Inc., Chicago, IL, USA).

4.3. Results and discussion

4.3.1. Characterization of CNCs

Cellulose nanocrystals (CNCs) were successfully isolated from *Sargassum fluitans*. Most amorphous regions of cellulose were removed by acid hydrolysis with sulfuric acid and mechanical treatment with the ultrasonicator. The crystalline parts remained due to their resistance to acid hydrolysis and mechanical force (Habibi et al., 2010; Sung et al., 2017). The CNCs were isolated with a total yield of about 42.7% when produced from fully dried cellulose. CNCs suspensions (0.005%) were analyzed with a zetasizer for determining particle size distribution, zeta potential, and PdI of the CNCs (Table 4.1). The length of CNCs was found to be 43.06 ± 8.94 nm and this result agreed with the TEM image shown in Fig. 4.2 (a). In addition, the TEM image showed that CNCs were short, rod shapes with some aggregates. According to the previous studies about isolated CNCs from the brown seaweed (kelp, *Laminaria japonica*), the length of CNCs varied 239 – 1300 nm, which was much smaller than suggested (Doh et al., 2020; Feng et al., 2015; Liu et al., 2017). This indicates that morphological traits can be affected by CNCs source. It is important because a higher aspect ratio is usually considered as having more reinforcement potential (Miao & Hamad, 2013). The zeta potential of CNCs was -37.4 ± 14.5 mV, which indicated that nanoparticles are stable in the suspension (Table 4.1). CNCs suspensions had a high standard deviation possibly due to agglomeration of CNCs. The result of PdI was 0.18 ± 0.01 and it indicated a stable status.

The results of FTIR spectra with *Sargassum fluitans*, cellulose, and CNCs are shown in Fig. 4.2 (b). In the range of 3000 – 3600 cm^{-1}, a hydroxyl group (O-H stretching vibration) was shown with a broad band in all cases. The peak turned weaker because the hydroxyl group of *Sargassum fluitans* reacted in the process and amorphous regions were removed during the extraction process. In the range of 2852 – 2923 cm^{-1}, C-H stretching vibration was also shown

in *Sargassum fluitans* but the peak was not on the cellulose and CNCs (Liu et al., 2017). It is likely when acid hydrolysis was carried out, hydrogen ions detached from carbon. FTIR spectra also demonstrated that the vibrations between 919 cm^{-1} and 1031 cm^{-1} (guaiacyl ring with C=O stretching) and the peak intensity of CNCs and cellulose was lower than that of *Sargassum fluitans*. This indicates that the amorphous regions around cellulose were mostly removed (Feng et al., 2015). Also, the peak of 1408 cm^{-1} was weakened from *Sargassum fluitans* to CNCs. This peak assigns the C=C stretching of aromatic hydrocarbons of lignin. Weakened peaks in the CNCs compared to the peaks in the *Sargassum fluitans* and cellulose indicated that content of lignin decreased. In addition, this band can also describe -CH_2 scissoring vibration in cellulose and disappeared due to acid hydrolysis (Kumar et al., 2014). In the range of 1568 cm^{-1} and 1632 cm^{-1}, bands were shifted or weakened from *Sargassum fluitans* to the CNCs (Łojewska et al., 2005). This indicated the hemiacetal bonds generated aldehyde groups (-CHO) by opening the terminal rings from bleaching and acid hydrolysis.

The XRD patterns of cellulose and CNCs from *Sargassum fluitans* are shown in Fig. 4.2 (c). The diffraction pattern of the CNCs was similar with previous studies (Feng et al., 2015; Liu et al., 2017; Sung et al., 2017). The main peaks were represented at $2\theta = 14.8^{\circ}$, 16.1°, 22.5°, and 34.5° and these peaks were well matched with cellulose type I. The spectra of the CNCs indicated higher crystallinity than extracted cellulose. The crystallinity index of cellulose and the CNCs were calculated to be 58.7% and 81.3%, respectively. It can be observed that the degree of crystallinity of CNCs increased 22.6% from extracted cellulose. With results of FTIR and XRD analysis, it was proven that the CNCs isolation process could remove amorphous regions effectively.

4.3.2. Characterization of alginate nanocomposite film

4.3.2.1. Morphological analysis of alginate nanocomposite films

Scanning electron microscopy (SEM) was used for morphological observation of cross-section and surface of Alg/CNCs film (Fig. 4.3). Fig. 4.3 (A) – (E) indicated the cross-section of the films and Fig. 4.3 (a) – (e) suggested the surface of the films. Compared with the control film (Fig. 4.3 (A)), Alg/CNCs films (Fig. 4.3 (B) – (E)) showed small particles with layered structure, indicating a filamentous aspect of the CNCs. The improved mechanical or barrier properties of Alg/CNCs film could be attributed to these structures (Huq et al., 2012). In addition, agglomeration of CNCs is observed (Fig. 4.3 (E)). It is likely that as CNCs concentration increased, they were not dispersed efficiently in suspension. Amiralian et al. (2015) also reported that using the ultrasonicator during the process could lead to inefficient dispersion of CNCs. In the case of film surfaces, the small wrinkles were observed on the surface of the all films due to the crosslinking (Fig. 4.3 (a) – (e)). Moreover, agglomeration of CNCs can be found which matched with cross-sectional observations. Similar results also have been observed in previous reports (Huq et al., 2012; Sung et al., 2017).

4.3.2.2. Analysis of chemical structures of alginate nanocomposite films

FTIR analysis was used to characterize the incorporation of CNCs into the Alg/CNCs film matrix. Fig. 4 (a) represent the spectra of components of Alg/CNCs film and Fig. 4 (b) shows Alg/CNCs films. Peaks are mainly shown at 3200 – 3600 cm^{-1}, which indicate mainly O-H stretching vibration. Some differences were observed in this broad band after adding crosslinking agent ($CaCl_2$) into the alginate matrix (Fig. 4. (a)). Other broad bands between 1025 and 1650 cm^{-1} changed their intensity. Crosslinking of alginate film changed their chemical structure mainly at 1025 cm^{-1}, 1416 cm^{-1}, and 1650 cm^{-1}, which is assigned to C-O, O-H, and ring structures (C=C), respectively. In addition, external deformational vibrations of C-H, C-OH, C-CO, and C-CH groups were also included in these regions. Previous studies also reported a decrease in the intensity of these regions (El miri et al., 2018; Wang et al.,

2017). As seen in Fig. 4 (b), adding more CNCs does not mean significant chemical structure changing. However, FTIR spectra of Alg/CNCs film provided the information about the effect of CNCs concentration on the position with width and intensity of peaks related to alginate-CNCs interactions. Although many bands from the alginate masked typical vibrations of CNCs, the fingerprint region (919 – 1632 cm^{-1}) indicated the bands were related to the degree of order of cellulosic materials.

4.3.2.2. Physical and mechanical properties of alginate nanocomposite films

Table 4.2 represents the physical and mechanical properties of Alg/CNCs films. Viscosity of film forming solutions decreased significantly as concentration of CNCs increased due to the expansion of alginate chains in film forming solutions. This expansion was caused by non-ionic properties of CNCs and previous report supports this explanation (Xiao et al., 2012). Average thickness of films was around 0.07 mm and there were no significant differences among films. Moisture content was slightly increased with CNCs addition, statistically. Abdollahi et al. (2013a) reported a similar moisture content with 3 – 4% of alginate film reinforced with CNCs.

Water absorption of films was in the range of around 40 – 60% and there were no significant differences. Alg/CNCs film surfaces turned hazy after immersion in water. This is because the alginate matrix captured water molecules in their matrix and this phenomenon lead to a high swelling capacity of Alg/CNCs film (Deepa et al., 2016). Besides, water solubility result indicates all Alg/CNCs films could hardly dissolve in water. Different from the result of this study, previous studies reported alginate-based film showed higher water solubility resulted to 5 – 40% (Deepa et al., 2016; El Miri et al., 2018; Wang et al., 2017). Water vapor permeability (WVP) and oxygen permeability (OP) were significantly decreased ($p < 0.05$) with addition of CNCs. WVP was decreased by 41.6%, 46.0%, 50.8%, and 45.1% with addition

of 1%, 3%, 5%, and 10% CNCs, respectively. As reported in previous studies, the incorporation of CNCs into the polymer matrix enhanced the complex path that water molecules must pass through the film, leading to a lower permeability (Abdollahi et al., 2013a; Deepa et al., 2016; Wang et al., 2017). Similarly, reduction of OP by 38.6%, 85.4%, 86.1%, and 93.3% were observed for the films with addition of 1%, 3%, 5%, and 10% CNCs, respectively.

The mechanical properties were determined with tensile strength (TS), elongation at break (EB), and Young's modulus and results are also shown in the Table 4.2. By adding 1% CNCs, TS was increased of 13.7% compared to the control film. Incorporation of 3 and 5% of CNCs raised the TS of Alg/CNCs films by 21.7% and 35.5%, respectively. However, when adding 10% CNCs, TS increased only 17.7% which was lower than with 3, 5% Alg/CNCs films. This can be attributed to the agglomeration of CNCs in the film-forming solution due to Van der Waals forces (Sung et al., 2017). The EB did not show big differences, statistically. Generally, EB decreased as TS increased in polymer films. However, it showed a different tendency. This is due to the physical effect of shrinkage when Alg/CNCs film crosslinked with calcium chloride rather than a chemical effect. Also, Young's modulus did not present significant differences because the tensile strain did not show consistency due to the brittleness of the alginate film. In this study, it can be described that agglomerations of CNCs indicated in the SEM result can lead to a decrease of tensile strength for alginate nanocomposite films. However, elongation and Young's modulus is hard to analyze the tendency due to its brittleness.

4.3.2.3. Optical and color properties of alginate nanocomposite films

The transmittance of UV light is one of the important factors for food packaging systems because foods can be degraded by oxidation, nutrient loss, and discoloration due to UV light. UV-A light in the wavelength range of 315 – 400 nm can damage foods because it is

far less absorbed by ozone in the atmosphere. Table 4.3 shows the light transmittance of the Alg/CNCs films with different wavelengths. As a result, the addition of CNCs into alginate film reduced light transmission for all measured wavelengths. In the range of UV-C light, most of the UV light was blocked. However, as the wavelength of UV increased, transmittance ranged from 45 – 88%. Based on the results, it was evident that light transmittance values would decrease when CNCs concentration increased. This is because Alg/CNCs films show higher haziness with increased addition of CNCs in the polymer matrix.

The color characteristics of the films are given in Table 4.4. The color of the film is also one of the important factors related to the appearance, which could influence consumer acceptance. Since increasing CNCs can affect the transparency of films, the whiteness index (WI) decreased when CNCs concentration increased. This result is in accordance with the light transmittance study. Due to this reason, total color difference (ΔE) of the films was increasing with addition of CNCs in the films. In addition, even though there were several significant differences between redness (a) and yellowness (b) value, it was difficult to visually distinguish.

4.3.2.4. Thermal properties of alginate nanocomposite films

Thermo-gravimetric analysis (TGA) graph of the films is shown in Fig. 4.5 (a). In all cases, a weight loss occurred at 30 – 140˚C, which indicates the evaporation of absorbed water in the polymer matrix. The onset thermal decomposition (T_{on}) occurred in the range of 202 – 208˚C. Thermal degradation was observed in the range of 300 – 380˚C, which indicated degradation of glycosidic bonds in cellulosic parts, decarboxylation, decarbonylation, and hydration of alginate (El Miri et al., 2018; Wang et al., 2017). CNCs could affect the weight loss of Alg/CNCs films. In the case of the control film, the decreasing rate of weight loss was the greatest among the samples and 1%, 3%, and 10% Alg/CNCs films showed a similar weight

loss. However, the least weight loss was observed in 5% Alg/CNCs film. The derivative thermogravimetry (DTG) graph agrees with the TGA graph. It showed the inflection point in which the addition of CNCs renders the graph shifting right; indicating higher thermal stabilities (Fig. 4.5 (b)). These results indicated better thermal stability of Alg/CNCs film.

Differential scanning calorimeter (DSC) analysis was performed and the results are shown in Fig. 4.5 (c), (d) and Table 4.5. The DSC heating cycle showed that all films displayed a similar shape, but the heat flow spectra differed according to the amount of addition of CNCs. Elimination of free water and the glass transition occurred in the region of 50 – 100˚C. According to the study by Sarmento et al., endothermic peaks that showed around 70 °C can be explained with loss of water associated to hydrophilic groups of alginate polymers (Sarmento et al., 2006). Russo et al. described the endotherm related to the elimination of free water, which can cover any signal related to the glass transition (Russo et al., 2007). Melting temperature (T_m), and decomposition temperature (T_d) which can be determined in first heating spectra (Fig. 5. (c)) did not show significant differences. Since melting temperature (T_m), and decomposition temperature (T_d) did not show significant differences. Since T_g, T_m, and T_d have complex phenomenon involving many factors, such as water evaporation, intermolecular interactions, molecular weight, chain flexibility, and crosslinking density, it is hard to find significant differences (Chaichi et al., 2017; Krishnamachari et al., 2009). However, there was a significant difference in the case of melting enthalpy (ΔH_m). ΔH_m showed the highest value with the 5% Alg/CNCs film. It can be attributed to an increase in the degree of crystallinity with CNCs incorporation (Sung et al., 2017).

4.4. Conclusions

Cellulose nanocrystals (CNCs) were successfully isolated from seaweed biomass, *Sargassum fluitans*, and proved its characteristics with zeta sizer, TEM, FTIR, and XRD analysis. Then, alginate nanocomposite films reinforced with CNCs were developed and characterized by physicochemical, mechanical, barrier, and thermal stability analysis. Morphological observations showed the possibilities of structural modifications and improvements of the mechanical, barrier, and thermal properties when CNCs were incorporated in nanocomposite films. Generally, as CNCs concentration increased, mechanical, water vapor, oxygen, and light barrier properties were increased but an agglomeration of CNCs could disturb the reinforcing effect on the mechanical properties of the films at a very high percentage of addition. No water solubility was observed in the films and the films showed around 50% of water absorption by weight. FTIR results indicate that alginate and CNCs mainly formed hydrogen bonding leading to a strength increase as CNCs addition increased. Through TGA and DSC tests, it was proven that adding CNCs could also increase thermal stability. Even though alginate film has been widely investigated for their applications such as food packaging, it presents some disadvantages in mechanical and barrier properties. Therefore, it is meaningful to use waste seaweed biomass (*Sargassum fluitans*) as the reinforcement agent of alginate film for developing alginate nanocomposite. Based on the results, CNCs from *Sargassum fluitans* can be used to overcome some disadvantages of alginate films that limit its applications in various fields, including food packaging and biomedical industry, with improved properties. Therefore, this study suggests that Alg/CNCs films have the potential as a novel biomaterial for packaging systems.

4.5. References

Abdollahi, M., Alboofetileh, M., Behrooz, R., Rezaei, M., & Miraki, R. (2013a). Reducing water sensitivity of alginate bio-nanocomposite film using cellulose nanoparticles. *International journal of biological macromolecules,* 54, 166-173.

Abdollahi, M., Alboofetileh, M., Rezaei, M., & Behrooz, R. (2013b). Comparing physico-mechanical and thermal properties of alginate nanocomposite films reinforced with organic and/or inorganic nanofillers. *Food Hydrocolloids*, 32(2), 416-424.

Amiralian, N., Annamalai, P. K., Memmott, P., & Martin, D. J. (2015). Isolation of cellulose nanofibrils from Triodia pungens via different mechanical methods. *Cellulose,* 22(4), 2483-2498.

ASTM D3985-17. (2017). Standard Test Method for Oxygen Gas Transmission Rate Through Plastic Film and Sheeting Using a Coulometric Sensor.

ASTM D882-02. (2002). Standard Test Method for Tensile Properties of Thin Plastic Sheeting.

ASTM F1249-13. (2013). Standard Test Method for Water Vapor Transmission Rate Through Plastic Film and Sheeting Using a Modulated Infrared Sensor.

Benavides, S., Villalobos-Carvajal, R., & Reyes, J. (2012). Physical, mechanical and antibacterial properties of alginate film: Effect of the crosslinking degree and oregano essential oil concentration. *Journal of Food Engineering,* 110(2), 232-239.

Blanco-Pascual, N., Montero, M., & Gómez-Guillén, M. (2014). Antioxidant film development from unrefined extracts of brown seaweeds Laminaria digitata and Ascophyllum nodosum. *Food hydrocolloids,* 37, 100-110.

Cao, Y., Duan, J., Guo, J., Li, W., & Tao, W. (2014). Pharmacokinetic properties of arsenic species after oral administration of Sargassum pallidum extract in rats using an HPLC-HG-AFS method. *Journal of pharmaceutical and biomedical analysis,* 96, 213-219.

Chaichi, M., Hashemi, M., Badii, F., & Mohammadi, A. (2017). Preparation and characterization of a novel bionanocomposite edible film based on pectin and

crystalline nanocellulose. *Carbohydrate Polymers,* 157, 167-175.

Chen, Y. W., Lee, H. V., Juan, J. C., & Phang, S.-M. (2016). Production of new cellulose nanomaterial from red algae marine biomass Gelidium elegans. *Carbohydrate polymers,* 151, 1210-1219.

Deepa, B., Abraham, E., Pothan, L. A., Cordeiro, N., Faria, M., & Thomas, S. (2016). Biodegradable nanocomposite films based on sodium alginate and cellulose nanofibrils. *Materials,* 9(1), 50.

Doh, H., Lee, M. H., & Whiteside, W. S. (2020). Physicochemical characteristics of cellulose nanocrystals isolated from seaweed biomass. *Food Hydrocolloids*, 102, 105542.

Doyle, E., & Franks, J. (2015). Sargassum fact sheet. Gulf and Caribbean Fisheries Institute.

El Miri, N., Aziz, F., Aboulkas, A., El Bouchti, M., Ben Youcef, H., & El Achaby, M. (2018). Effect of plasticizers on physicochemical properties of cellulose nanocrystals filled alginate bionanocomposite films. *Advances in Polymer Technology,* 37(8), 3171-3185.

Feng, X., Meng, X., Zhao, J., Miao, M., Shi, L., Zhang, S., & Fang, J. (2015). Extraction and preparation of cellulose nanocrystals from dealginate kelp residue: structures and morphological characterization. *Cellulose,* 22(3), 1763-1772.

George, J. (2012). High performance edible nanocomposite films containing bacterial cellulose nanocrystals. *Carbohydrate Polymers*, 87(3), 2031-2037.

Habibi, Y., Lucia, L. A., & Rojas, O. J. (2010). Cellulose nanocrystals: chemistry, self-assembly, and applications. *Chemical reviews,* 110(6), 3479-3500.

Huq, T., Salmieri, S., Khan, A., Khan, R. A., Le Tien, C., Riedl, B., . . . Kamal, M. R. (2012). Nanocrystalline cellulose (NCC) reinforced alginate based biodegradable nanocomposite film. *Carbohydrate Polymers,* 90(4), 1757-1763.

Krishnamachari, P., Zhang, J., Lou, J., Yan, J., & Uitenham, L. (2009). Biodegradable poly (lactic acid)/clay nanocomposites by melt intercalation: a study of morphological,

thermal, and mechanical properties. *International Journal of Polymer Analysis and Characterization,* 14(4), 336-350.

Kumar, A., Negi, Y. S., Choudhary, V., & Bhardwaj, N. K. (2014). Characterization of cellulose nanocrystals produced by acid-hydrolysis from sugarcane bagasse as agro-waste. *Journal of Materials Physics and Chemistry,* 2(1), 1-8.

Liu, Z., Li, X., Xie, W., & Deng, H. (2017). Extraction, isolation and characterization of nanocrystalline cellulose from industrial kelp (Laminaria japonica) waste. *Carbohydrate polymers,* 173, 353-359.

Łojewska, J., Miśkowiec, P., Łojewski, T., & Proniewicz, L. (2005). Cellulose oxidative and hydrolytic degradation: In situ FTIR approach. *Polymer Degradation and Stability,* 88(3), 512-520.

Miao, C., & Hamad, W. Y. (2013). Cellulose reinforced polymer composites and nanocomposites: a critical review. Cellulose, 20(5), 2221-2262.

Milledge, J. J., & Harvey, P. J. (2016). Golden Tides: Problem or golden opportunity? The valorisation of Sargassum from beach inundations. *Journal of Marine Science and Engineering,* 4(3), 60.

Pranoto, Y., Salokhe, V. M., & Rakshit, S. K. (2005). Physical and antibacte rial properties of alginate-based edible film incorporated with garlic oil. *Food research international,* 38(3), 267-272.

Rosa, M., Medeiros, E., Malmonge, J., Gregorski, K., Wood, D., Mattoso, L., . . . Imam, S. (2010). Cellulose nanowhiskers from coconut husk fibers: Effect of preparation conditions on their thermal and morphological behavior. *Carbohydrate polymers,* 81(1), 83-92.

Russo, R., Malinconico, M., & Santagata, G. (2007). Effect of cross-linking with calcium ions on the physical properties of alginate films. Biomacromolecules, 8(10), 3193-3197.

Sarmento, B., Ferreira, D., Veiga, F., & Ribeiro, A. (2006). Characterization of insulin-loaded alginate nanoparticles produced by ionotropic pre-gelation through DSC and FTIR studies. Carbohydrate polymers, 66(1), 1-7.

Segal, L., Creely, J., Martin Jr, A., & Conrad, C. (1959). An empirical method for estimating the degree of crystallinity of native cellulose using the X-ray diffractometer. *Textile Research Journal,* 29(10), 786-794.

Sirviö, J. A., Kolehmainen, A., Liimatainen, H., Niinimäki, J., & Hormi, O. E. (2014). Biocomposite cellulose-alginate films: Promising packaging materials. *Food chemistry,* 151, 343-351.

Sung, S. H., Chang, Y., & Han, J. (2017). Development of polylactic acid nanocomposite films reinforced with cellulose nanocrystals derived from coffee silverskin. *Carbohydrate Polymers,* 169, 495-503.

Wang, L.-F., Shankar, S., & Rhim, J.-W. (2017). Properties of alginate-based films reinforced with cellulose fibers and cellulose nanowhiskers isolated from mulberry pulp. *Food Hydrocolloids,* 63, 201-208.

Xiao, Q., Tong, Q., & Lim, L.-T. (2012). Pullulan-sodium alginate based edible films: Rheological properties of film forming solutions. *Carbohydrate polymers,* 87(2), 1689-1695

Zhou, C., Shi, Q., Guo, W., Terrell, L., Qureshi, A. T., Hayes, D. J., & Wu, Q. (2013). Electrospun bio-nanocomposite scaffolds for bone tissue engineering by cellulose nanocrystals reinforcing maleic anhydride grafted PLA. *ACS applied materials & interfaces*, 5(9), 3847-3

Table 4.1. Particle size distribution, zeta potential, and PdI of the cellulose nanocrystals.

Sample	Size (nm)	Zeta potential (mV)	PdI
CNCs	43.06 ± 8.94	-37.4 ± 14.5	0.18 ± 0.01

(1) Data are mean ± S.D.

Table 4.2. Physical and mechanical properties of the alginate-CNCs nanocomposite films.

wt% CNCs	Viscosity (cP)	Thickness (mm)	Moisture content (%)	Water absorption (%)	Water solubility (%)	Tensile strength (MPa)	Elongation at break (%)	Young's modulus (MPa) $\times 10^{-2}$	WVP (g/m·s·Pa) $\times 10^{-13}$	OP (g/m·s·Pa) $\times 10^{-14}$
0	4354.0 ± 14.94^{a}	0.073 ± 0.008^{a}	1.27 ± 0.35^{a}	57.01 ± 4.62^{a}	-3.01 ± 1.19^{a}	123.8 ± 10.8^{a}	3.4 ± 1.8^{a}	48.29 ± 28.35^{a}	16.15 ± 3.34^{a}	49.92 ± 5.49^{a}
1	4062.65 ± 3.61^{b}	0.075 ± 0.001^{a}	1.91 ± 1.31^{b}	55.16 ± 3.47^{a}	-1.75 ± 1.63^{a}	141.2 ± 4.8^{b}	6.3 ± 1.0^{ab}	23.05 ± 4.64^{a}	9.43 ± 2.26^{b}	30.67 ± 1.13^{b}
3	3692.45 ± 24.40^{c}	0.071 ± 0.006^{a}	2.12 ± 0.27^{b}	48.20 ± 5.96^{a}	-2.53 ± 1.55^{a}	150.8 ± 3.9^{b}	7.9 ± 3.0^{b}	20.86 ± 6.28^{a}	8.72 ± 1.68^{b}	7.27 ± 0.69^{c}
5	2311.95 ± 8.56^{d}	0.073 ± 0.006^{a}	2.11 ± 0.21^{b}	46.88 ± 4.52^{a}	-2.94 ± 2.10^{a}	168.2 ± 19.4^{c}	5.6 ± 1.9^{ab}	33.51 ± 14.51^{a}	7.95 ± 2.01^{b}	6.96 ± 0.14^{d}
10	534.83 ± 22.54^{e}	0.075 ± 0.008^{a}	2.19 ± 0.36^{b}	52.76 ± 6.36^{a}	-0.92 ± 1.79^{a}	146.2 ± 8.7^{b}	5.0 ± 2.7^{ab}	36.12 ± 14.40^{a}	8.86 ± 1.26^{b}	3.36 ± 0.32^{e}

(1) Data are mean ± S.D.

(2) Mean values with different letters within a column are significantly different ($p < 0.05$) by ANOVA with Duncan's multiple comparison test, n=5.

(3) WVP is 'water vapor permeability'; OP is 'oxygen permeability'.

Table 4.3. Light transmittance values of the alginate-CNCs nanocomposite films measured at 190 nm (UV-C), 300 nm (UV-B), 360 nm (UV-A), and 600 nm (visible).

wt% CNCs	%T at 190 nm (UV-C)	%T at 300 nm (UV-B)	%T at 360 nm (UV-A)	%T at 600 nm (visible)
0	0.11 ± 0.01^{a}	67.20 ± 3.20^{a}	75.65 ± 4.46^{ab}	86.79 ± 1.78^{a}
1	0.11 ± 0.01^{a}	63.94 ± 1.81^{ab}	77.08 ± 2.28^{a}	86.78 ± 1.14^{a}
3	0.10 ± 0.01^{a}	60.61 ± 4.32^{bc}	73.46 ± 2.88^{ab}	84.62 ± 1.48^{ab}
5	0.10 ± 0.01^{a}	58.99 ± 3.35^{c}	71.69 ± 2.63^{b}	82.81 ± 1.60^{b}
10	0.07 ± 0.01^{b}	48.59 ± 3.64^{d}	64.96 ± 3.28^{c}	77.03 ± 2.89^{c}

(1) Data are mean ± S.D.

(2) Mean values with different letters within a column are significantly different ($p < 0.05$) by ANOVA with Duncan's multiple comparison test, n=5.

Table 4.4. Color parameters of the alginate-CNCs nanocomposite films.

wt% CNCs	*L*	*a*	*b*	*ΔE*	WI
0	89.17 ± 1.50[a]	-0.97 ± 0.30[a]	6.34 ± 0.46[b]	5.42 ± 0.96[a]	87.37 ± 1.15[a]
1	86.94 ± 0.94[b]	-0.86 ± 0.21[ab]	5.44 ± 0.29[a]	6.93 ± 0.95[ab]	85.85 ± 0.94[b]
3	87.26 ± 0.79[c]	-0.74 ± 0.17[ab]	5.17 ± 0.57[a]	6.56 ± 0.70[c]	86.22 ± 0.67[b]
5	84.73 ± 0.47[c]	-0.70 ± 0.14[ab]	5.06 ± 0.54[a]	8.99 ± 0.47[d]	83.89 ± 0.48[ab]
10	83.06 ± 1.42[d]	-0.63 ± 0.18[b]	5.12 ± 0.19[a]	10.63 ± 1.40[e]	82.29 ± 1.36[b]

(1) Data are mean ± S.D.

(2) Mean values with different letters within a column are significantly different ($p < 0.05$) by ANOVA with Duncan's multiple comparison test, n=5.

(3) *ΔE* is 'total color difference'; WI is 'whiteness index'.

Table 4.5. Thermal properties of the alginate-CNCs nanocomposite films from DSC measurements.

wt% CNCs	T_m (˚C)	T_d (˚C)	ΔH_m (J/g)
0	119.62 ± 1.32[a]	216.20 ± 0.62[a]	256.77 ± 12.41[a]
1	119.79 ± 2.73[a]	215.83 ± 1.03[a]	252.70 ± 8.56[a]
3	121.76 ± 1.81[a]	216.50 ± 1.61[a]	260.63 ± 15.92[a]
5	123.44 ± 0.81[a]	214.97 ± 0.76[a]	312.77 ± 26.27[b]
10	123.14 ± 4.99[a]	216.30 ± 1.11[a]	255.63 ± 15.40[a]

(1) Data are mean ± S.D.

(2) Mean values with different letters within a column are significantly different ($p < 0.05$) by ANOVA with Duncan's multiple comparison test, n=5.

(3) T_g = glass transition temperature; T_m = melting temperature; T_d = decomposition temperature; ΔH_m = the enthalpy of melting.

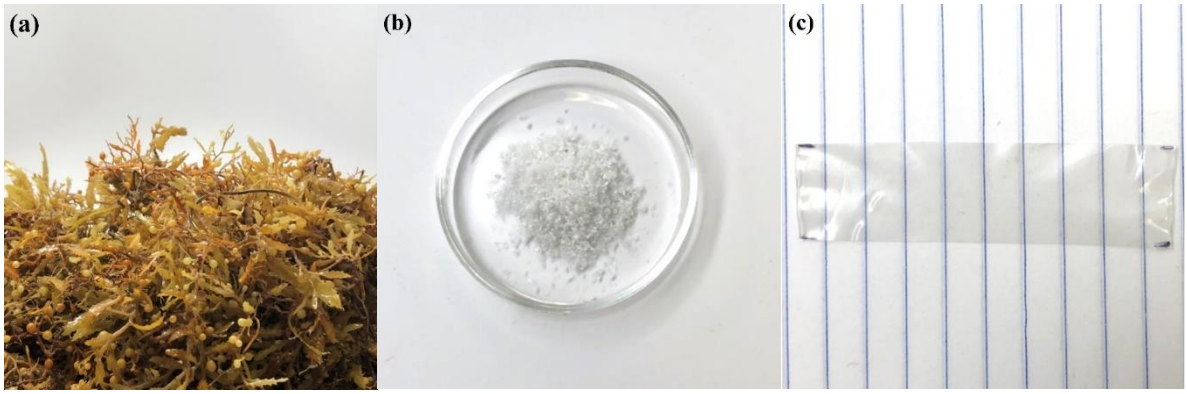

Figure 4.1. Images of the *Sargassum fluitans* (a), cellulose nanocrystals (b), 5% Alg/CNCs film (c).

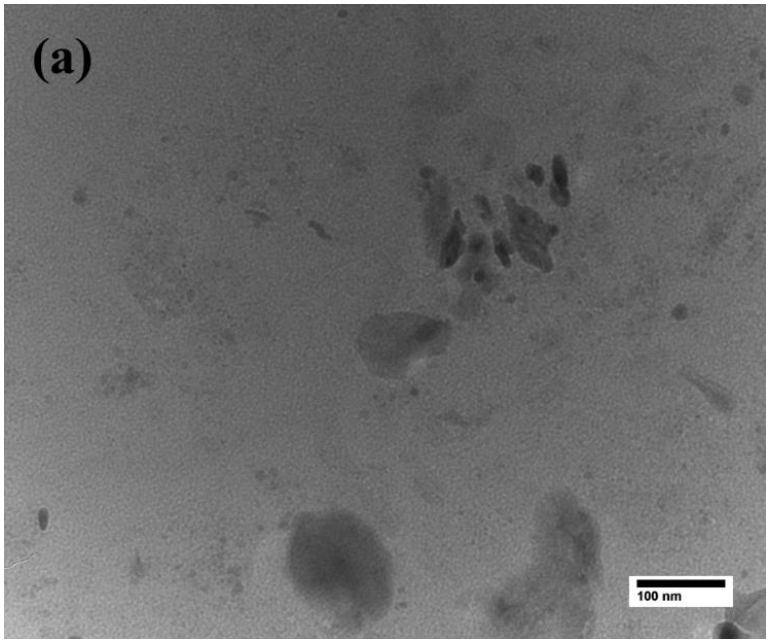
(a)
100 nm

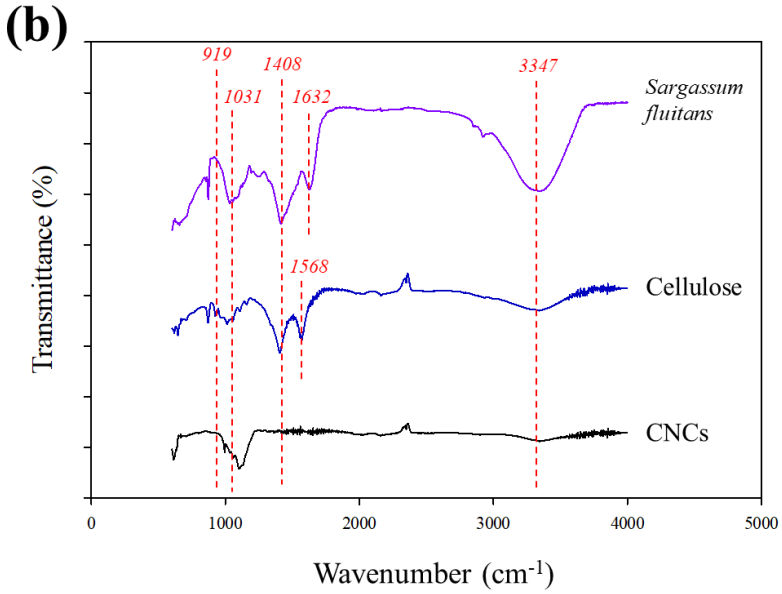
(b)
919
1031
1408
1568
1632
3347
Sargassum fluitans
Cellulose
CNCs
Transmittance (%)
0
1000
2000
3000
4000
5000
Wavenumber (cm-1)

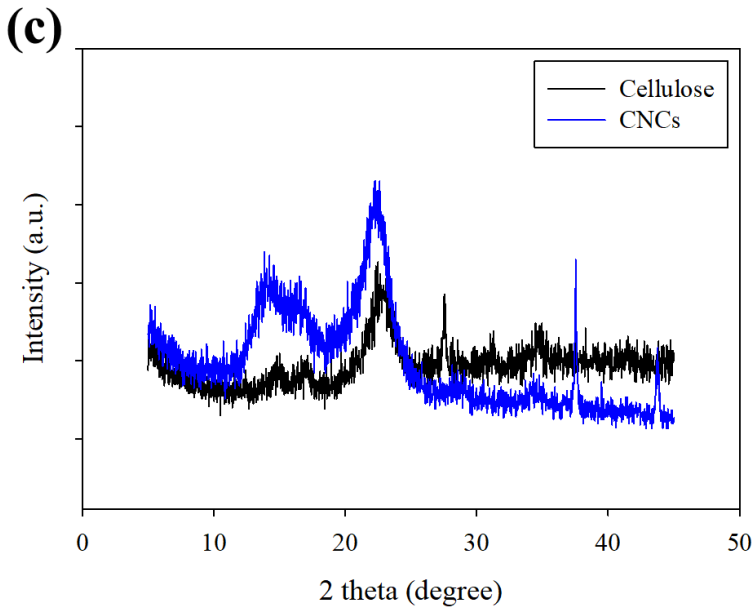

Figure 4.2. TEM image of the CNCs, (a); FTIR spectra of the *Sargassum fluitans*, extracted cellulose, and CNCs, (b); XRD patterns of the extracted cellulose and CNCs, (c).

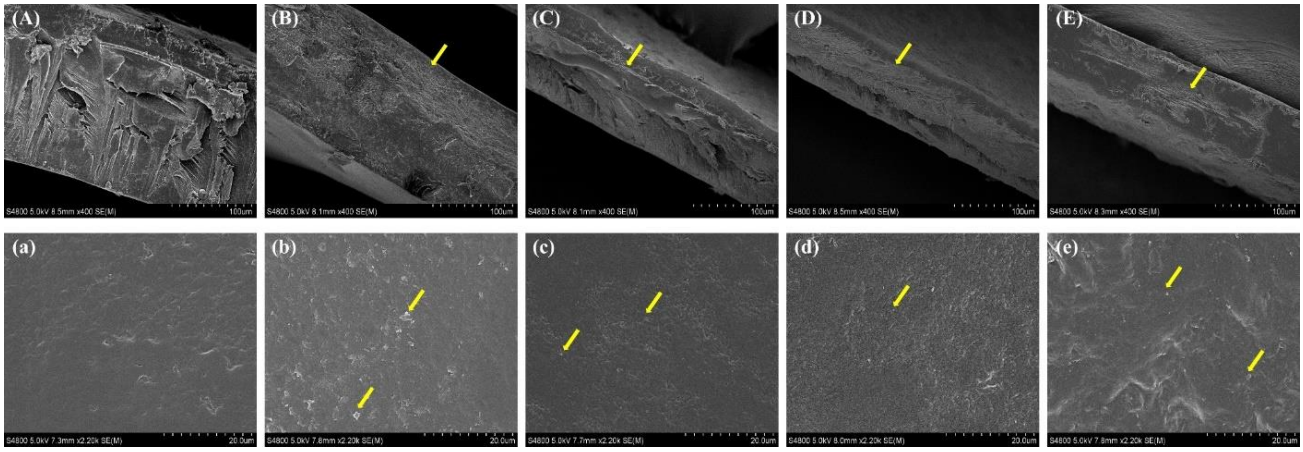

Figure 4.3. SEM images of cross-sections and surface of control film, (A) and (a); 1% Alg/CNCs film, (B) and (b); 3% Alg/CNCs film, (C) and (c); 5% Alg/CNCs film, (D) and (d); 10% Alg/CNCs film, (E) and (e).

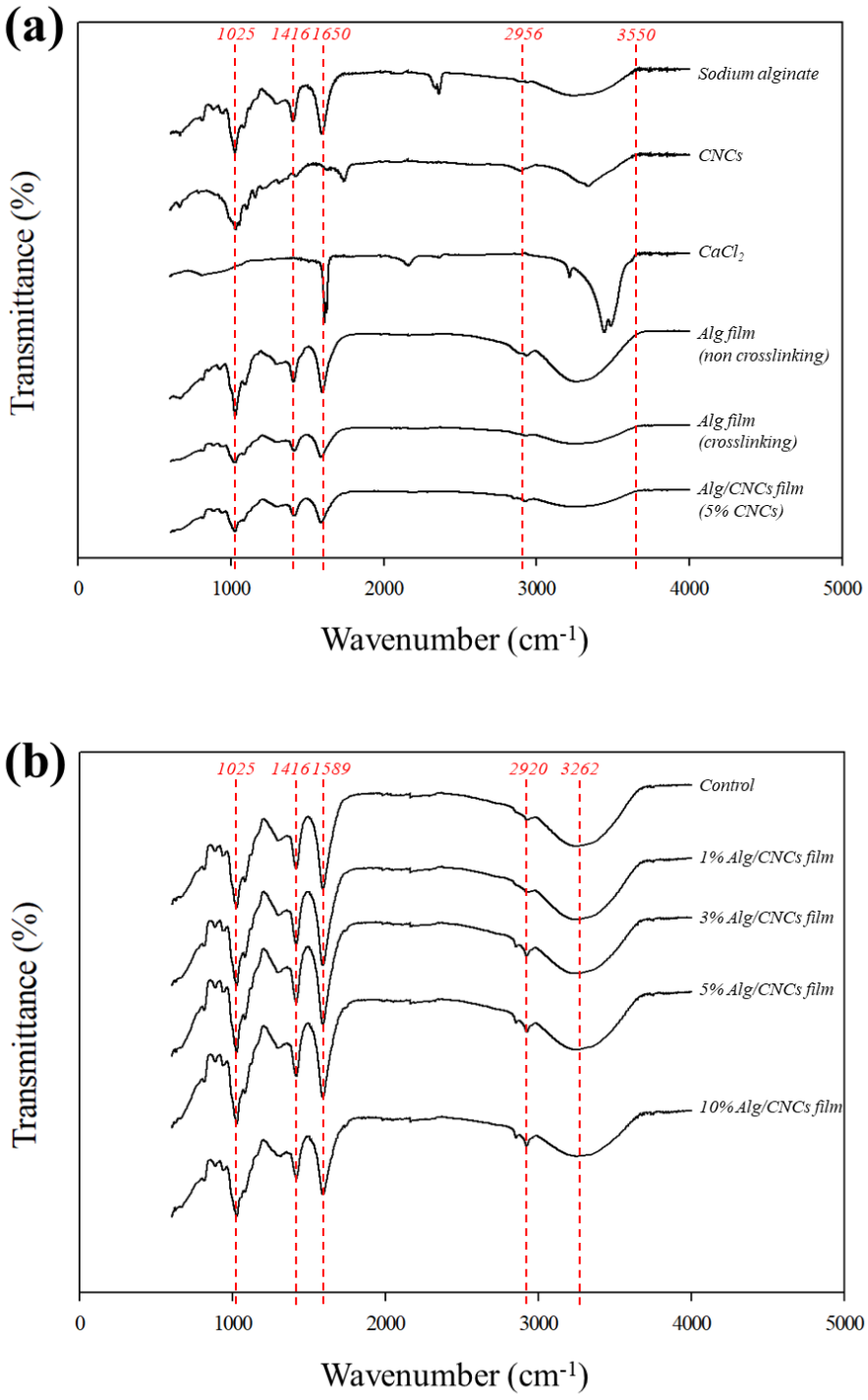

Figure 4.4. FTIR spectra of materials for developing Alg/CNCs film, (a); 0 – 10% Alg/CNCs film, (b).

(a)

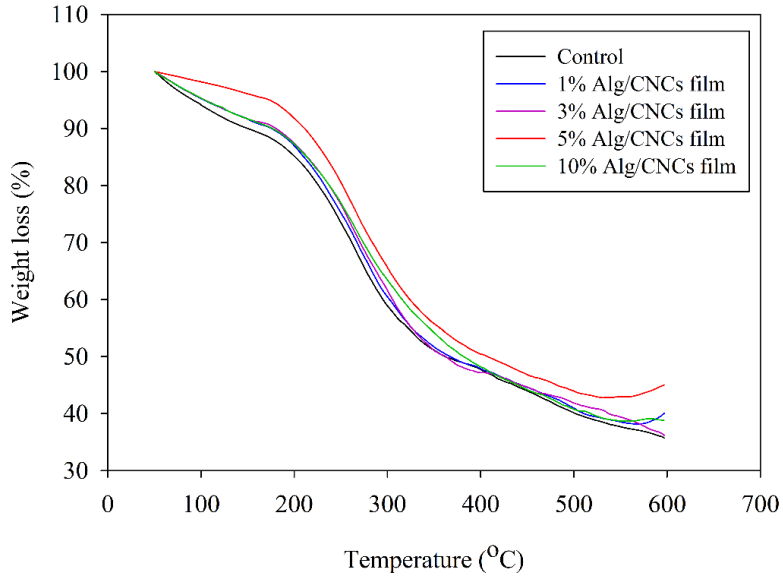
Control
1% Alg/CNCs film
3% Alg/CNCs film
5% Alg/CNCs film
10% Alg/CNCs film
Weight loss (%)
110
100
90
80
70
60
50
40
30
0
100
200
300
400
500
600
700
Temperature (°C)

(b)

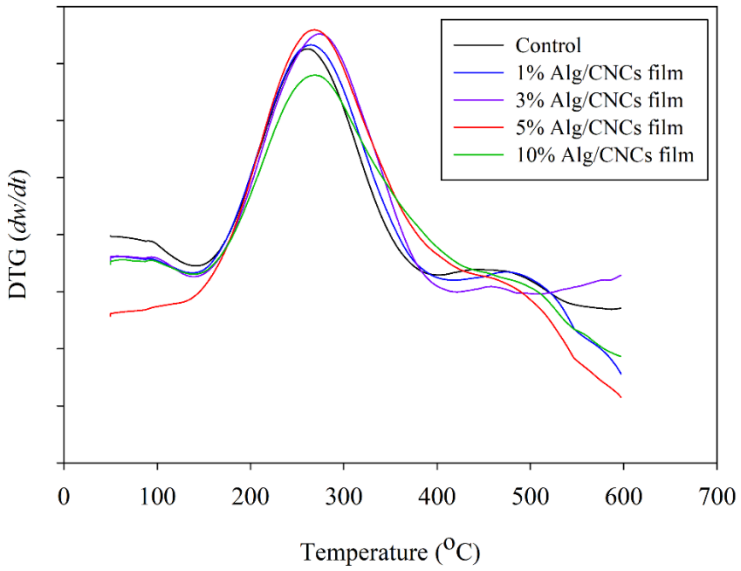
Control
1% Alg/CNCs film
3% Alg/CNCs film
5% Alg/CNCs film
10% Alg/CNCs film
DTG (dw/dt)
0
100
200
300
400
500
600
700
Temperature (°C)

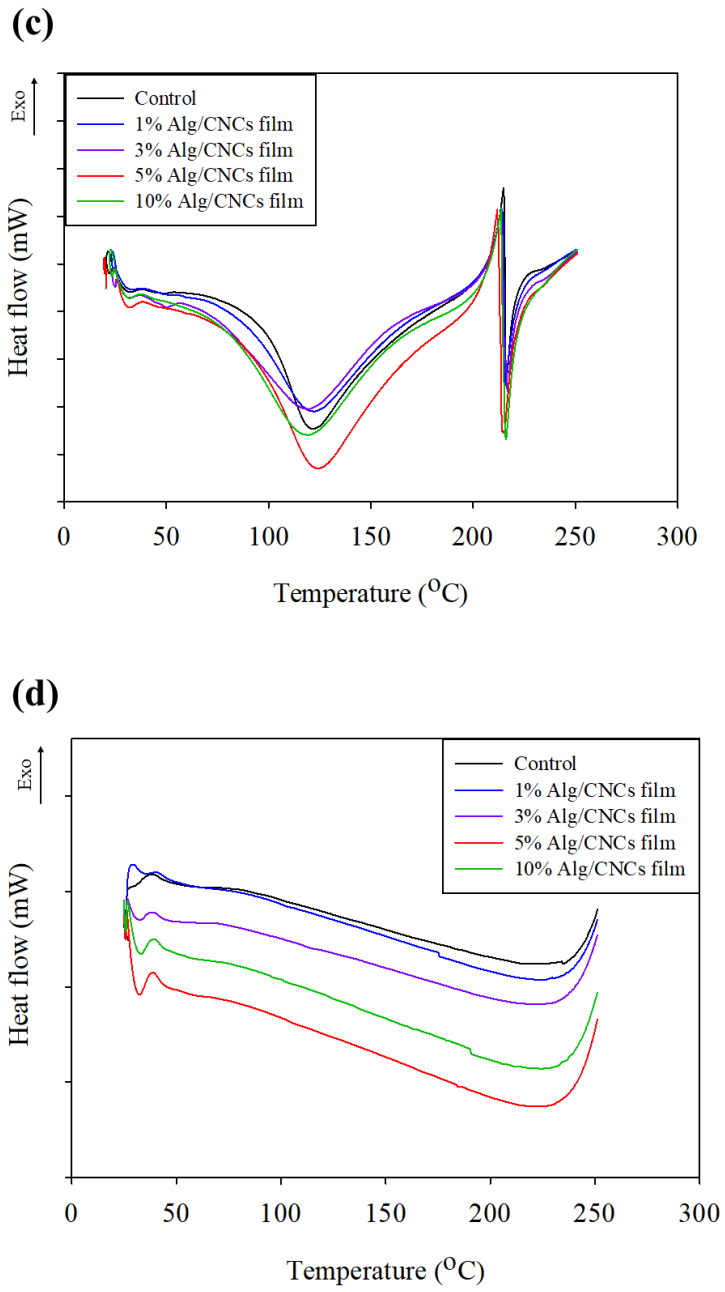

Figure 4.5. TGA, DTG, and DSC graphs of control film and 1 – 10% Alg/CNCs films. TGA, (a); DTG, (b); DSC 1st heating, (c); DSC 2nd heating, (d).

CHAPTER FIVE

Preparation of novel seaweed nanocomposite film from brown seaweeds *Laminaria japonica* and *Sargassum natans*

Abstract

Seaweed nanocomposite films were manufactured with brown seaweeds, kombu (*Laminaria japonica*) and sargassum (*Sargassum natans*). With the supernatant obtained after the acid-base pretreatment, a film-forming solution was prepared and seaweed biopolymer film formed using a cast-evaporating method. Additionally, cellulose nanocrystals (CNCs) were isolated from the residues of the film formulation process and were applied to seaweed biopolymer film. As a result, seaweed nanocomposite films were developed. Their physicochemical properties were investigated to determine viability as a packaging substrate. Kombu film was visible as a dark brown and sargassum film appeared light brown in color. The addition of CNCs did not affect the color of films. The morphological observation revealed the addition of CNCs could fill the void space including holes and fractures. FTIR spectra indicated hydrogen bonding was increased and XRD results showed higher crystallinity after the addition of the CNCs. The addition of CNCs into the film led to improving not only the physical properties such as thickness, moisture content, and water solubility, but also mechanical properties. Similarly, barrier properties to water, oxygen, and light were reinforced. It was found that CNCs also enhanced thermal properties in TGA and DSC tests. Total phenolic contents, DPPH radical scavenging effect, and reducing power assay indicated that kombu film showed higher antioxidant properties than sargassum film and not related to the CNCs addition.

5.1. Introduction

Biopolymer films have been considered as an attractive replacement of petroleum-based packaging films for numerous years (Lee et al., 2018; Mir et al., 2018; Siracusa et al., 2008). Packaging films are one of the important parts in all industrial fields, as they not only act as a role in preserving and protecting for the product through distribution but also offer convenience and communication to consumers (Mihindukulasuriya & Lim, 2014; Tharanathan, 2003). Traditional packaging materials have been converted using petroleum-based polymers due to their low cost, good barrier properties, and strong mechanical characteristics. However, these packaging materials can lead to severe environmental problems because they are not easily degraded in current landfill operations (Emadian et al., 2017). However, the challenge of degradation can be overcome through the use of biopolymer films since they typically degrade more rapidly in natural environments as compared to petroleum-based films. Biopolymer films have been investigated by various researchers using a range of materials such as starch (Jaramillo et al., 2016), alginate (Tavassoli-Kafrani et al., 2016), and chitosan (Lee et al., 2018).

Among the strong candidates for the development of biopolymer films are brown seaweeds. Brown seaweeds have potential to be used as a biopolymer film because their cell walls are rich in carbohydrates which can be used for the backbone of the biopolymer film (Blanco-Pascual et al., 2014; Gomaa et al., 2018; Tavassoli-Kafrani et al., 2016; Vijayan et al., 2016). For instance, alginate, which is abundant in the cell wall of brown seaweed, has a linear molecular structure that can form a strong polymer matrix and structures (Rinaudo, 2008). Kombu (*Laminaria japonica*) and sargassum (*Sargassum natans*) are representative brown seaweeds in the world. In 2014, 7.7 million ton of kombu were produced representing 43% of world seaweed production used for items such as foods, pharmaceuticals, and biomaterials in

industrial fields (Rioux et al., 2017; FAO, 2016). Besides, *Sargassum* spp. has made inundations of beaches for numerous years, recently becoming more of an issue along the North Atlantic and Caribbean seashore. The amount of seaweed washing up on the coastal shores has contributed to economic disruptions related to tourism, aquaculture, and traditional fisheries (Milledge & Harvey, 2016). As a result, if sargassum biopolymer films can be shown to be produced successfully, it will be helpful to economic as well as environmental issues. Also, brown seaweed extracts are usually rich in phenolic compounds having antioxidant properties (Cardozo et al., 2007; Gupta & Abu-Ghannam, 2011). Therefore, the crude extract of these brown seaweeds was used for manufacturing biopolymer films in this study.

Cellulose nanocrystals (CNCs) were isolated by using the residual parts obtained during the process for producing seaweed biopolymer films from brown seaweeds. Biopolymer films have continued to possess limited scalability due to their poor physical, mechanical, and barrier properties compared to petroleum-based packaging materials (Blanco-Pascual et al., 2014; Gomaa et al., 2018). However, research has indicated some of these inherent challenges with using biopolymers can be overcome by adding CNCs to reinforce these weak properties of biopolymer films (Chaichi et al., 2017; Huq et al., 2012; Sung et al., 2017). The implementation of CNCs into the polymer matrix increased the mechanical and barrier properties remarkably, indicating CNCs could be a suitable material platform for the packaging industry (George & Sabapathi, 2015; Sung et al., 2017).

The objective of this research project was to produce a seaweed biopolymer nanocomposite film. The seaweed biopolymer films were prepared with crude extract of two different brown seaweeds, kombu (*Laminaria japonica*) and sargassum (*Sargassum natans*), and reinforced with CNCs that were derived from residue obtained in the process of manufacturing a seaweed biopolymer nanocomposite film. The physical, chemical, thermal,

and antioxidant properties of films were investigated for potential in applications for the packaging industry.

5.2. Materials and methods

5.2.1. Seaweed preparation

Laminaria japonica (kombu) and *Sargassum natans* (sargassum) were collected and shipped from the North Atlantic seashore. These brown seaweeds were washed with running tap water for several minutes and then fully dried. The dried seaweeds were pulverized by a commercial blender for 10 min for homogenizing and stored in a dry oven at 30˚C for further use.

5.2.2. Seaweed extraction

Seaweed extraction was performed with a slight modification of previous studies (Blanco-Pascual et al., 2014). Extractions were treated with 0.2M hydrochloric acid and followed with a 4% sodium hydroxide solution. Dried seaweeds were immersed in the hydrochloric acid solution in a 1:10 (w/v) proportion and homogenized with a magnetic stirrer for 2 h at 30˚C. Then, these colloidal suspensions were washed with distilled water until pH 7 was reached. Neutralized seaweeds were filled with distilled water in a 1:60 proportion (w/v) and adjusted until pH 10 with a 4% sodium hydroxide solution. Then, the suspension was subjected to continuous stirring for 3 h at 75˚C. A pH of 10 was maintained during the treatment. After treatment, colloidal suspensions were centrifuged at 10,000 rpm for 10 min. The supernatants and residues were separated and dried at 75˚C, respectively.

5.2.3. Cellulose nanocrystals (CNCs) preparation

CNCs were produced from residual parts obtained in the seaweed extraction process of a previous study (Doh et al., 2020). Residues were stirred with 10% of potassium hydroxide for removing possible interrupted polysaccharides for 3 h at 80˚C. Then, residues were washed with distilled water and treated with excess amounts of 6.5% (w/v) sodium hypochlorite. After a pH of 5 was reached by adding glacial acetic acid, the sample was reacted for 2 h with magnetic stirring at 75˚C. Then, 10% of active hydrogen peroxide was used for another bleaching process at 80˚C for 70 min. At last, cellulose could be obtained after removing the supernatant. Acid hydrolysis was performed with obtained cellulose at 45˚C for 45 min with 51% sulfuric acid under constant stirring. The suspension was diluted with ice water to stop the reaction and the sample was centrifuged to remove excess sulfuric acid. The suspensions were adjusted to a pH 7 with distilled water and using 4% sodium hydroxide. The suspension was homogenized with an ultrasonicator for 15 min. CNCs suspension was lyophilized to obtain a powdered form of CNCs.

5.2.4. Characterization of cellulose nanocrystals

To analyze the morphological properties of the CNCs from kombu (*Laminaria japonica*) and sargassum (*Sargassum natans*), 0.005% (w/v) of CNCs suspension dissolved in distilled water was prepared and a drop of the suspension was placed on a carbon-coated copper grid. After drying for overnight, the grids were observed with a high-resolution transmission electron microscope (TEM, H-9500; Hitachi, USA), operating at an accelerating voltage of 20 kV. Image J software (National Institute of Health, Bethesda, MD., USA) was used for analyzing the length and width of CNCs particles. 50 measurements were analyzed for calculating the aspect ratio (L/d, where L is the length and d is the width).

Crystallinity was determined by an X-ray diffractometer (Rigaku Ultima IV, Tokyo, Japan). Scanning rate was 5˚/min from 5˚ to 45˚ with Cu K_α radiation (λ = 1.5418 Å) using a

voltage and current of 40 kV and 40 mA, respectively. The crystallinity index of the sample was calculated by the Segal method (Segal et al., 1959) using the following equation:

$$\text{Crystallinity index (\%)} = \frac{I_{200} - I_{am}}{I_{200}} \times 100 \qquad \text{(Eq. 11)}$$

where, I_{200} is the maximum intensity at the plane and I_{am} is the minimum intensity at the valley between planes.

5.2.5. Film preparation

Film-forming solutions were prepared by suspending 1.5% (w/v) dried residues from supernatant obtained as a product of the seaweed extraction process (Blanco-Pascual et al., 2014). Glycerol was used as a plasticizer and added with 30% of total dried residues. This suspension was homogenized with an ultrasonicatior for 10 min. At last, the homogenized suspension was cast into the Petri dish and dried at 35˚C. Films were removed from the Petri dish once fully dried.

Films reinforced with CNCs were prepared as follows. Before homogenizing with ultrasonicator, a certain amount of CNCs based on the dried weight of total dried residue was added into the suspension. Kombu enhanced with 5% CNCs and sargassum reinforced with 5% and 25% CNCs were produced as seaweed nanocomposite films for this study and were named KNF-5, SNF-5, and SNF-25, respectively. Films without CNCs were used as control and named as KF (kombu film) and SF (sargassum film). Films were kept at 25˚C and 56% relative humidity (RH) for 48 h before testing.

5.2.6. Physicochemical characterization of biopolymer films

5.2.6.1. Color

The color of the developed films was assessed by a colorimeter (Aeros Spectrophotometer, Hunter Associates Laboratory, Inc., VA, USA). The values of *L* (lightness), *a* (redness), and *b* (yellowness) of the films were measured. The background value was estimated to L^*= 95.98, a^*= -1.36, and b^*= 1.63. Measurements were performed four times for each sample. The parameters of total color difference (*ΔE*) and whiteness index (WI) were calculated as follow:

$$\Delta E = \sqrt{(L^* - L)^2 + (a^* - a)^2 + (b^* - b)^2} \quad \text{(Eq. 12)}$$

$$\text{WI} = 100 - \sqrt{(100 - L)^2 + a^2 + b^2} \quad \text{(Eq. 13)}$$

where, *L*, *a*, and *b* are the color parameter values of the film sample.

5.2.6.2. Morphology analysis

The morphological properties of the seaweed nanocomposite films were observed at their topographical surface and cross-section using field emission scanning electron microscope S4800 (Hitach High Technologies America, Inc., USA) operated with a voltage of 15.0 kV. The samples were coated with platinum under a vacuum for 2 min before the image was captured.

5.2.6.3. Fourier transform infrared (FTIR) spectroscopy

The FTIR spectra of films were recorded in the infrared range of 4000 – 600 cm^{-1} using an FTIR spectrometer (Nicolet iS10, Thermo Fisher Scientific, USA). The spectra were collected in 128 scans at a resolution of 4 cm^{-1} for each sample.

5.2.6.4. X-ray diffraction (XRD)

Crystallinity was determined by X-ray diffraction with an X-ray diffractometer (Rigaku Ultima IV, Tokyo, Japan) at a scanning rate of 2˚/min from 5˚ to 80˚ with Cu K_α radiation (λ = 1.5418 Å) using a voltage and current of 40 kV and 40 mA, respectively. The crystallinity index of the sample was calculated by the Segal method (Segal et al., 1959).

5.2.6.5. Thickness and moisture content

The thickness for every film was determined using a device with 0.001 mm accuracy (Excel technologies, Inc, Arizona, USA). Measurements were performed at five different locations with five repetitions per film. The moisture content of the films was determined by the dry oven method. Five film specimens per each sample were dried for 24 h at 105˚C until the films reached an equilibrium weight. Once an equilibrium weight was observed, the differences in initial and final moisture content measurements were calculated to obtain moisture content.

5.2.6.6. Mechanical properties

Tensile strength (TS), elongation at break (EB), and tensile energy to break (J) were estimated by using a universal testing machine (5900 Series, Instron Engineering Co., USA) following ASTM D882-02. Each sample was prepared with the dimensions of 10 × 70 mm and placed between grip heads of the testing machine. The cross-head speed and the initial gauge length were 50 mm/min and 50 mm, respectively. Five specimens were tested for each sample.

5.2.6.7. Water solubility

The water solubility of the films was determined gravimetrically (Blanco-Pascual et al., 2014; Lee et al., 2018). Film samples measuring 20 mm × 20 mm were dried at 75˚C to obtain

a constant weight. Then, film samples were immersed in 30 mL of distilled water and stored at 25˚C for 24 h. The suspension was filtered through Whatman # 1 filter paper to recover the remaining undissolved film at 105˚C for 24 h. The water solubility of the films was calculated using the following formula:

$$\text{Water solubility (\%)} = \frac{W_1 - W_2}{W_1} \times 100 \qquad \text{(Eq. 14)}$$

where, W_1 represents the weight of the film sample before immersion and W_2 is the final dried weight of the film sample. Five repetitions were performed for each biopolymer film sample.

5.2.6.8. Water vapor permeability (WVP) and Oxygen permeability (OP)

To determine WVP, water vapor transmission rate (WVTR) was tested using a Mocon Permatran 3/33 Model G (Mocon Inc., Minneapolis, USA) following ASTM F1249-13. The tests were conducted at 23˚C and 90% RH. Water vapor partial pressure at 90% RH is 0.0253 bar at 23˚C. WVP for each sample was estimated according to the following equation:

$$WVP = \frac{WVTR \times l}{\Delta p} \qquad \text{(Eq. 15)}$$

where l corresponds to film thickness and Δp is the partial pressure difference across the films.

OP was calculated from the oxygen transmission rate (OTR) that was collected by using an oxygen permeation analyzer (OX-TRAN Model 2/21; Mocon Inc., Minneapolis, MN, USA) according to ASTM D3985-17 at 23˚C and 100% RH. The OP was calculated by the following equation:

$$OP = \frac{OTR \times l}{\Delta p} \qquad \text{(Eq. 16)}$$

where l is the thickness of the film, and Δp is the difference between oxygen partial pressure across the film ($\Delta p = p_1 - p_2$, where p_1 is the oxygen partial pressure at 23˚C, p_2 is equal to zero on the detector side).

5.2.6.9. Light absorption and transparency

The light barrier properties and transparency of the films were determined by Genesys 10S UV-VIS Spectrophotometer (Thermo Fisher Scientific, Waltham, WA, USA) at selected wavelengths of 190, 300, 360, and 600 nm. The film sample (30 mm × 10 mm) was placed on the quartz cell and the transparency of the film was estimated. Five specimens from each sample were used to determine the light transmittance of the biopolymer film.

5.2.7. Thermodynamic Analysis

Thermal properties of the seaweed biopolymer films were measured using a thermogravimetric analysis (TGA; TA Instruments Inc., New Castle, USA) and differential scanning calorimeter (DSC; TA Instruments Inc., New Castle, USA). Both experiments were performed under a nitrogen atmosphere. For the TGA test, 3 mg of the test sample was placed into an aluminum pan and a scan was performed encompassing a range from 30 to 600˚C. The heating rate was 10˚C/min.

In the DSC experiment, approximately 5 mg of the test sample was sealed in an aluminum pan with an aluminum lid. Samples were first heated from 30˚C to 300˚C at a heating rate of 10˚C/min. The glass transition temperature (T_g), melting temperature (T_m), cold crystallization temperature (T_{cc}), and the enthalpy of melting (ΔH_m) of the samples was obtained from the DSC thermograms. The DSC test was performed in triplicate.

5.2.8. Antioxidant activities of films

5.2.8.1. Determination of total phenol compounds

Folin-Ciocalteu method was used for estimating the total phenolic contents in seaweed biopolymer films with slight modification (Abdollahi et al., 2012; Blanco-Pascual et al., 2014). 20 mg of the film sample was immersed in 5 mL of distilled water overnight. 0.1 mL of the

film extract solution was mixed with a mixture of 7 mL of distilled water and 0.5 mL of Folin and Ciocalteu's phenol solution for 8 min. Then, 1.5 mL of 0.1M sodium carbonate solution and 0.9 mL of distilled water were added to the mixture. The mixture was stored in darkness at room temperature for 2 h after 1 min vortexing. The absorbance of the mixture at 765 nm was determined using a UV/Vis spectrophotometer (Thermo Fisher Scientific, Waltham, WA, USA). The total phenol contents are expressed as mg of gallic acid equivalent (GAE) per gram of the film. The experiment was performed in triplicate for each film sample.

5.2.8.2. DPPH assay

The free radical scavenging activity was determined by the DPPH (2,2-Diphenyl-1-picrylhydrazyl) assay. The measurement was performed with slight modifications (Blois, 1958). 20 mg of film sample was added to 5 mL of distilled water and then stored at 25˚C for 12 h. Afterward, 0.2 mL of the film extract solution was blended with 2 mL of a DPPH solution (0.025 g/L, in methanol). The absorbance was measured at 517 nm after the mixture was stored in darkness for 30 min at 25˚C. The percentage of DPPH radical-scavenging activity is calculated as follows:

$$\text{DPPH scavenging effect (\%)} = \frac{A_{DPPH} - A_{extract}}{A_{DPPH}} \times 100 \qquad \text{(Eq. 17)}$$

where, A_{DPPH} and $A_{extract}$ are the absorbance values of the solution of DPPH and the sample extracts, respectively. The experiment was carried out in triplicate for each film sample.

5.2.8.3. Reducing power assay

The reducing power of the film samples was determined with slight modifications of a previously reported study (Oyaizu, 1986). 20 mg of the film sample was added to 5 mL of distilled water and incubated for 12 h at 25˚C. 0.8 mL of the film extract was blended with 2

mL of a phosphate buffer (0.1 M, pH 6.6) and 2 mL of potassium ferricyanide (1%, w/v). The mixture was stored at 50˚C for 20 min. After being stored, 2 mL of trichloroacetic acid (10%, w/v) was added to the mixture and then centrifuged at 2500 rpm for 10 min. The supernatant (1 mL) was mixed with 2 mL of distilled water and 0.2 mL of a ferric chloride solution (0.1%, w/v). The absorbance was determined at 700 nm. It is determined that increased absorbance indicates increasing reducing power. The experiment was performed in triplicate for each film sample.

5.2.9. Statistical analysis

All data from this research experiment will be presented as the mean ± standard deviation (S.D). The data were analyzed using an analysis of variance (ANOVA). The ANOVA statistical analysis with Duncan's multiple comparison tests at a significance level of $p \leq 0.05$ was applied to the results using the Statistical Package for the Social Sciences software (SPSS, Version 20.0, SPSS Inc., Chicago, IL, USA).

5.3. Results and discussion

5.3.1. Characterization of cellulose nanocrystals

CNCs were successfully isolated from kombu (*Laminaria japonica*) and sargassum (*Sargassum natans*). Acid hydrolysis and mechanical treatment helped to remove the most parts of the amorphous region of cellulose and the crystalline parts remained due to their resistance to acid hydrolysis and mechanical force (Habibi & Sheiban, 2010; Sung et al., 2017). Total yields of CNCs are 26.7% and 42.7% of kombu and sargassum when CNCs were isolated from fully dried cellulose. Morphology, aspect ratio, and crystallinity of CNCs were analyzed since these properties are considered one of the most important factors for nanocomposites

which mainly determined by the cellulose source and the preparation conditions (Miao & Hamad, 2013; Börjesson & Westman, 2015).

Table 5.1 showed the length, width, and aspect ratio of CNCs. This result is in accordance with the TEM images (Fig. 5.1). The aspect ratio of CNCs from kombu and sargassum was calculated as 11.13 ± 1.84 and 6.11 ± 1.85, respectively. Miao & Hamad (2013) reported the typical range of CNCs aspect ratio as 1 – 100 and CNCs aspect ratio indicated in this study is in accordance with this range.

TEM images showed short, rod shapes of CNCs with some aggregates in both cases (Fig. 5.1). These aggregates appeared in the drying step for CNCs preparation due to its strong intermolecular hydrogen bonds between the CNCs particles (Agustin et al., 2014). Previous studies where CNCs were extracted from the brown seaweed (*Laminaria* spp.) showed a length of about 365 - 1300 nm longer than CNCs of this study (Feng et al., 2015; Liu et al., 2017). This is considered caused by the effect of mechanical dispersion of sonication.

The crystallinity of kombu and sargassum showed 98.85 ± 0.65% and 85.06 ± 3.55%, respectively (Table 5.1). The XRD spectra of CNCs from kombu and sargassum are shown in Fig. 5.5 and the shape of CNCs patterns was similar to previous reports (Feng et al., 2015; Liu et al., 2017; Sung et al., 2017). The main peaks were observed at 2θ = 14.9˚, 18.4˚, and 22.5˚ which accordance with cellulose type I.

5.3.2. Morphological analysis

5.3.2.1. Color

Images of seaweed biopolymer films are shown in Fig. 5.2 and data of the samples in agreement with the Hunter system are given in Table 5.2. The color of the film is one of the most important factors related to the appearance of influencing consumer acceptance (Garavand et al., 2017). As shown in Fig. 5.2, kombu films appeared dark brown color and

sargassum films showed a light brown color. Color values are significantly affected ($p < 0.05$) between seaweed sources. There are no significant differences observed between the films enhanced with CNCs or those not containing CNCs. Since sargassum films showed a higher *L* value, but lower *a* and *b* values than kombu films, *ΔE* and WI did not show the significant differences between kombu and sargassum films. Blanco-Pascual et al., (2014) developed kombu (*Laminaria digitate*) film and reported different colorimeter results than our study. The samples from the previously reported study appeared darker green and blue than this study. Another research report by Gomaa et al. (2018) investigated sargassum (*Sargassum latifolium*) film and it showed lower *L* value (57 – 65%) than that of our sargassum film. These comparative results indicate that although the same species was used for manufacturing the biopolymer films, factors such as extraction conditions and experimental methods can affect the color of seaweed biopolymer films as well as regions, feed, and the other numerous natural factors (Beratto et al., 2017).

5.3.2.2. Scanning electron microscopy (SEM)

Scanning electron microscopy (SEM) results were analyzed focusing on the morphological surface along with the cross-section of seaweed biopolymer films (Fig. 5.3). Fig. 5.3 (A) – (E) showed the surface of the film, while Fig. 5.3 (a) – (e) indicated the cross section of the film. As shown in Fig. 5.3 (A) and (C), KF and SF showed cracks on their surfaces. These cracks are a result of the seaweed polymer matrix not forming strong interactions in these areas. However, KNF-5, SNF-5, and SNF-25 did not show evidence of cracks on their surface. This is due to the addition of CNCs as they were able to form and maintain strong interactions through hydrogen bonding in the polymer matrix (Fig. 5.3 (B) and (E)) (Huq et al., 2012; Sung et al., 2017). Although SNF-5 displayed a small fracture on the film surface, it showed significant improvement compared to SF (Fig. 5.3 (D)). Similar to

surface morphology, small holes were observed in the cross-section of certain films as shown in Fig. 5.3 (a), (c), and (d). KNF-5 and SNF-25 did not indicate the presence of holes at the cross-section. These samples reported a smooth transition across the matrix indicating strong interactions between polymer matrix and CNCs. CNCs applied in biopolymer films such as alginate or polylactic acid (PLA) showed the agglomeration in polymer matrix when the amount of CNCs increased (Doh et al., 2020; Huq et al., 2012; Sung et al., 2017). However, there were no observations of agglomeration of CNCs in the polymer matrix up to 5% for kombu and 25% for sargassum.

5.3.3. Chemical structure analysis

5.3.3.1. FTIR analysis

FTIR spectra of seaweed nanocomposite films are shown in Fig. 5.4. The peaks at 990 – 1200 cm^{-1} indicated the presence of C-C and C-O pyranoid ring stretching and C-O-C glycosidic bond stretching (Gómez-Ordóñez & Rupérez, 2011). The peak around the 1029 cm^{-1} and 1031 cm^{-1} also appeared due to OH-guluronate bending possibly indicating the fingerprints of alginate. However, KNF-5 showed a decrease of this peak intensity due to the addition of CNCs. Besides, a peak appeared at 1133 cm^{-1} after the addition of CNCs due to the increment of crystallinity (Jipa et al., 2012). As CNCs addition, peak shifts occurred at 1248 cm^{-1} for kombu film (a) and 1232 cm^{-1} for sargassum film (b) which indicate the shift of hydrogen bond (Takahashi, R., & Noguchi, T., 2007). These indicate kombu film showed donor-acceptor form and sargassum film showed acceptor form when new hydrogen bonds were formed due to the addition of CNCs. Bands between 1400 cm^{-1} and 1600 cm^{-1} which indicate the asymmetric and symmetric carboxylate group stretching vibrations (-COO) on the polymeric backbone show the presence of alginate. The carbonyl group appears shifted as carboxylate anion to 1600 cm^{-1} (Gómez-Ordóñez & Rupérez, 2011; Paşcalău et al., 2012).

These results can describe the formation of new hydrogen bonds due to the addition of CNCs including the polar groups between polymer matrix and CNCs (Nešić et al., 2017). The band at 2934 cm^{-1} is associated with C-H stretching. The broad band at 3000 – 3600 cm^{-1} is assigned to the vibrational stretching related to hydroxyl groups. It can be caused by hydrogen bonds between CNCs and polymer matrix or captured water molecules. Marques et al., (2006) and Paula et al., (2015) suggested the formation of more hydrogen bonds in these bands, however, it is hard to analyze whether this band is attributed to hydrogen bond or captured water molecules because the seaweed polymer band absorbs water molecules very easily in the atmosphere.

5.3.3.2. XRD analysis

XRD analysis was performed to find the crystalline characteristics of kombu and sargassum biopolymer films. XRD spectra of CNCs showed the peaks at 2θ = 14.8˚ and 20 - 22˚ depended on crystalline order and corresponding to 1 1 0 and 2 0 0 planes of cellulose type I, respectively (Li et al., 2009; Shin & Exarhos, 2007). KF and SF did not show the peaks typically observed for cellulose. However, KNF-5, SNF-5, and SNF-25 showed the peaks at 14.8˚ and 22.6˚ which indicate the cellulose type I. Crystallinity index of KNF-5 was reported to be 77.2%. The crystallinity index of 76.3% and 83.3% was shown in SNF-5 and SNF-25, respectively. As CNCs were added to the polymer matrix, the crystallinity index also increased as shown in the XRD spectra (Fig. 5.5). These results are supported by the analysis observed from the FTIR because of the high intensity of the band between 2800 – 3200 cm^{-1} can lead to high crystallinity. Also, an increased crystallinity index of films could indicate increased biopolymer film strength characteristics, such as stiffness and rigidity. This means CNCs from brown seaweed have high potential to be used for enhancing the mechanical properties of seaweed biopolymer films.

5.3.4. Physical properties of seaweed nanocomposite films

Table 5.3 represents the physical properties of seaweed biopolymer films. Conversely, the thickness of sargassum-based film ranged from 0.039 mm to 0.058 mm which showed significant differences ($p < 0.05$). As the amount of CNCs increased, the film thickness was increased. Moisture content results showed that kombu-based film reported a lower moisture content than sargassum-based film. Compared to films without the addition of CNCs and nanocomposite films, as CNCs addition increased, moisture content was significantly decreased ($p < 0.05$).

Water solubility is one of the biggest challenges preventing biopolymer films from being introduced as viable replacements to petroleum-based plastics. In the result of the water solubility test, KF showed 70.23 ± 5.85% of water solubility and that of KNF-5 was 59.02 ± 3.99%, which showed a 16% reduction in water solubility. Similarly, SF showed a reduction of water solubility when CNCs was added the addition of CNCs in the polymer matrix (59.09 ± 5.04% and 41.74 ± 1.97% for CNF-5 and CNF-25, respectively). SF completely dissolved into solution after being immersed for 24 h. Water vapor permeability (WVP) and oxygen permeability (OP) were also analyzed (Table 5.3). Kombu films showed the values were reduced when 5% CNCs added to the polymer matrix, but the difference was not significant. On the other hand, WVP of sargassum films was significantly different when CNCs were added to the polymer matrix ($p < 0.05$). KF and SF showed a 66% reduction in the OP with KNF-5. SNF-5 and SNF-25 reported significant reductions of 91.8% and 97.1% respectively ($p < 0.05$). This shows that as the CNCs concentration was increased in the seaweed polymer matrix, it created a tortuous path making it difficult for water and oxygen molecules must pass through (Huq et al., 2012; Sanchez-Garcia & Lagaron, 2010; Sung et al., 2017). As a result, the higher the concentration of CNCs in the polymer matrix, the lower the permeability.

The transmittance of UV light is an important factor for food packaging systems because foods can be degraded by oxidation, nutrient loss, and discoloration due to UV light (Lee et al., 2018). UV-C light (100 – 280 nm), UV-B light (280 – 315 nm), and UV-A light (315 – 400 nm) were used as light wavelength in this study. Among these, UV-A light can damage foods directly due to its far less absorbed by the ozone layer in the atmosphere (Sobrino et al., 2004). In Table 4, all films exhibited very low light transmittance in the UV range up to 360 nm which agrees with previously reported results (Blanco-Pascual et al., 2014). However, when transmittance was investigated at 600 nm, the values were significantly increased. Some previous reports indicated this results from the possible presence of chlorophyll *a* and *b*, β-carotene, phaeophytin or some protein complexes in thylakoids which are acting as a light-harvesting system from 437 nm to 675 nm (Blanco-Pascual et al., 2014; de Quirós et al., 2010; Gildenhoff et al., 2010). The kombu-based film showed significantly lower light transmittance than sargassum-based film and both films showed less light transmittance when CNCs added ($p < 0.05$). Light transmittance was lowered 5.8% comparing KF to KNF-5 and 28.7% when samples of SF were compared to that of SNF-5. SNF-25 showed a dramatic 38.2% reduction in transmittance when compared to SF.

5.3.5. Mechanical properties of seaweed nanocomposite films

The mechanical properties of seaweed biopolymer films were investigated to evaluate the tensile strength (TS), elongation at break (EB), and tensile energy to break for determining the effects of CNCs as a reinforcing agent (Table 5.3). TS of KF showed 15.36 ± 2.24 MPa and that of KNF-5 showed 19.54 ± 2.89 MPa which indicates a 21.4% improvement in tensile strength. Similarly, TS of SF (3.96 ± 0.65 MPa) showed gradual increase when CNCs were added (4.61 ± 1.0 MPa and 9.08 ± 1.14 MPa with SNF-5 and SNF-25, respectively). Films reinforced with CNCs showed significantly higher TS than films without CNCs both in kombu

and sargassum ($p < 0.05$). In the SEM results from this study, cracks to the matrix were observed for films without CNCs in seaweed biopolymer films, which translated to lower TS results due to the cracks increasing the stress concentrations in the film. Also, FTIR results indicated that when CNCs amounts increased, hydrogen bonding was enhanced which could be correlated to the increased TS. XRD results were also in agreeance with the TS results. The crystallinity being increased led to an increase in the TS due to the intermolecular bonding being stronger due to the addition of the CNCs ($p < 0.05$) (Balani et al., 2015). According to previous reports, Huq et al. (2012) reported that when CNCs were added over 5% in alginate suspension, TS of alginate nanocomposite film was decreased.

When evaluating the elongation at break (EB) of the films, KNF-5 had an average EB of 4.2 ± 1.40% which was lower than KF film samples (8.9 ± 1.65%). SF had an average EB of 58.6 ± 5.59%, and like the KF films, as the concentration of CNCs was increased, the EB was reduced (43.6 ± 8.71% and 28.2 ± 5.36% with SNF-5 and SNF-25, respectively). EB showed an inverse relationship with tensile strength, which agrees with previous reports (Chaichi et al., 2017; Cian et al., 2014; Huq et al., 2012; Sung et al., 2017). These results from previous reports are attributed to the agglomerations of CNCs, mainly via Van der Waals forces (Haafiz et al., 2013).

The result of tensile energy to break indicates the toughness of the composition of seaweed biopolymer film and its ability to withstand the conditions it will be applied to in use. This concept can be defined as the material energy that can be absorbed before rupturing and is measured by the area under the stress-strain curve. In this study, KF has 0.020 ± 0.005 J, KNF-5 showed 0.062 ± 0.037 J, and in the case of sargassum film, 0.028 ± 0.005 J, 0.028 ± 0.010 J, and 0.036 ± 0.008 J as ordered SF, SNF-5, and SNF-25, respectively. As the amount of CNCs increased, tensile energy showed an increasing tendency similar to the TS results.

These results show that the toughness of the biopolymer film matrix can be increased by increasing the concentration of CNCs in the polymer matrix.

5.3.6. Thermodynamics

Thermo-gravimetric analysis (TGA) and derivative thermogravimetry (DTG) curves for seaweed biopolymer films are represented in Fig. 5.6 (a) and (b). The initial weight loss by water evaporation was observed in the range of 0 – 100˚C in all cases. Initial decomposition of kombu film ranged in 100 – 140˚C can be attributed to bound water molecules inside of the film (Huq et al., 2012). The same phenomena could be found in sargassum film in the range of 100 – 160˚C. Next, the second decomposition of kombu film is shown in 239.11˚C and 250.33˚C for KF and KNF-5. Besides, sargassum film showed their second decomposition in 201.88˚C, 209.57˚C, and 228.21˚C for SF, SNF-5, and SNF-25, respectively. According to the previous report, these results indicated a thermal decomposition of glycerol (Han et al., 2018). The third decomposition was assigned at temperatures higher than 350˚C in both kombu (375.15˚C and 386.11˚C) and sargassum (475.11˚C, 374.05˚C, and 486.07˚C) films. These occurred due to the degradation of seaweed crude extract backbones. CNCs could not affect the decomposition of films due to their high thermal stability (Doh et al., 2020). It is clear from the results that CNCs in the polymer matrix can decrease the weight loss ratio and increase the onset thermal decomposition temperature (T_{on}) of seaweed films (198.67˚C, KF; 218.57˚C, KNF-5 and 128.13˚C, SF; 161.27˚C, SNF-5; 197.71˚C, SNF-25, respectively). The results showed that TGA curves were shifted to higher temperatures with CNCs. This suggests higher thermal stability can be obtained by adding CNCs to films and indicates strong interactions can be formed between seaweed polymer matrix and CNCs. DTG curves also agreed with the results of TGA curves and therefore showed an increase of an inflection point when CNCs were added. SNF-25 showed a significant increase compared to SF and SNF-5. XRD result

agrees with TGA data that at high concentrations of CNCs can lead to high thermal stability attributed to high crystallinity (Balani et al., 2015).

The DSC thermograms showed endothermic and exothermic spectra when the temperature goes up from 25˚C to 300˚C (Fig. 5.7). Due to the high moisture content of kombu and sargassum films, it is hard to find the degradation temperature. However, DSC spectra showed the evaporation of bound water molecules of the films in the range of 100 – 140˚C for kombu film and 100 – 160˚C for sargassum film, in accordance with the TGA data. In addition, the second decomposition observed in TGA results could be found in 235 – 260˚C for kombu film and 200 – 230˚C attributed from the glycerol degradation. Also, DSC spectra showed that the addition of CNCs could render the water and glycerol molecules hard to evaporate or degrade by forming a complicated path inside of the polymer matrix. Therefore, TGA and DSC spectra showed the addition of CNCs in seaweed nanocomposite films contributed to a substantial improvement in their thermal stability.

5.3.7. Antioxidant properties

The total phenolic contents, DPPH assay, and reducing power assay of seaweed nanocomposite films are presented in Fig. 5.8. Kombu films showed higher results in total phenolic contents, DPPH, and reducing power assay than that of sargassum film ($p < 0.05$). However, the antioxidant properties were not changed even though the amounts of CNCs were added to the films. Seaweed is well known for its antioxidant properties. According to previous research by Heffernan et al., (2015), the total phenol content of *Laminaria digitata*, which is one of the genera of kombu, ranged from 2.1 to 22.8 ug GAE mg^{-1} and was dependent on the extraction method utilized. Kombu film showed about 8 – 10 mg GAE/g, comparable to the range of total phenol content (Figure 8. (a)). Also, this study reported that DPPH scavenging activity ranged from 0.2 to 0.8 ARP (antiradical power) which means 40 – 80% depended on

the calculation method in this study. Similar to the total phenolic content, the results agree with a previous report (Heffernan et al., 2015). In the case of *Sargassum* spp., (*Sargassum pallidum*), previous research stated that total phenolic content of it was determined to be 52.08 ± 0.02 mg CHA (chlorogenic acid)/g extract and DPPH showed about 40 – 50% antioxidant activities which are higher than the result of our study (Ye et al., 2009). A previous study reported DPPH scavenging activity of film samples decreased with the increasing CNCs content, due to the addition of CNCs that could slow down the release of the extract of a grape from the chitosan matrix due to the strong matrix-filler interaction (Sogut & Seydim, 2018). However, another study reported the higher concentration of CNCs can attribute to the deposition of dense PANI (polyaniline) layer which leads to increasing the antioxidant activity (Rehim et al., 2019). In the present study, the higher content of CNCs (SNF-25) help assembles the polymer matrix in sargassum film which led to higher observed DPPH scavenging activities than the other sargassum film ($p < 0.05$). Reducing power assay showed the same tendency with total phenolic content and DPPH scavenging activity. As a result, total phenolic content is related to the DPPH scavenging activity and reducing power assay (Lee et al., 2018). Also, the total phenol content of seaweed film could be deeply affected by season, region, and a lot of other factors.

5.4. Conclusions

Laminaria japonica and *Sargassum natans* crude extracts would be novel sources for biopolymer nanocomposite films with cellulose nanocrystals from residues of these seaweeds. Generally, physicochemical, mechanical, barrier and thermal properties were improved by adding CNCs and kombu biopolymer films showed better characteristics than that of sargassum films. Morphological observations showed that structural modifications with the CNC layer

led to an improved mechanical, barrier, and thermal properties. As CNCs concentration increased, tensile strength and tensile energy were increased and elongation was decreased. Water, oxygen, and light barrier properties were significantly improved by adding CNCs and it was proven that the addition of CNCs could increase thermal stability through TGA and DSC results. Seaweed biopolymer films have been facing challenges of industry acceptance due to concerns of poor mechanical and barrier properties. However, these properties were improved by adding CNCs. Therefore, results from this study suggest support seaweed biopolymer nanocomposite films have shown the potential to be used as a novel biopolymer film for food packaging systems. Additionally, antioxidant properties investigated in this study proved seaweed biopolymer films could be used to improve food preservation or to design functional foods.

5.5. References

Abdollahi, M., Rezaei, M., & Farzi, G. (2012). Improvement of active chitosan film properties with rosemary essential oil for food packaging. *International Journal of Food Science & Technology, 47*(4), 847-853.

Agustin, M. B., Ahmmad, B., Alonzo, S. M. M., & Patriana, F. M. (2014). Bioplastic based on starch and cellulose nanocrystals from rice straw. Journal of Reinforced Plastics and Composites, 33(24), 2205-2213.

ASTM D3985-17. (2017). Standard Test Method for Oxygen Gas Transmission Rate Through Plastic Film and Sheeting Using a Coulometric Sensor.

ASTM D882-02. (2002). Standard Test Method for Tensile Properties of Thin Plastic Sheeting.

ASTM F1249-13. (2013). Standard Test Method for Water Vapor Transmission Rate Through Plastic Film and Sheeting Using a Modulated Infrared Sensor.

Balani, K., Verma, V., Agarwal, A., & Narayan, R. (2015). *A Materials Science and Engineering Perspective*: Wiley Online Library.

Beratto, A., Agurto, C., Freer, J., Peña-Farfal, C., Troncoso, N., Agurto, A., & Castillo, R. d. P. (2017). Chemical characterization and determination of the anti-oxidant capacity of two brown algae with respect to sampling season and morphological structures using infrared spectroscopy and multivariate analyses. *Applied spectroscopy, 71*(10), 2263-2277.

Blanco-Pascual, N., Montero, M., & Gómez-Guillén, M. (2014). Antioxidant film development from unrefined extracts of brown seaweeds Laminaria digitata and Ascophyllum nodosum. *Food hydrocolloids, 37*, 100-110.

Blois, M. S. (1958). Antioxidant determinations by the use of a stable free radical. *Nature, 181*(4617), 1199.

Börjesson, M., & Westman, G. (2015). Crystalline nanocellulose—preparation, modification, and properties. Cellulose-fundamental aspects and current trends, 159-191.

Cardozo, K. H., Guaratini, T., Barros, M. P., Falcão, V. R., Tonon, A. P., Lopes, N. P., Campos, S., Torres, M. A., Souza, A. O., & Colepicolo, P. (2007). Metabolites from algae with economical impact. *Comparative Biochemistry and Physiology Part C: Toxicology & Pharmacology, 146*(1-2), 60-78.

Chaichi, M., Hashemi, M., Badii, F., & Mohammadi, A. (2017). Preparation and characterization of a novel bionanocomposite edible film based on pectin and crystalline nanocellulose. *Carbohydrate Polymers, 157*, 167-175.

Cian, R. E., Salgado, P. R., Drago, S. R., González, R. J., & Mauri, A. N. (2014). Development of naturally activated edible films with antioxidant properties prepared from red seaweed Porphyra columbina biopolymers. *Food chemistry, 146*, 6-14.

de Quirós, A. R.-B., Frecha-Ferreiro, S., Vidal-Pérez, A., & López-Hernández, J. (2010).

Antioxidant compounds in edible brown seaweeds. *European Food Research and Technology, 231*(3), 495-498.

Doh, H., Lee, M. H., & Whiteside, W. S. (2020). Physicochemical characteristics of cellulose nanocrystals isolated from seaweed biomass. Food Hydrocolloids, 102, 105542.

Emadian, S. M., Onay, T. T., & Demirel, B. (2017). Biodegradation of bioplastics in natural environments. *Waste management, 59*, 526-536.

FAO. (2016). Fishery and Aquaculture Statistics. Global production by production source 1950-2014. *FishstatJ*. http://www.fao.org/fishery/statistics/software/fishstatj/en

Feng, X., Meng, X., Zhao, J., Miao, M., Shi, L., Zhang, S., & Fang, J. (2015). Extraction and preparation of cellulose nanocrystals from dealginate kelp residue: structures and morphological characterization. Cellulose, 22(3), 1763-1772.

Garavand, F., Rouhi, M., Razavi, S. H., Cacciotti, I., & Mohammadi, R. (2017). Improving the integrity of natural biopolymer films used in food packaging by crosslinking approach: A review. *International journal of biological macromolecules, 104*, 687-707.

George, J., & Sabapathi, S. (2015). Cellulose nanocrystals: synthesis, functional properties, and applications. *Nanotechnology, science and applications, 8*, 45.

Gildenhoff, N., Amarie, S., Gundermann, K., Beer, A., Büchel, C., & Wachtveitl, J. (2010). Oligomerization and pigmentation dependent excitation energy transfer in fucoxanthin–chlorophyll proteins. *Biochimica et Biophysica Acta (BBA)-Bioenergetics, 1797*(5), 543-549.

Gomaa, M., Fawzy, M. A., Hifney, A. F., & Abdel-Gawad, K. M. (2018). Use of the brown seaweed Sargassum latifolium in the design of alginate-fucoidan based films with natural antioxidant properties and kinetic modeling of moisture sorption and polyphenolic release. *Food hydrocolloids, 82*, 64-72.

Gómez-Ordóñez, E., & Rupérez, P. (2011). FTIR-ATR spectroscopy as a tool for

polysaccharide identification in edible brown and red seaweeds. *Food hydrocolloids, 25*(6), 1514-1520.

Gupta, S., & Abu-Ghannam, N. (2011). Recent developments in the application of seaweeds or seaweed extracts as a means for enhancing the safety and quality attributes of foods. *Innovative Food Science & Emerging Technologies, 12*(4), 600-609.

Haafiz, M. M., Hassan, A., Zakaria, Z., Inuwa, I. M., Islam, M. S., & Jawaid, M. (2013). Properties of polylactic acid composites reinforced with oil palm biomass microcrystalline cellulose. *Carbohydrate Polymers, 98*(1), 139-145.

Habibi, M. H., & Sheibani, R. (2010). Removal of 2-mercaptobenzoxazole from water as model of odorous mercaptan compounds by a heterogenous photocatalytic process using Ag-ZnO nanocomposite coated thin film on glass plate. Bulletin of environmental contamination and toxicology, 85(6), 589-592.

Han, Y., Yu, M., & Wang, L. (2018). Soy protein isolate nanocomposites reinforced with nanocellulose isolated from licorice residue: Water sensitivity and mechanical strength. Industrial Crops and Products, 117, 252-259.

Heffernan, N., Smyth, T., Soler-Villa, A., Fitzgerald, R., & Brunton, N. (2015). Phenolic content and antioxidant activity of fractions obtained from selected Irish macroalgae species (*Laminaria digitata*, *Fucus serratus*, *Gracilaria gracilis* and *Codium fragile*). *Journal of applied phycology, 27*(1), 519-530.

Huq, T., Salmieri, S., Khan, A., Khan, R. A., Le Tien, C., Riedl, B., Fraschini, C., Bouchard, J., Uribe-Calderon, J., & Kamal, M. R. (2012). Nanocrystalline cellulose (NCC) reinforced alginate based biodegradable nanocomposite film. *Carbohydrate Polymers, 90*(4), 1757-1763.

Jaramillo, C. M., Gutiérrez, T. J., Goyanes, S., Bernal, C., & Famá, L. (2016). Biodegradability and plasticizing effect of yerba mate extract on cassava starch edible films.

Carbohydrate Polymers, 151, 150-159.

Jipa, I. M., Dobre, L., Stroescu, M., Stoica-Guzun, A., Jinga, S., & Dobre, T. (2012). Preparation and characterization of bacterial cellulose-poly (vinyl alcohol) films with antimicrobial properties. Materials Letters, 66(1), 125-127.

Lee, M. H., Kim, S. Y., & Park, H. J. (2018). Effect of halloysite nanoclay on the physical, mechanical, and antioxidant properties of chitosan films incorporated with clove essential oil. *Food Hydrocolloids*.

Li, Q., Zhou, J., & Zhang, L. (2009). Structure and properties of the nanocomposite films of chitosan reinforced with cellulose whiskers. *Journal of Polymer Science Part B: Polymer Physics, 47*(11), 1069-1077.

Liu, Z., Li, X., Xie, W., & Deng, H. (2017). Extraction, isolation and characterization of nanocrystalline cellulose from industrial kelp (Laminaria japonica) waste. Carbohydrate polymers, 173, 353-359.

Marques, P. T., Lima, A., Bianco, G., Laurindo, J., Borsali, R., Le Meins, J.-F., & Soldi, V. (2006). Thermal properties and stability of cassava starch films cross-linked with tetraethylene glycol diacrylate. *Polymer degradation and stability, 91*(4), 726-732.

Miao, C., & Hamad, W. Y. (2013). Cellulose reinforced polymer composites and nanocomposites: a critical review. *Cellulose*, 20(5), 2221-2262.

Mihindukulasuriya, S., & Lim, L.-T. (2014). Nanotechnology development in food packaging: A review. *Trends in Food Science & Technology, 40*(2), 149-167.

Milledge, J., & Harvey, P. (2016). Golden Tides: Problem or golden opportunity? The valorisation of Sargassum from beach inundations. *Journal of Marine Science and Engineering, 4*(3), 60.

Mir, S. A., Dar, B., Wani, A. A., & Shah, M. A. (2018). Effect of plant extracts on the techno-functional properties of biodegradable packaging films. *Trends in Food Science &*

Technology.

Nešić, A., Onjia, A., Davidović, S., Dimitrijević, S., Errico, M. E., Santagata, G., & Malinconico, M. (2017). Design of pectin-sodium alginate based films for potential healthcare application: Study of chemico-physical interactions between the components of films and assessment of their antimicrobial activity. *Carbohydrate Polymers, 157*, 981-990.

Oyaizu, M. (1986). Studies on products of browning reaction: antioxidative activity of products of browning reaction. *Jpn. J. Nutr, 44*(6), 307-315.

Paşcalău, V., Popescu, V., Popescu, G., Dudescu, M., Borodi, G., Dinescu, A., Perhaiţa, I., & Paul, M. (2012). The alginate/k-carrageenan ratio's influence on the properties of the cross-linked composite films. *Journal of Alloys and Compounds, 536*, S418-S423.

Paula, G. A., Benevides, N. M., Cunha, A. P., de Oliveira, A. V., Pinto, A. M., Morais, J. P. S., & Azeredo, H. M. (2015). Development and characterization of edible films from mixtures of κ-carrageenan, ι-carrageenan, and alginate. *Food hydrocolloids, 47*, 140-145.

Rehim, M. H. A., Yassin, M. A., Zahran, H., Kamel, S., Moharam, M. E., & Turky, G. (2019). Rational design of active packaging films based on polyaniline-coated polymethyl methacrylate/nanocellulose composites. *Polymer Bulletin*, 1-15.

Rinaudo, M. (2008). Main properties and current applications of some polysaccharides as biomaterials. *Polymer International, 57*(3), 397-430.

Rioux, L.-E., Beaulieu, L., & Turgeon, S. L. (2017). Seaweeds: A traditional ingredients for new gastronomic sensation. *Food hydrocolloids, 68*, 255-265.

Sanchez-Garcia, M. D., & Lagaron, J. M. (2010). On the use of plant cellulose nanowhiskers to enhance the barrier properties of polylactic acid. *Cellulose, 17*(5), 987-1004.

Segal, L., Creely, J., Martin Jr, A., & Conrad, C. (1959). An empirical method for estimating

the degree of crystallinity of native cellulose using the X-ray diffractometer. *Textile Research Journal, 29*(10), 786-794.

Shin, Y., & Exarhos, G. J. (2007). Template synthesis of porous titania using cellulose nanocrystals. *Materials Letters, 61*(11-12), 2594-2597.

Siracusa, V., Rocculi, P., Romani, S., & Dalla Rosa, M. (2008). Biodegradable polymers for food packaging: a review. *Trends in Food Science & Technology, 19*(12), 634-643.

Sobrino, C., Montero, O., & Lubián, L. M. (2004). UV-B radiation increases cell permeability and damages nitrogen incorporation mechanisms in Nannochloropsis gaditana. *Aquatic Sciences, 66*(4), 421-429.

Sogut, E., & Seydim, A. C. (2018). Development of Chitosan and Polycaprolactone based active bilayer films enhanced with nanocellulose and grape seed extract. *Carbohydrate Polymers, 195*, 180-188.

Sung, S. H., Chang, Y., & Han, J. (2017). Development of polylactic acid nanocomposite films reinforced with cellulose nanocrystals derived from coffee silverskin. *Carbohydrate Polymers, 169*, 495-503.

Takahashi, R., & Noguchi, T. (2007). Criteria for determining the hydrogen-bond structures of a tyrosine side chain by Fourier transform infrared spectroscopy: Density functional theory analyses of model hydrogen-bonded complexes of p-cresol. The Journal of Physical Chemistry B, 111(49), 13833-13844.

Tavassoli-Kafrani, E., Shekarchizadeh, H., & Masoudpour-Behabadi, M. (2016). Development of edible films and coatings from alginates and carrageenans. *Carbohydrate Polymers, 137*, 360-374.

Tharanathan, R. (2003). Biodegradable films and composite coatings: past, present and future. *Trends in Food Science & Technology, 14*(3), 71-78.

Vijayan, S. R., Santhiyagu, P., Ramasamy, R., Arivalagan, P., Kumar, G., Ethiraj, K., &

Ramaswamy, B. R. (2016). Seaweeds: a resource for marine bionanotechnology. *Enzyme and microbial technology, 95*, 45-57.

Ye, H., Zhou, C., Sun, Y., Zhang, X., Liu, J., Hu, Q., & Zeng, X. (2009). Antioxidant activities in vitro of ethanol extract from brown seaweed Sargassum pallidum. *European Food Research and Technology, 230*(1), 101.

Table 5.1. Characteristics of CNCs on the CNCs source.

CNCs source	Length (nm)	Width (nm)	Aspect ratio (L/D)	Crystallinity (%)
Kombu (*Laminaria japonica*)	228.14 ± 46.07	20.96 ± 5.11	11.13 ± 1.84	98.85 ± 0.65
Sargassum (*Sargassum natans*)	49.30 ± 11.73	8.55 ± 2.11	6.11 ± 1.85	85.06 ± 3.55

(1) Data are mean ± S.D.

Table 5.2. Color parameters of seaweed films formulated with CNCs.

Sample	*L*	*a*	*b*	*ΔE*	WI
KF	54.83 ± 3.28[a]	18.14 ± 2.08[a]	28.84 ± 5.05[a]	53.10 ± 5.76[a]	43.36 ± 5.64[a]
KNF-5	54.70 ± 3.22[a]	18.13 ± 0.49[a]	26.64 ± 1.95[a]	51.98 ± 2.17[a]	44.35 ± 2.18[a]
SF	89.55 ± 0.32[b]	4.70 ± 0.44[b]	55.58 ± 1.42[b]	54.66 ± 1.47[a]	43.25 ± 1.48[a]
SNF-5	89.07 ± 1.43[b]	3.86 ± 0.96[b]	52.72 ± 1.56[b]	51.82 ± 1.78[a]	46.01 ± 1.84[a]
SNF-25	88.24 ± 0.79[b]	3.34 ± 0.41[b]	51.28 ± 0.78[b]	50.45 ± 0.82[a]	47.28 ± 0.82[a]

(1) Data are mean ± S.D.

(2) Mean values with different letters within a column are significantly different ($p < 0.05$) by ANOVA with Duncan's multiple comparison test, n=5.

(3) *ΔE* is the total color difference; WI is a whiteness index.

Table 5.3. Physical and mechanical properties of seaweed films.

Sample	Thickness (mm)	Moisture content (%)	Tensile strength (MPa)	Elongation at break (%)	Tensile energy to break (J)	Water solubility (%)	WVP ($g/m \cdot s \cdot Pa \times 10^{-12}$)	OP ($cm^{-3}/m \cdot s \cdot Pa \times 10^{-14}$)
KF	0.046 ± 0.008^{ab}	15.73 ± 2.24^{a}	15.36 ± 2.24^{a}	8.90 ± 1.65^{a}	0.020 ± 0.005^{a}	70.23 ± 5.85^{a}	1.78 ± 0.33^{a}	12.66 ± 1.5^{a}
KNF-5	0.045 ± 0.003^{ab}	11.45 ± 2.34^{b}	19.54 ± 2.89^{b}	4.20 ± 1.40^{a}	0.062 ± 0.037^{b}	59.02 ± 3.99^{b}	1.21 ± 0.20^{a}	4.29 ± 0.25^{b}
SF	0.039 ± 0.002^{a}	33.39 ± 1.44^{c}	3.96 ± 0.65^{c}	58.60 ± 5.59^{c}	0.028 ± 0.005^{a}	N.D.	4.70 ± 0.54^{b}	31.11 ± 1.63^{c}
SNF-5	0.051 ± 0.003^{b}	22.15 ± 1.84^{d}	4.61 ± 1.00^{c}	43.60 ± 8.71^{d}	0.028 ± 0.010^{a}	59.09 ± 5.04^{b}	1.02 ± 0.07^{c}	2.56 ± 1.15^{b}
SNF-25	0.058 ± 0.006^{c}	12.60 ± 0.59^{b}	9.08 ± 1.14^{d}	28.20 ± 5.36^{e}	0.036 ± 0.008^{a}	41.74 ± 1.97^{c}	1.06 ± 0.09^{c}	0.91 ± 0.14^{d}

(1) Data are mean ± S.D.

(2) Mean values with different letters within a column are significantly different ($p < 0.05$) by ANOVA with Duncan's multiple comparison test, n=5.

(3) N.D. mean 'not detected'.

(4) WVP is 'water vapor permeability'; OP is 'oxygen permeability'.

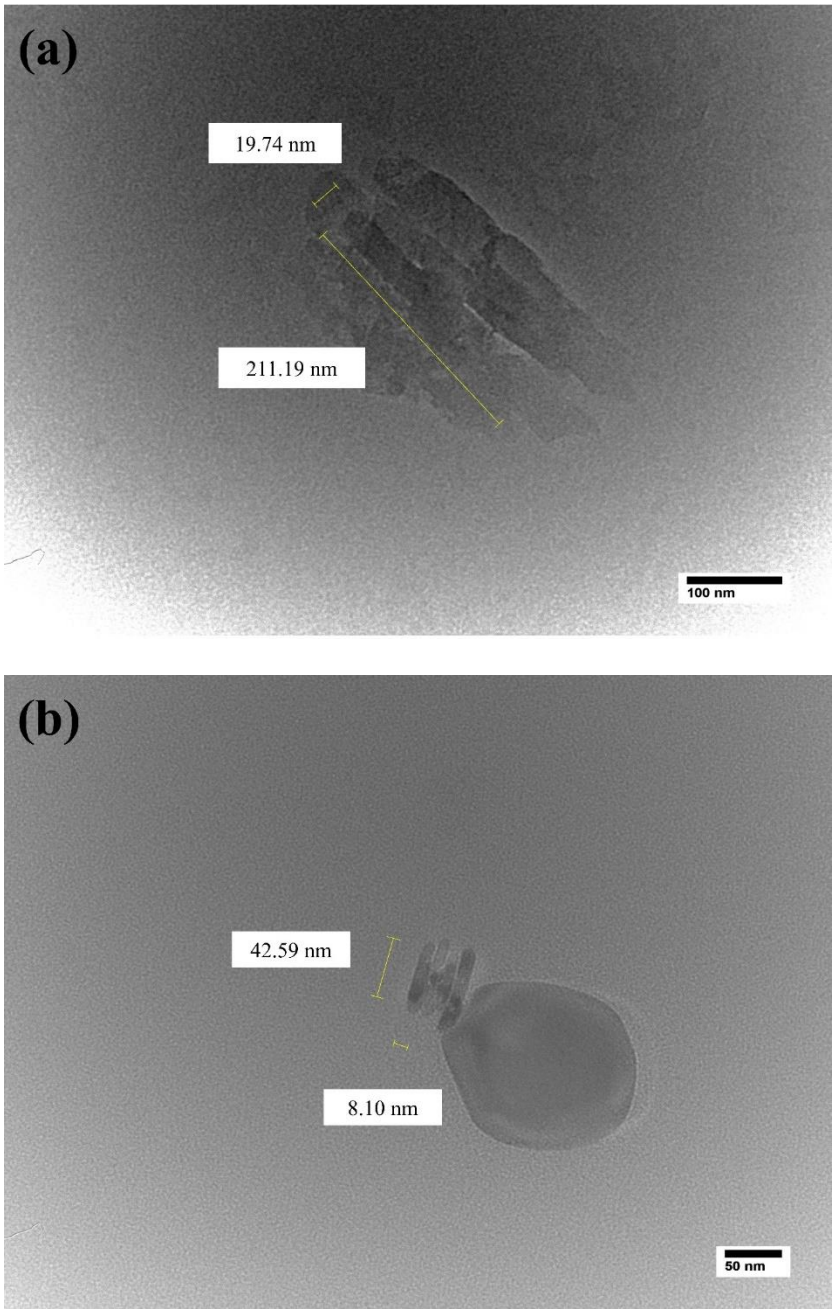

Figure 5.1. TEM images of CNCs from kombu (*Laminaria japonica*), (a); sargassum (*Sargassum natans*), (b).

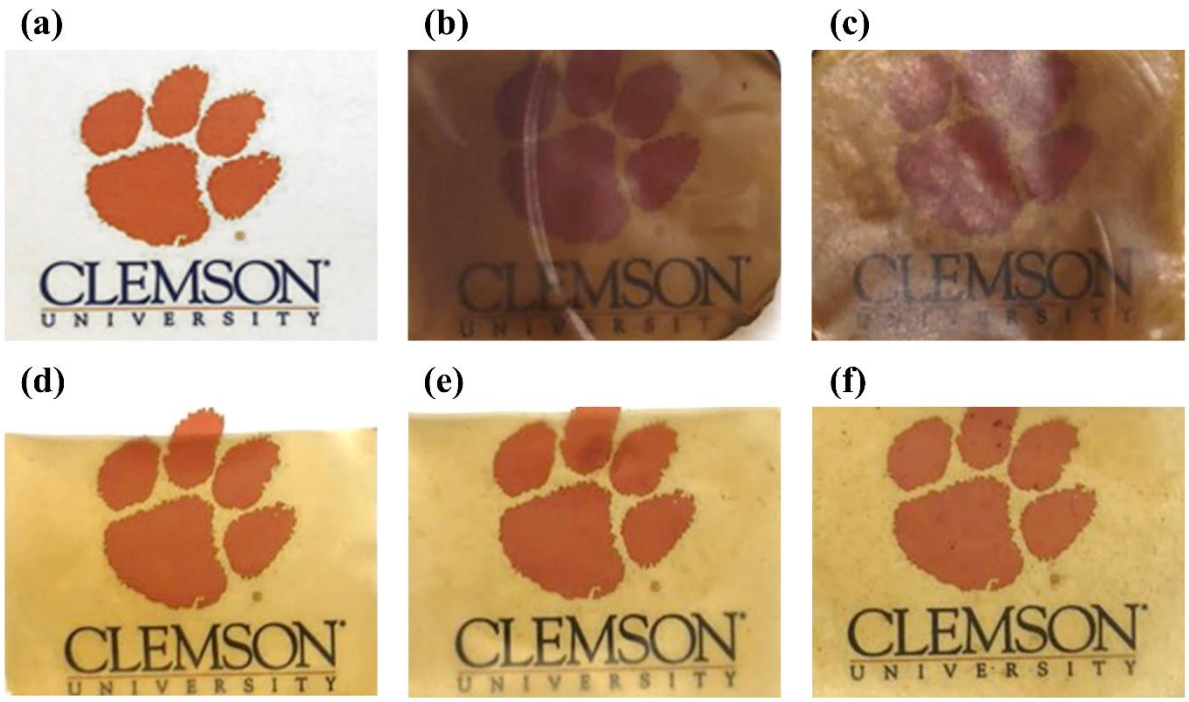

Figure 5.2. Optical images of the seaweed films. None, (a); KF, (b); KNF-5, (c); SF, (d); SNF-5, (e); SNF-25, (f).

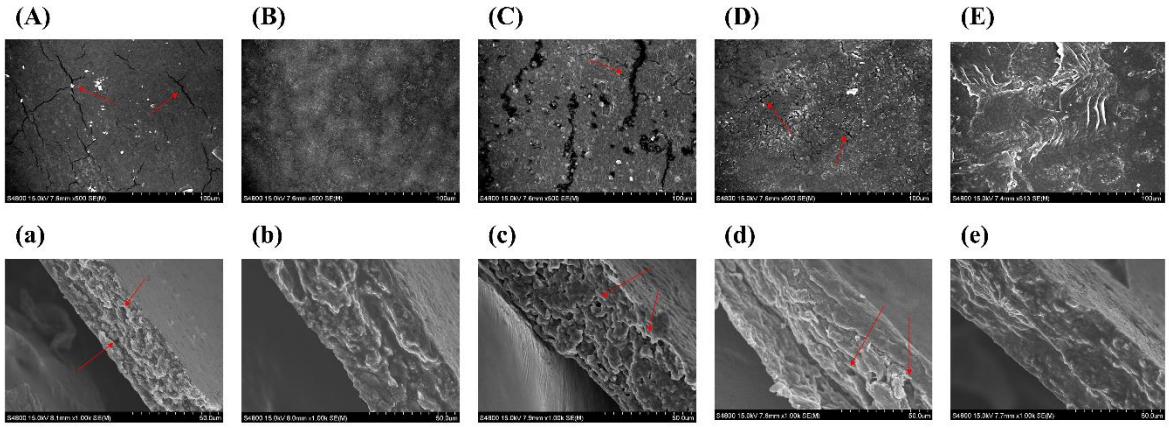

Figure 5.3**.** Scanning electron microscope images of surface and cross section of seaweed films. KF, (A) and (a); KNF-5, (B) and (b); SF, (C) and (c); SNF-5, (D) and (d); SNF-25, (E) and (e).

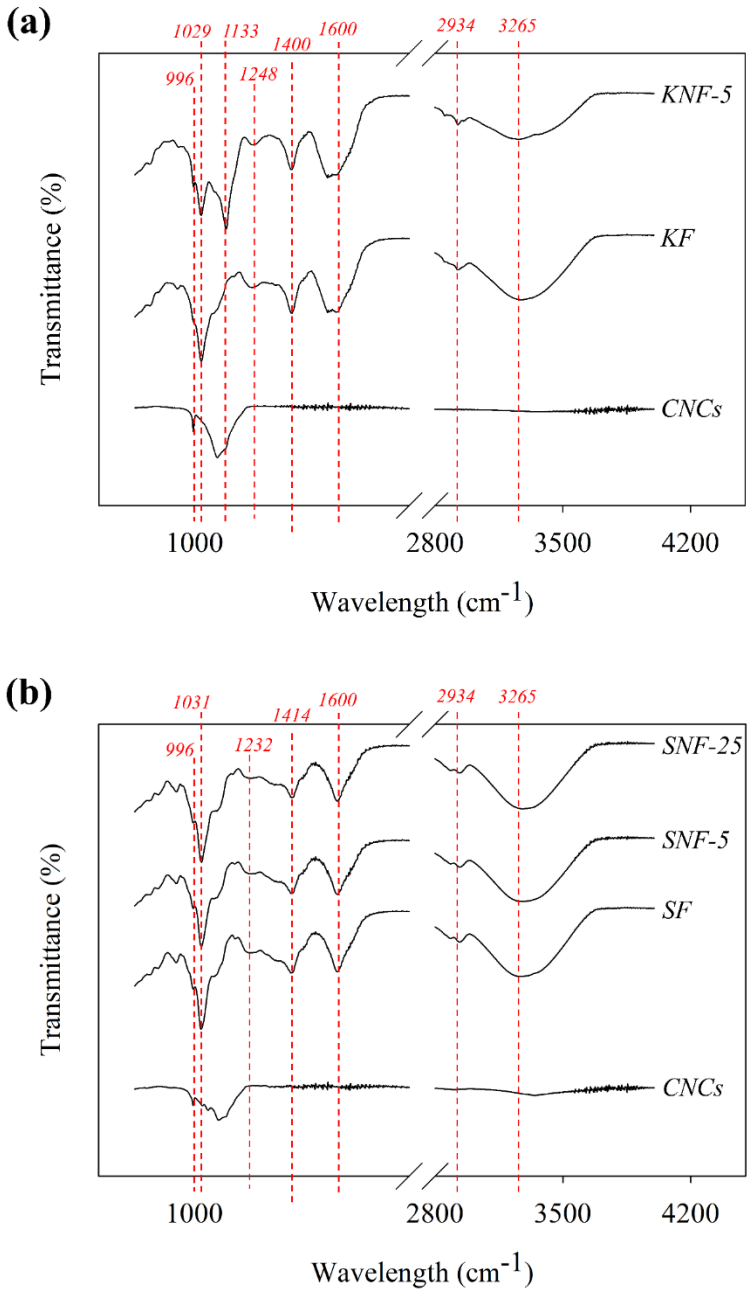

Figure 5.4. FTIR spectra of CNCs and seaweed films.

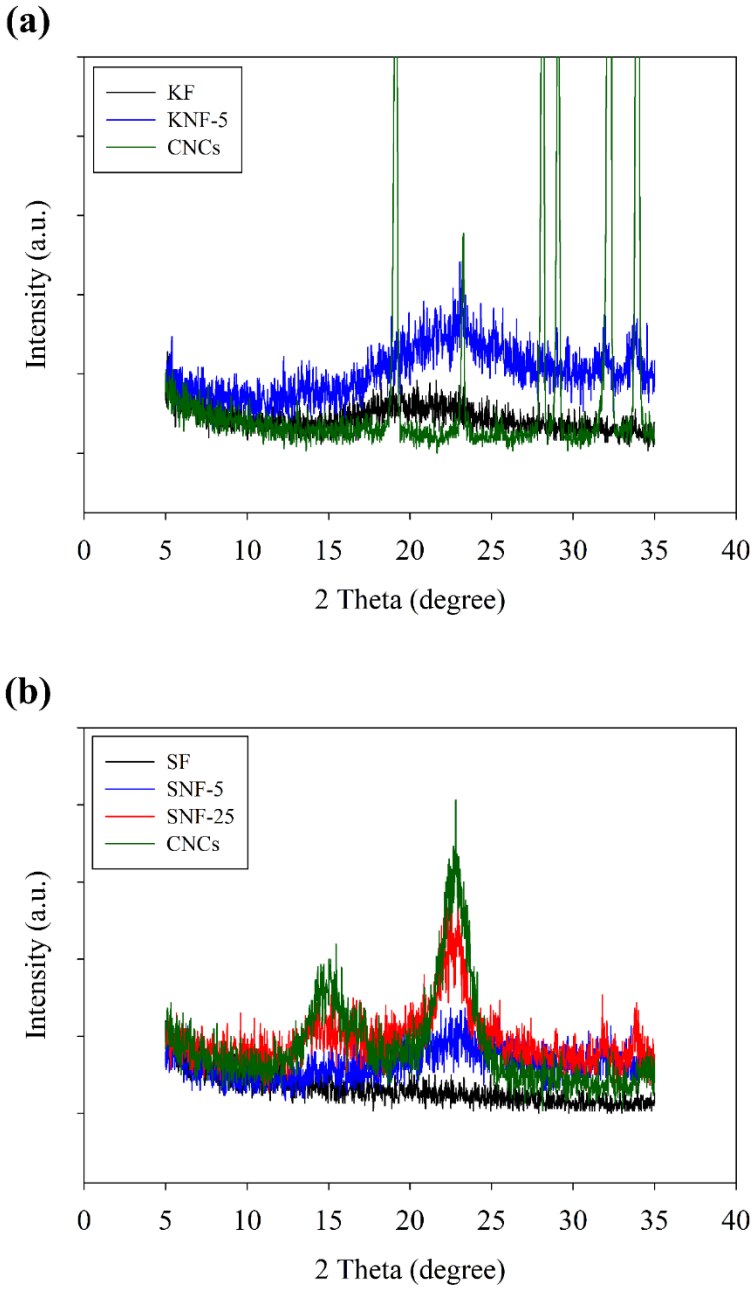

Figure 5.5. X-ray diffractograms for CNCs and seaweed films. Kombu-based film, (a); Sargassum-based film, (b).

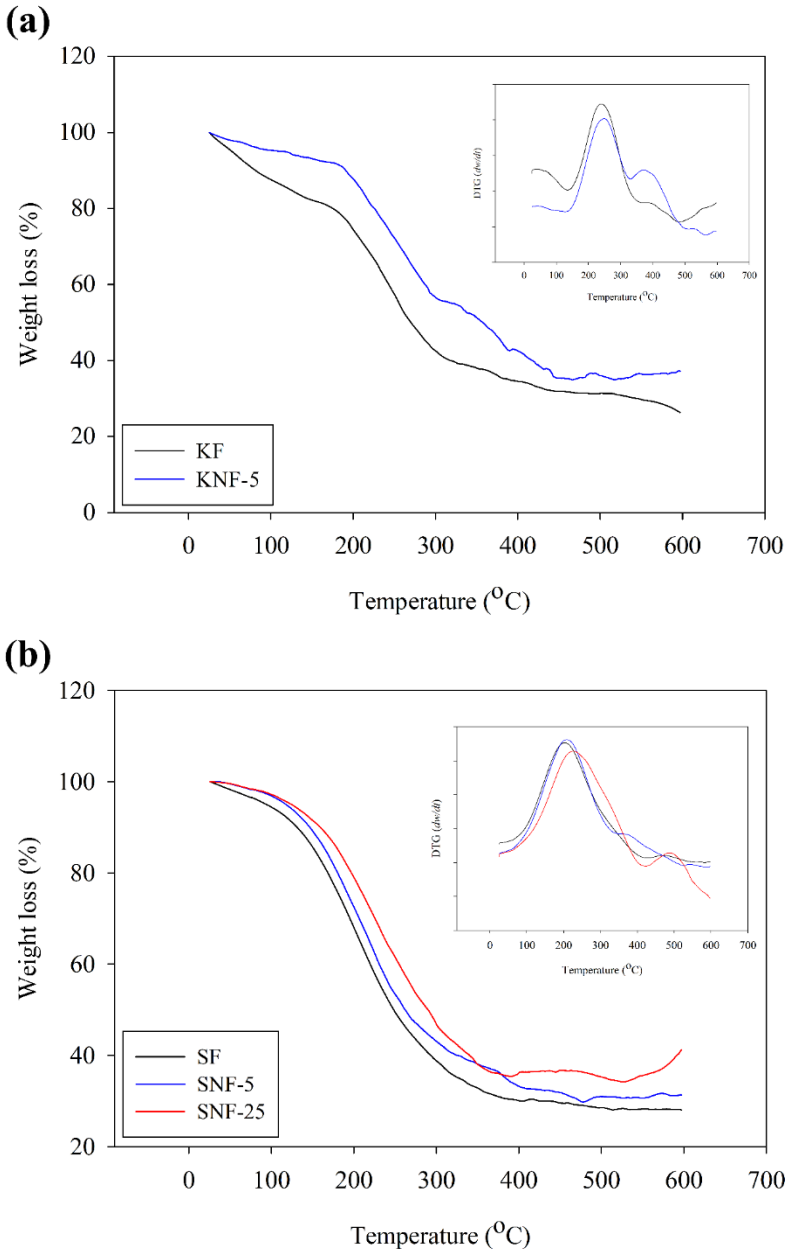

Figure 5.6. TGA and DTG curve for seaweed films. Kombu-based film, (a); Sargassum-based film, (b).

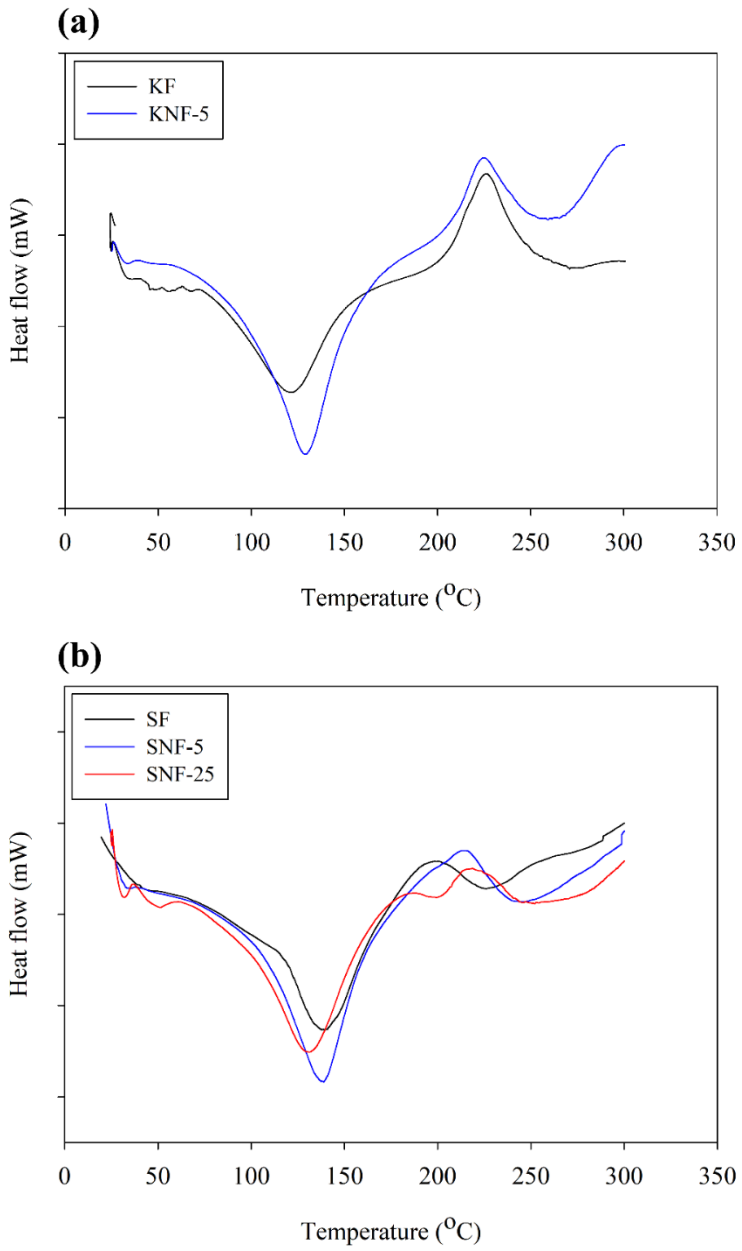

Figure 5.7. DSC curves for seaweed films. Kombu-based film, (a); Sargassum-based film, (b).

(a)

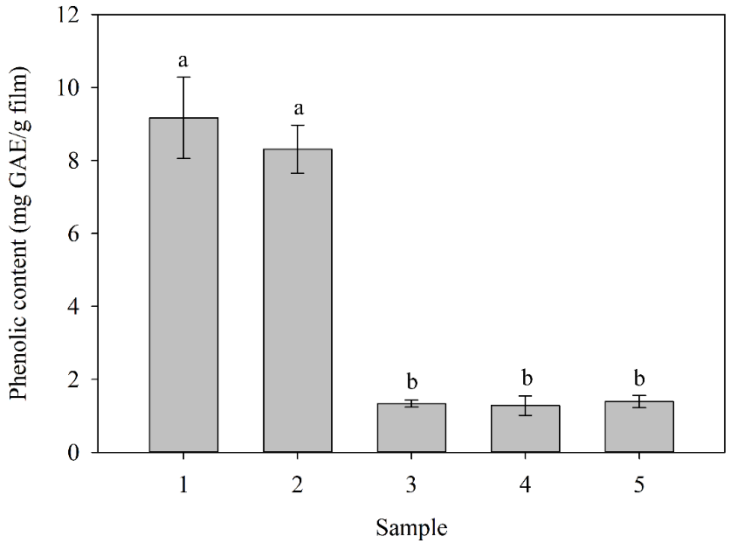
Phenolic content (mg GAE/g film)
12
10
8
6
4
2
0
a
a
b
b
b
1
2
3
4
5
Sample

(b)

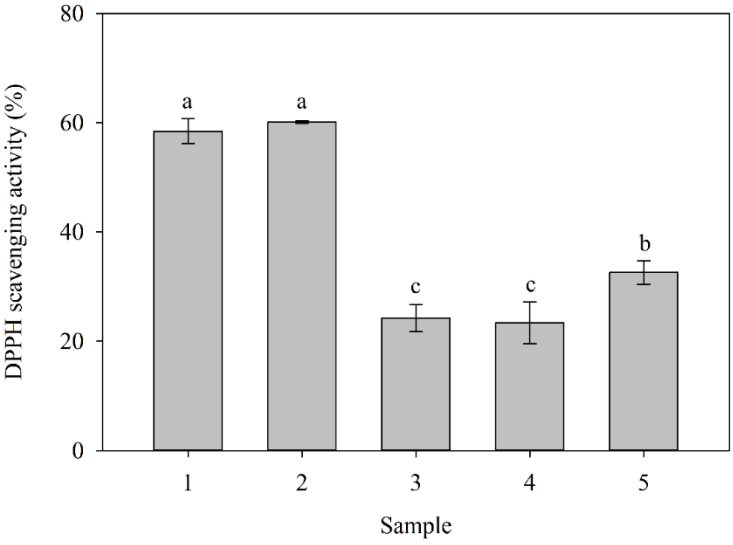
DPPH scavenging activity (%)
80
60
40
20
0
a
a
c
c
b
1
2
3
4
5
Sample

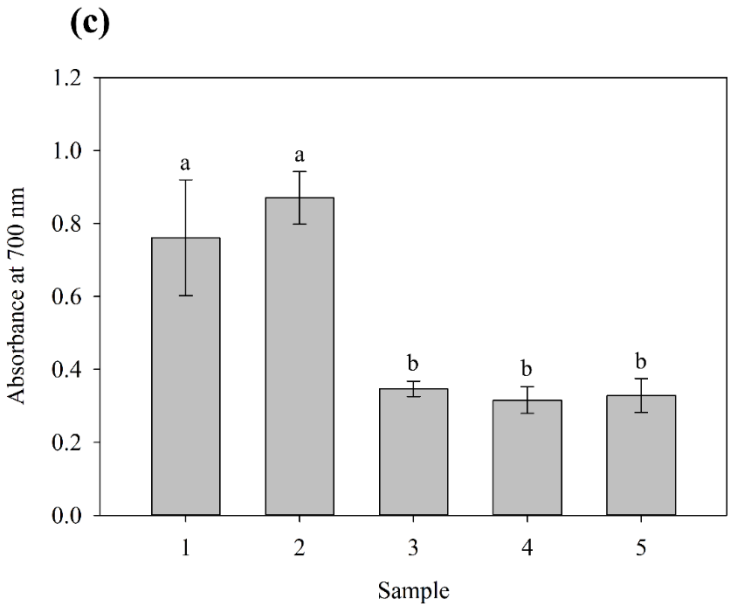

Figure 5.8. Total phenolic contents (a), DPPH radical scavenging effect (b), and reducing power (c) of seaweed films. KF, (1); KNF-5, (2); SF, (3); SNF-5, (4); SNF-25, (5).

CHAPTER SIX

Effect of cellulose nanocrystals to biodegradability with alginate and seaweed crude extracts nanocomposite films

Abstract

Petroleum-based, non-degradable plastics and their use in commercial applications cause ecological issues due to their inability to degrade or decompose naturally in the environment. Therefore, biopolymers including alginate and seaweed crude extracts with kombu (*Laminaria japonical*) and sargassum (*Sargassum natans*) were used to produce biodegradable films. These films were reinforced with cellulose nanocrystals (CNCs) isolated from seaweeds. Degradability was determined by using an indoor soil burial and lake water immersion system for a duration of 35 days. The degradation rate was evaluated by monitoring the weight loss of the films. Alginate-based films degraded up to 35% in soil burial with 28 days and 53% in lake water immersion with 7 days. Morphological observations showed wrinkles, pores, and cracks of the films after soil burial and lake water immersion. Additionally, chemical structure analysis revealed molecular interactions in polymer matrix diminished after degradation test. Thermogravimetric analysis (TGA) test results were analyzed to determine the thermal decomposition of nanocomposite films. Results from this study showed the developed films have the potential to be a novel biodegradable film that can break down naturally in the environment.

6.1. Introduction

Traditional petroleum-based, non-degradable plastics have been used for decades in various industrial applications due to their great mechanical and barrier abilities as well as cost-effectiveness (Gironi & Piemonte, 2011). However, these traditional plastics such as polyethylene (PE) and polypropylene (PP) do not degrade naturally in normal landfill operations, contributing to the potential of severe ecological problems. Over 300 million tons of petroleum-based plastics were produced in 2015; of which 34 million tons were generated as waste, with 93% of them disposed of in landfills or oceans (Mekonnen et al., 2013; Pathak et al., 2014). European countries including Germany, Netherlands, Sweden, Denmark, and Austria are achieving 80 – 100% in the recovery of the plastic wastes, however, they can only successfully recycle about 28% based on their recycling infrastructure. Also, the consumption and landfilling of petroleum-based plastics in developing countries are still rising despite the efforts to increase awareness about recycling (Muenmee et al., 2016). Therefore, the need and interest to develop biodegradable plastics have significantly increased.

The definition of biodegradation involves three important steps (Emadian et al., 2017): (1) Depolymerization: It changes the mechanical and physicochemical properties of the polymer matrix due to the activities of microorganisms or environmental factors. (2) Fragmentation: It converts from complicated polymer matrix to low carbon polymers by the action of microorganisms or surrounding conditions. (3) Mineralization: Microorganisms are supplied the energy from the fragmented low carbon polymers or carbon dioxide (CO_2), water, and biomass from the plastics. To fulfill these steps, factors

in the environment such as pH, temperature, moisture content, oxygen content, and microorganism activity should be considered (Kale et al., 2007; Massardier-Nageotte et al., 2006). Once films are exposed to these processes, the chemical structure of the film is altered in their morphology, polymer chain, crystallinity, and the complexity of polymer formula, all of which are related to the biodegradation parameters (Emadian et al., 2017).

Alginate and seaweeds biopolymers have previously been investigated as a biodegradable material and their physicochemical characteristics, material performances, and biodegradation properties have been examined (de Oliveira Filho et al., 2019; Deepa et al., 2016; Huq et al., 2012; H. Khalil et al., 2017; H. A. Khalil et al., 2017; Tran et al., 2020). Additionally, previous studies have reported cellulose nanocrystals (CNCs) can improve physical, mechanical, barrier, thermal, and biodegradation properties of biopolymer films when they acted as a reinforcement agent in the packaging system (El Achaby et al., 2018; Neto et al., 2016; Sirviö et al., 2014; Son & Seo, 2015). In our preliminary experiment, when alginate film was reinforced with 5% CNCs, the tensile strength of the film increased by approximately 35.5%. The tensile strength of kombu (*Laminaria japonica*; brown seaweed) film was increased by 21.4% when 5% CNCs were applied to the film matrix. Also, the tensile strength of sargassum (*Sargassum natans*; brown seaweed) film was increased by 14.1% and 56.3% when 5% and 25% CNCs were added, respectively. In addition to the increase in tensile strength, barrier properties including water, oxygen, and light, and the other physicochemical properties also improved (Doh, Dunno, & Whiteside, 2020). From these studies, it can be concluded that biopolymer nanocomposite films based on alginate and brown seaweed crude extract films reinforced

with CNCs show the potential of becoming a biodegradable film for a food packaging system. However, the biodegradability of the films must be further understood to determine its rate of degradation after use and disposal.

Previous studies have already tried to evaluate the biodegradability of biodegradable films with weight loss test (Dalev et al., 2000; Martucci & Ruseckaite, 2009; Patil et al., 2000; Yamano et al., 2019). The present study is designed to investigate weight loss in soil burial and lake water immersion system with alginate and seaweed biopolymer films, which are generally recognized as a biodegradable film. In addition, morphological, chemical structure, and thermal stability changes were analyzed for proving the effect of CNCs on the films and their degradation properties. Therefore, the aims of this study were: (1) to determine the biodegradation effect of alginate and seaweed crude extract films with CNCs and (2) to evaluate the physicochemical characteristics of films during the degradation test.

6.2. Materials and methods

6.2.1. Isolation of cellulose nanocrystals from brown seaweeds

Cellulose nanocrystals (CNCs) were isolated from residues after an acid-base pretreatment process of brown seaweeds (kombu; *Laminaria japonica*, sargassum; *sargassum natans*) described in a previous study (Doh, Lee, & Whiteside, 2020). Residues were stirred with 10% of potassium hydroxide to remove possible interrupted polysaccharides for 3 h at 80˚C. Then, residues were washed with distilled water and treated with excess amounts of 6.5% (w/v) sodium hypochlorite for bleaching. After that,

a pH of 5 was reached by glacial acetic acid and the sample was reacted for 2 h with magnetic stirring at 75˚C. Then, 10% of active hydrogen peroxide was used for another bleaching process at 80˚C for 70 min. Obtained cellulose went through the acid hydrolysis at 45˚C for 30 min with 51% sulfuric acid. The suspension was diluted with ice water to stop the reaction and the sample was centrifuged and washed with distilled water to eliminate the rest of the sulfuric acid. After the suspensions were adjusted to reach a pH 7, it was homogenized with ultrasonicator for 15 min with 30% amplitude (Q500 sonicator, Qsonica, USA). CNCs suspension was lyophilized to obtain powdered form of CNCs.

6.2.2. CNCs characterization

6.2.2.1. TEM

Morphological properties were analyzed with a transmission electron microscope (TEM, H-9500; Hitachi, USA). 0.005% of CNCs dissolved in distilled water was prepared and a drop of the suspension was deposited on a carbon-coated copper grid and dried overnight. The TEM grids were observed through TEM operating at an accelerating voltage of 120 kV. Image J software was used for determining the length and width of CNC particles (National Institute of Health, Bethesda, MD, USA).

6.2.2.2. FTIR

The chemical structure changes between brown seaweeds (kombu and sargassum) and CNCs were evaluated through FTIR spectrophotometer in the infrared range of 4000

– 600 cm^{-1} (Nicolet iS10, Thermo Fisher Scientific, USA). The spectra were collected in 128 scans at a resolution of 4 cm^{-1}.

6.2.2.3. XRD

X-ray diffractometer (Rigaku Ultima IV, Tokyo, Japan) was used for determining crystallinity index at a scanning rate of 5˚/min from 5˚ to 45˚ with Cu K_α radiation (λ = 1.5418 Å) using a voltage and current of 40 kV and 40 mA. The crystallinity index of the sample was calculated by the Segal method (Segal et al., 1959) using the following equation:

$$\text{Crystallinity index (\%)} = \frac{I_{200} - I_{am}}{I_{200}} \times 100$$

where, I_{200} is the maximum intensity at the plane and I_{am} is the minimum intensity at the valley between planes.

6.2.3. Film preparation

Sodium alginate (3%, w/v) was dissolved in distilled water and glycerol was added with 30% (w/w, based on the weight of sodium alginate) as a plasticizer. 5% (w/w, based on the weight of solid material) of CNCs isolated from sargassum (*Sargassum natans*; brown seaweed) were added for manufacturing alginate nanocomposite film and homogenized with an ultrasonicator for 10 min at 25% amplitude. Then, suspensions were cast by pouring into Petri dishes with 90 mm inner diameter and fully dried at 35˚C. The films were detached from the Petri dishes and soaked with 1% calcium chloride solution for 30 min for crosslinking. Films were washed several times with distilled water to remove

the excess calcium chloride present on the surface of the films. These films were dried again at 35˚C with 5 N on the film to prevent critical shrinkage of the films.

Seaweed crude extract films were formed by suspending 1.5% (w/v) crude extracts from supernatant obtained in acid-base treatment from brown seaweed, *Laminaria japonica* (kombu) and *Sargassum natans* (Sargassum) with slight modification of previous studies (Blanco-Pascual et al., 2014; Doh, Dunno, & Whiteside, 2020). Glycerol was used as plasticizer and added with 30% of the total weight of solid content. 5% and 25% of CNCs based on the dried weight of total seaweed residues was added into the suspension to kombu and sargassum film each for obtaining seaweed nanocomposite films. After homogenizing with ultrasonicator, suspension was cast into the Petri dish and dried at 35˚C. Films were detached from Petri dish after fully dried.

Alginate film without CNCs (AF), alginate film with 5% CNCs (ANF-5), kombu film without CNCs (KF), kombu film with 5% CNCs (KNF-5), sargassum film without CNCs (SF), sargassum film with 5% CNCs (SNF-5), and sargassum film with 25% CNCs (SNF-25) were developed for the experiments. Films were kept at 25˚C and 56% relative humidity (RH) for 48 h before testing for conditioning.

6.2.4 Biodegradation test

6.2.4.1. Soil degradation

Experiments were performed using plastic boxes (35 cm × 20 cm × 10 cm) contain approximately 2 kg of characterized compost soil purchased from local market (total nitrogen (ammoniacal nitrogen, nitrate nitrogen), 0.21%; available phosphate (P_2O_5),

0.11%; soluble potash (K_2O), 0.16%). Film samples were cut into square shapes (3 cm × 3 cm) and then dried until constant weight obtained. Specimens were put on an aluminum mesh to permit the access of microorganisms, moisture, and to prevent extra loss of film from soil. Specimens were buried at 6 cm depth from the soil surface to ensure aerobic conditions of degradation. The moisture content of soil was maintained around 70% (70.24 ± 1.17%) in the period of process. The pH recorded during the period of the testing was 4.51 ± 0.05. The experiment was performed at 22.85 ± 1.00˚C and 64.43 ± 3.11% relative humidity (RH) conditions. The experiment was carried out triplicate.

6.2.4.2. Lake water degradation

Lake water was obtained from in local lake park (34°42'08.3"N 82°50'28.9"W, Clemson, South Carolina). Film specimens were cut into square shapes (3 cm × 3 cm) and then dried until constant weight obtained. Specimen were placed into membrane bags with a molecular weight of 12 – 14 kDa (Sigma-Aldrich Co., St. Louis, MO, USA) for preventing extra loss of film fragments from lake water. Half of the lake water inside of the membrane was removed and replaced with fresh lake water every 1.5 days. The membrane was immersed in 1 L of lake water. Mild magnetic stirring was used for mimic water oscillation of a lake. Film fragments were collected on filter paper (Whatman No. 1) and dried. The experiment was performed at 22.85 ± 1.00˚C and 64.43 ± 3.11% RH conditions. This lake water maintained a pH of 7.37 ± 0.07 during the experimentation process. The experiment was carried out triplicate.

6.2.4.3. Weight loss determination

Initial mass of specimen was estimated after drying to minimize the effect of moisture content of the film samples. For each date of observation for soil burial and lake water immersion, the specimen was retrieved and dried at 95˚C to eliminate absorbed water molecules. The specimens were weighed to determine the average weight loss (%WL).

$$\%\mathrm{WL} = \frac{W_1 - W_2}{W_1} \times 100$$

where, W_1 is the initial mass of specimen, W_2 is the final mass after drying of specimen.

6.2.5. Morphology observation

The morphological properties of the nanocomposite films were observed using field emission scanning electron microscope S4800 (SEM; Hitach High Technologies America, Inc., USA) operated with a voltage of 15.0 kV. The samples were coated with platinum under a vacuum for 2 min.

6.2.6. Chemical structure analysis

The FTIR spectra of films were recorded in the infrared range of 4000 – 600 cm^{-1} using an FTIR spectrometer (Nicolet iS10, Thermo Fisher Scientific, USA). The spectra were collected in 128 scans at a resolution of 4 cm^{-1} for each sample.

6.2.7. Thermal stabilities analysis

Thermal properties of the biodegradable films were measured using a thermo gravimetric analysis (TGA; TA Instruments Inc., New Castle, USA). Experiment was

performed using nitrogen atmosphere. The mass of the sample (approximately 3 mg) was placed in an aluminum pan and scanned from a range of 30 to 600˚C. Heating rate was 10˚C/min.

6.2.8. Statistical analysis

All data from this research experiment is presented as the mean ± standard deviation (S.D). The data were analyzed using an analysis of variance (ANOVA). The ANOVA statistical analysis with Duncan's multiple comparison tests at a significance level of $p \leq 0.05$ was applied to the results using the Statistical Package for the Social Sciences software (SPSS, Version 20.0, SPSS Inc., Chicago, IL, USA).

6.3. Results and discussion

6.3.1. Characteristics of CNCs from seaweed biomass

CNCs were isolated from kombu (*Laminaria japonica*) and sargassum (*Sargassum natans)*. Most of the amorphous parts were successfully removed by acid hydrolysis and mechanical force. Crystalline regions were remained because of their resistance to acid hydrolysis and mechanical force (Doh, Lee, & Whiteside, 2020).

TEM images are shown in Fig. 6.1 (a). CNCs display rod and needle shapes with some aggregates. The length of CNCs was determined to be 204.3 nm and 53.6 nm from kombu and sargassum, respectively. Previous studies reported that isolated CNCs from kelp, *Laminaria japonica*, indicated the similar length varied from 239 – 1300 nm and CNCs from sargassum, *Sargassum fluitans*, also showed the similar length approximately

40 – 55 nm (Doh, Lee, & Whiteside, 2020; Feng et al., 2015; Liu et al., 2017). Morphological traits of CNCs are depended on its source. This is important because crystallinity, crystal size, and aspect ratio are usually considered as a critical factor for determining the reinforcement effect when it is applied to the polymer matrix for nanocomposite (Miao & Hamad, 2013).

FTIR spectra of kombu (*Laminaria japonica*), sargassum (*Sargassum natans)*, and their CNCs are shown in Fig. 6.1 (b). The vibrations between 1025 cm^{-1} and 1031 cm^{-1} indicated the guaiacyl ring with C=O stretching and the peak intensity of CNCs were lower than that of pure seaweeds. This is due to the amorphous parts being mostly removed (Feng et al., 2015). In addition, the peak intensities of 1416 cm^{-1} indicated the C=C stretching of aromatic hydrocarbons of lignin were weakened from seaweeds to the CNCs. These bands can also be attributed to $-CH_2$ scissoring vibration in seaweeds and disappeared due to acid hydrolysis and mechanical treatment (Kumar et al., 2014). Bands were shifted or weakened in the range of 1568 cm^{-1} and 1611 cm^{-1} from kombu and sargassum to the CNCs (Łojewska et al., 2005). This result shows the hemiacetal bonds from aldehyde groups (-CHO) opened the terminal rings by the isolation process. C-H stretching vibrations were present in the range of 2852 – 2923 cm^{-1} from kombu and sargassum, but the peaks were not on the CNCs. This is because when acid hydrolysis was performed, hydrogen ions detached from carbon (Liu et al., 2017). The intensity of bands in the range of 3000 – 3600 cm^{-1} were attributed to a hydroxyl group (O-H stretching vibration) turned weaker because the hydroxyl group of kombu and sargassum reacted in the process and amorphous regions were removed during the isolation process.

The XRD graphs of kombu (*Laminaria japonica*) and sargassum (*Sargassum natans*) and their CNCs are shown in Fig. 6.1 (c). The diffraction pattern of the CNCs was similar to previous studies (Feng et al., 2015; Liu et al., 2017; Sung et al., 2017). Previous studies indicated that the main peaks of CNCs were represented at 2θ = 14˚, 16˚, 22˚, and 34˚. CNCs isolated from kombu showed its peak at 22˚ and 34˚. In the case of sargassum CNCs, peaks were represented at 14˚, 16˚, and 22˚. Therefore, peaks of CNCs matched with peaks of cellulose type I (Rosa et al., 2010). Also, it can be found that the crystallinity index increased from seaweeds. The crystallinity index of CNCs were determined to be 98.1% and 87.3% for kombu and sargassum, respectively. With the results of TEM, FTIR, and XRD analysis, it was observed that CNCs isolation process could remove amorphous regions effectively.

6.3.2. Weight loss of biopolymer nanocomposite films

Recently, not only in landfill pollution, but also water pollution such as ocean and river, has shown to be a potential critical problem, since aquatic systems offer semi-permanent stability to organic matters (Kale et al., 2007; Sekiguchi et al., 2011; Volova et al., 2010). Therefore, this study investigated the potential of biodegradable ability by using both soil burial and lake water immersion. The weight loss test for evaluating biodegradation properties in soil and lake water system were challenging due to factors such as attached debris to the specimen and difficult to collect without damaging (Alvarez et al., 2006; Di Franco et al., 2004; Goheen & Wool, 1991; Martucci & Ruseckaite, 2009). To help the offset of these issues, the morphology, chemical structure analysis, and thermal

stabilities were determined to evaluate the degradability of the samples. Fig. 6.2 and 6.3 illustrate the images of films after different exposure times during the soil burial and lake water immersion test. Overall, each film type degraded in the process. Alginate films showed higher stability than seaweed films and seaweed nanocomposite films reinforced with CNCs could survive longer than the pure films.

Fig. 6.4 indicated the weight loss after 35 days buried in the soil. During the first day of soil burial, samples lost approximately 2% (alginate films) and 20% (seaweed films) of their initial weight due to the loss of low molecular weight compounds (Gu, 2003). According to previous reports, this results largely from glycerol and oligomers leaching out from the polymer matrix which can indicate depolymerization and fragmentation of the biodegradation process (Alvarez et al., 2006; Di Franco et al., 2004; Martucci & Ruseckaite, 2009). As storage time went by, it can be observed that glycerol, oligomers, and parts of cellulose and alginate would be adsorbed by soil debris, passed through the aluminum mesh. Both AF and ANF-5 had kept their weight loss up to 35% in Day 35 (Fig. 6.4 (a)). However, ANF-5 showed a slightly lower degradation rate than AF. The reason for weight loss in later days can be explained by metabolization of the microorganisms, which indicate mineralization (Martucci & Ruseckaite, 2009). Compared to a previous study, B. Deepa et al. reported that degradability of alginate film without cellulose nanofibril (CNF) increased up to 90% in soil with 60% of moisture content in 35 days and alginate nanocomposite film including 10% of CNF showed around 60% weight loss in the same period (Deepa et al., 2016). Conversely, seaweed crude extract films showed 88 – 100% of weight loss results at Day 28 (Fig. 6.4 (b) and (c)). Generally, kombu film showed

lower weight loss percentage compared to sargassum film, indicating higher stability. In the case of the weight loss percentage of sargassum film, SF achieved about 92% at Day 7 and that of SNF-5, SNF-25 showed about 97% and 95% at Day 28, respectively (Fig. 6.4 (c)). Previously reported results are in agreement with this study as the kombu film generally showed higher stability than sargassum film in physical, mechanical, and barrier properties (Doh, Dunno, & Whiteside, 2020). It can be inferred that the enhanced bonding strength affected the weight loss in the soil burial system as the films were more stable as CNCs concentration increased. Also, it is in accordance with Fig. 6.2. The main reason for weight loss for the seaweed films was the biodegradation process including depolymerization, fragmentation, and mineralization, as well as the effect of burial conditions, such as a high moisture environment.

In the case of in lake water immersion system, alginate films did not show any deformation, however, seaweed film dissolved very easily (Fig. 6.5). Besides, degradability was higher than the soil burial system. Seaweed films showed a significantly higher degradation rate compared to alginate films ($p < 0.05$). Also, nanocomposite films were more stable than films without CNCs. The result of weight loss in AF and ANF-5 was not constant but trends showed ANF-5 had slightly lower weight loss percentage than AF. AF had a 53.65 ± 4.25% weight loss at Day 28 and ANF-5 reported 25.01 ± 9.47% weight loss at Day 35. This weight loss was mainly attributed to small molecules such as glycerol or oligomers which are easily dissolved in the lake water system (Kale et al., 2007; Martucci & Ruseckaite, 2009). In the case of seaweed films, they were fully degraded in 7 days. KF was dissolved in 3 days and SF was not even able to be observed after one day.

SNF-5 remained at Day 3 with 93.07 ± 2.81% of weight loss and KNF-5 and SNF-25 could survive by 7 days (96.04 ± 0.99% and 93.18 ± 0.89% of weight loss, respectively). There are two main reasons of weight loss. According to a previous study, the lake water derived for this study was from Lake Keowee, includes many microorganisms such as *Psudomonas*, *Bacillus*, *Streptococcus,* and *Aerobacter spp.* (Guthrie et al., 1974). Activities of these microorganism activities could affect the degradation of films. Since AF and ANF-5 showed higher water resistance ability in the previous study, it can be inferred that this is the main reason for weight loss of alginate films. However, in the case of seaweeds crude extract films, high moisture condition is probably more attributed to weight loss than microbial activity in lake water immersion system due to its high water sensitivities Doh, Dunno, & Whiteside, 2020). Chemically modified gelatin films showed similar degradation rates in lake and river water systems (Patil et al., 2000).

Some studies reported the addition of CNCs to polymer matrix can improve biodegradation properties (F. Ferreira et al., 2018; Rhim & Kim, 2014). The reason for this tendency is related to the depolymerization of the polymer matrix by hydrophilic nature of CNCs. Biodegradation by microorganisms with enzyme is usually hydrophilic and can consume the CNCs during degradation which leads to the more porous polymer matrix. As a result, the addition of CNCs can enhance biodegradation (Dieckow et al., 2009; Garcia-Garcia et al., 2018). Also, degradation rate of polymer matrix can be significantly promoted by water molecules due to the hydrolysis of polymer chains, especially for heterogeneous polymers such as composite materials (F. V. Ferreira et al., 2019; Mohanty & Nayak, 2012). However, it was observed that the opposite result happened for this study in that the

nanocomposite film showed lower degradability than pure film. This is because of the crystallinity and crystal size of the CNCs from seaweeds (kombu and sargassum) (Arrieta et al., 2015; Bahari et al., 1998; El-Hadi et al., 2002; Kanesawa et al., 1994; Tomasi, Scandola et al., 1996). Since crystalline regions are more resistant to the hydrolysis, the crystallinity and crystal size affects the degradation rate of the polymer matrix (F. Ferreira et al., 2018). As already mentioned, crystallinity of CNCs of this study was very high, for instance, 98.1% and 87.3% for CNCs from kombu and sargassum. With the high crystallinity, crystal sizes are also relatively short compared to the previous studies, 204.3 nm and 53.6 nm for CNCs from kombu and sargassum (Miao & Hamad, 2013; Son & Seo, 2015). These factors can affect the degradation ratio by biodegradation process or hydrolysis with water molecules. This phenomenon indicates there might be an increased potential to use seaweed biopolymer films as packaging materials due to the polymer matrix needing more molecular interaction due to its lower bonding strength.

6.3.3. Morphological analysis

Fig. 6.6 shows SEM images of film surfaces after exposure to soil burial and lake water immersion. AF and ANF-5 at Day 0 showed a smooth surface (Fig. 6.6 (a)). However, at Day 35 of the soil burial, both the surfaces of AF and ANF-5 displayed wrinkles and pinholes due to the degradation of polymeric matrix (Ikada, 1999). This can be attributed to the fragmentation or hydrolysis of water-soluble compounds including glycerol, parts of cellulose, monomers, and alginate that are not strongly connected in the

polymer matrix (Martucci & Ruseckaite, 2009; Patil et al., 2000). Surfaces of films in lake water system at Day 35 showed similar wrinkles and pinholes as well.

In contrast, the seaweed nanocomposite films showed significant changes on the surface compared to alginate films KNF-5 and SNF-25 indicated in Fig. 6.6 (b). Before exposing to the soil or lake water system (time: Day 0), the surface of seaweed films presented some heterogeneousity because of solvent evaporations from film casting process (Doh, Dunno, & Whiteside, 2020). After 14 days in soil burial, surface showed irregular surface with lots of porosity, cracks, and channels as a result of the depolymerization, fragmentation, and leaching of compounds including glycerol, polysaccharides of seaweed biomass by microbial activity and hydrolysis. These factors intensified as burial time was prolonged and attributable to the disconnection of molecular interactions. Fig. 6.2 supports this statement. When the seaweed nanocomposite film samples were tested in the lake water systems, specimen also showed surface deformations for both KNF-5 and SNF-5 at Day 3. This is mainly attributed to hydrolysis of molecular interactions by water molecules could be dissolved in the lake water system. The observations of Fig. 6.6 suggested that after degradation process, films were able to be invaded not only the surfaces but also penetrated into the polymer matrix.

6.3.4. Chemical structure analysis

FTIR results indicated there were changes in the chemical structures of the films (Fig. 6.7). Since crude extract suspension for producing seaweed films mostly includes alginate, the spectra of alginate and seaweed films showed similar shape (Blanco-Pascual

et al., 2014; Doh, Dunno, & Whiteside, 2020). The absorption peaks shown at around 1025 and 1031 cm^{-1} indicate the presence of guluronic and mannuronic acids which are the part of alginate, respectively (Paula et al., 2015). Besides, the absorption peaks at near 1416 and 1600 cm^{-1} are related to the asymmetric and symmetric stretching vibrations of the carboxyl group of alginate and CNCs (Gao et al., 2017). Also, peaks around 1589 and 1600 cm^{-1} can correspond to the -CHO and carbonyl bond (C=O) which can indicate glycerol or low carbon biomass. The absorption bands at 2930 cm^{-1} are mainly attributed to the symmetric and asymmetric stretching vibration of C-H bonds in aliphatic chains (Gao et al., 2017; Huq et al., 2012). Peaks at 3200 cm^{-1} are mainly ascribed to the stretching vibration of O-H group in aliphatic chain (El Miri et al., 2018).

It was observed that the main peaks of AF were decreased significantly after exposure to both soil burial and lake water immersion system (Fig. 6.7 (a)). ANF-5 showed similar trends but showed that the ratio of decreased intensities was much lower than that of AF due to the addition of the CNCs (Fig. 6.7 (b)). The addition of CNCs improves the bonding strength inside of the backbone polymer matrix. This result correlates well with the weight loss test. Fig. 6.7 (c) and (d) showed the spectra of KNF-5 and SNF-25, respectively. Similar to alginate films, the result of KNF-5 and SNF-25 indicated significant decreasing of intensities occurred in all main peaks. Additionally, intensities of peaks shown at 1133 cm^{-1} and 1248 cm^{-1} correspond to C-O stretching shown in KNF-5 and 996 cm^{-1}, indicating C=C bending in SNF-25 was decreased.

Intensities of peaks were decreased in the FTIR spectra as biodegradation process time went by and these results agreed with the reduction of chemical interaction. This

indicates the obvious evidence for degradation in soil burial and lake water immersion system. Observations from the morphology test also support these results, suggesting that the molecular bonding can be disconnected after the degradation test.

6.3.5. Thermal stabilities analysis

Fig. 6.8 shows the thermogravimetric analysis (TGA) graph and derivative thermogravimetry (DTG) curves of the films at Day 0 and after exposure to soil burial and lake water immersion. The onset thermal decomposition temperature (T_{on}) of AF and ANF-5 have been appeared in the different temperature, however, the tendency is similar (Fig. 6.8 (a) and (b)). Prior to the degradation tests, the T_{on} of AF and ANF-5 was analyzed to 202˚C and 208˚C, respectively. After 35 days, AF showed 186˚C and 184˚C, ANF-5 presented 191˚C and 189˚C of T_{on} when they were exposed to soil and lake water system, respectively. These results indicated that the addition of CNCs can improve the thermal stability of the film. Also, as it can be found in the DTG graphs, the results indicate that the films prior to the degradation test showed lower weight loss and higher inflection point which suggest higher thermal stability. Ferreira et al. supports these claims, reporting that since the CNCs are the nucleating agent, it can lead to an increase of melting temperature (T_m), crystallization temperature (T_c), and degree of crystallinity (X_c) of the polymer (F. Ferreira et al., 2018). In the case of ANF-5, second degradation which occurred by the degradation of glycosidic bonds in cellulosic parts, decarboxylation, decarbonylation, and hydration of alginate was found after the degradation process. The second degradation in lake water system (458˚C) showed faster degradation than soil system (490˚C) and both

results were lower than that for pure film. This occurrence can be attributed from its weakened bonding strength (El Miri et al., 2018; Huq et al., 2012).

Fig. 6.8. (c) and (d) presented the results of KNF-5 and SNF-25. After degradation test, both films showed different tendency compared to AF and ANF-5, and unstable thermal degradation. T_{on} of KNF-5 is 218˚C and it increased as 231˚C and 222˚C after soil burial and lake water immersion test. Similar to KNF-5, T_{on} of SNF-25 is 198˚C and it increased as 230˚C and 247˚C after soil burial and lake water immersion test. Previous studies reported this result was due to the anti-nucleating agent activity of CNCs (Chen et al., 2017; Lv et al., 2017). When CNCs acted as an anti-nucleating agent, crystallinity of nanocomposite matrix was lower than pure polymer matrix. However, since crystallinity index of kombu and sargassum film increased after CNCs addition (Doh, Dunno, & Whiteside, 2020), the TGA results from this study show the effect of many factors including molecular interactions, molecular weight, and chain flexibility in the thermal stability test (Chaichi et al., 2017; Krishnamachari et al., 2009). In addition, small debris, many random extracts from seaweeds, and the other interrupted particles attached on the surface could influence the ability to determine thermal stability of the films.

6.4. Conclusions

Effect of cellulose nanocrystals after biodegradation test with indoor soil burial and lake water immersion was performed with alginate and seaweed nanocomposite films reinforced with cellulose nanocrystals (CNCs). CNCs were successfully isolated from two different brown seaweeds, kombu and sargassum. Biodegradation mainly occurred due to

microbial activities and hydrolysis by water molecules in the soil burial and lake water systems. Weight loss test showed the addition of CNCs to the films rendered degradation rate slower than the films without the addition of the CNCs due to its reinforcement effect to molecular bonding strength in the polymer matrix, especially for the high crystallinity and small crystal size of CNCs from seaweeds. SEM images showed that wrinkles, holes, pores, and cracks were observed in the later stages of the degradation process. These results are in agreement with chemical structure analysis data. FTIR spectra showed the diminishing intensity of peaks after the degradation process around 1025, 1416, 1589, 1600, 2930 and 3200 cm^{-1} indicated the main molecular interactions of alginate and CNCs. At last, TGA and DTG plots showed nanocomposite films presented higher thermal stabilities due to the nucleating effect of CNCs. Results reported in this study suggest that the degradation of biopolymer nanocomposite films with CNCs could be prolonged during the biodegradation process with enhanced molecular bonding strength.

6.5. References

Alvarez, V. A., Ruseckaite, R., & Vazquez, A. (2006). Degradation of sisal fibre/Mater Bi-Y biocomposites buried in soil. *Polymer Degradation and Stability, 91*(12), 3156-3162.

Arrieta, M. P., Fortunati, E., Dominici, F., López, J., & Kenny, J. M. (2015). Bionanocomposite films based on plasticized PLA–PHB/cellulose nanocrystal blends. *Carbohydrate polymers, 121*, 265-275.

Bahari, K., Mitomo, H., Enjoji, T., Yoshii, F., & Makuuchi, K. (1998). Degradability of

poly (3-hydroxybutyrate) and its copolymer grafted with styrene by radiation. *Polymer Degradation and Stability, 61*(2), 245-252.

Blanco-Pascual, N., Montero, M., & Gómez-Guillén, M. (2014). Antioxidant film development from unrefined extracts of brown seaweeds Laminaria digitata and Ascophyllum nodosum. *Food hydrocolloids, 37*, 100-110.

Chaichi, M., Hashemi, M., Badii, F., & Mohammadi, A. (2017). Preparation and characterization of a novel bionanocomposite edible film based on pectin and crystalline nanocellulose. *Carbohydrate polymers, 157*, 167-175.

Chen, J., Wu, D., Tam, K. C., Pan, K., & Zheng, Z. (2017). Effect of surface modification of cellulose nanocrystal on nonisothermal crystallization of poly (β-hydroxybutyrate) composites. *Carbohydrate polymers, 157*, 1821-1829.

Dalev, P., Patil, R., Mark, J., Vassileva, E., & Fakirov, S. (2000). Biodegradation of chemically modified gelatin films in soil. *Journal of applied polymer science, 78*(7), 1341-1347.

de Oliveira Filho, J. G., Rodrigues, J. M., Valadares, A. C. F., de Almeida, A. B., de Lima, T. M., Takeuchi, K. P., . . . Dyszy, F. H. (2019). Active food packaging: Alginate films with cottonseed protein hydrolysates. *Food hydrocolloids*.

Deepa, B., Abraham, E., Pothan, L. A., Cordeiro, N., Faria, M., & Thomas, S. (2016). Biodegradable nanocomposite films based on sodium alginate and cellulose nanofibrils. *Materials, 9*(1), 50.

Di Franco, C., Cyras, V. P., Busalmen, J. P., Ruseckaite, R. A., & Vázquez, A. (2004). Degradation of polycaprolactone/starch blends and composites with sisal fibre.

Polymer Degradation and Stability, 86(1), 95-103.

Dieckow, J., Bayer, C., Conceição, P., Zanatta, J., Martin-Neto, L., Milori, D., . . . Hernani, L. (2009). Land use, tillage, texture and organic matter stock and composition in tropical and subtropical Brazilian soils. *European Journal of Soil Science, 60*(2), 240-249.

Doh, H., Dunno, K. D., & Whiteside, W. S. (2020). Preparation of novel seaweed nanocomposite film from brown seaweeds Laminaria japonica and Sargassum natans. *Food hydrocolloids, 105*, 105744.

Doh, H., Lee, M. H., & Whiteside, W. S. (2020). Physicochemical characteristics of cellulose nanocrystals isolated from seaweed biomass. *Food hydrocolloids, 102*, 105542.

El-Hadi, A., Schnabel, R., Straube, E., Müller, G., & Henning, S. (2002). Correlation between degree of crystallinity, morphology, glass temperature, mechanical properties and biodegradation of poly (3-hydroxyalkanoate) PHAs and their blends. *Polymer testing, 21*(6), 665-674.

El Achaby, M., Kassab, Z., Aboulkas, A., Gaillard, C., & Barakat, A. (2018). Reuse of red algae waste for the production of cellulose nanocrystals and its application in polymer nanocomposites. *International journal of biological macromolecules, 106*, 681-691.

El Miri, N., Aziz, F., Aboulkas, A., El Bouchti, M., Ben Youcef, H., & El Achaby, M. (2018). Effect of plasticizers on physicochemical properties of cellulose nanocrystals filled alginate bionanocomposite films. *Advances in Polymer Technology, 37*(8), 3171-

3185.

Emadian, S. M., Onay, T. T., & Demirel, B. (2017). Biodegradation of bioplastics in natural environments. *Waste management, 59*, 526-536.

Feng, X., Meng, X., Zhao, J., Miao, M., Shi, L., Zhang, S., & Fang, J. (2015). Extraction and preparation of cellulose nanocrystals from dealginate kelp residue: structures and morphological characterization. *Cellulose, 22*(3), 1763-1772.

Ferreira, F., Dufresne, A., Pinheiro, I., Souza, D., Gouveia, R., Mei, L., & Lona, L. (2018). How do cellulose nanocrystals affect the overall properties of biodegradable polymer nanocomposites: a comprehensive review. *European Polymer Journal, 108*, 274-285.

Ferreira, F. V., Cividanes, L. S., Gouveia, R. F., & Lona, L. M. (2019). An overview on properties and applications of poly (butylene adipate-co-terephthalate)–PBAT based composites. *Polymer Engineering & Science, 59*(s2), E7-E15.

Gao, C., Pollet, E., & Avérous, L. (2017). Properties of glycerol-plasticized alginate films obtained by thermo-mechanical mixing. *Food hydrocolloids, 63*, 414-420.

Garcia-Garcia, D., Lopez-Martinez, J., Balart, R., Strömberg, E., & Moriana, R. (2018). Reinforcing capability of cellulose nanocrystals obtained from pine cones in a biodegradable poly (3-hydroxybutyrate)/poly (ε-caprolactone)(PHB/PCL) thermoplastic blend. *European Polymer Journal, 104*, 10-18.

Gironi, F., & Piemonte, V. (2011). Bioplastics and petroleum-based plastics: strengths and weaknesses. *Energy Sources, Part A: Recovery, Utilization, and Environmental Effects, 33*(21), 1949-1959.

Goheen, S., & Wool, R. (1991). Degradation of polyethylene–starch blends in soil. *Journal of applied polymer science, 42*(10), 2691-2701.

Gu, J.-D. (2003). Microbiological deterioration and degradation of synthetic polymeric materials: recent research advances. *International Biodeterioration & Biodegradation, 52*(2), 69-91.

Guthrie, R., Cherry, D. t., & Ferebee, R. (1974). A comparison of thermal loading effects on bacterial populations in polluted and non-polluted aquatic systems. *Water Research, 8*(3), 143-148.

Huq, T., Salmieri, S., Khan, A., Khan, R. A., Le Tien, C., Riedl, B., . . . Kamal, M. R. (2012). Nanocrystalline cellulose (NCC) reinforced alginate based biodegradable nanocomposite film. *Carbohydrate polymers, 90*(4), 1757-1763.

Ikada, E. (1999). Electron microscope observation of biodegradation of polymers. *Journal of environmental polymer degradation, 7*(4), 197-201.

Kale, G., Kijchavengkul, T., Auras, R., Rubino, M., Selke, S. E., & Singh, S. P. (2007). Compostability of bioplastic packaging materials: an overview. *Macromolecular bioscience, 7*(3), 255-277.

Kanesawa, Y., Tanahashi, N., Doi, Y., & Saito, T. (1994). Enzymatic degradation of microbial poly (3-hydroxyalkanoates). *Polymer Degradation and Stability, 45*(2), 179-185.

Khalil, H., Tye, Y., Saurabh, C., Leh, C., Lai, T., Chong, E., . . . Syakir, M. (2017). Biodegradable polymer films from seaweed polysaccharides: A review on cellulose as a reinforcement material. *Express Polymer Letters, 11*(4).

Khalil, H. A., Saurabh, C. K., Tye, Y., Lai, T., Easa, A., Rosamah, E., . . . Fizree, H. (2017). Seaweed based sustainable films and composites for food and pharmaceutical applications: A review. *Renewable and Sustainable Energy Reviews, 77*, 353-362.

Krishnamachari, P., Zhang, J., Lou, J., Yan, J., & Uitenham, L. (2009). Biodegradable poly (lactic acid)/clay nanocomposites by melt intercalation: a study of morphological, thermal, and mechanical properties. *International Journal of Polymer Analysis and Characterization, 14*(4), 336-350.

Kumar, A., Negi, Y. S., Choudhary, V., & Bhardwaj, N. K. (2014). Characterization of cellulose nanocrystals produced by acid-hydrolysis from sugarcane bagasse as agro-waste. *Journal of Materials Physics and Chemistry, 2*(1), 1-8.

Liu, Z., Li, X., Xie, W., & Deng, H. (2017). Extraction, isolation and characterization of nanocrystalline cellulose from industrial kelp (Laminaria japonica) waste. *Carbohydrate polymers, 173*, 353-359.

Łojewska, J., Miśkowiec, P., Łojewski, T., & Proniewicz, L. (2005). Cellulose oxidative and hydrolytic degradation: In situ FTIR approach. *Polymer Degradation and Stability, 88*(3), 512-520.

Lv, Q., Xu, C., Wu, D., Wang, Z., Lan, R., & Wu, L. (2017). The role of nanocrystalline cellulose during crystallization of poly (ε-caprolactone) composites: Nucleation agent or not? *Composites Part A: Applied Science and Manufacturing, 92*, 17-26.

Martucci, J. F., & Ruseckaite, R. A. (2009). Biodegradation of three-layer laminate films based on gelatin under indoor soil conditions. *Polymer Degradation and Stability, 94*(8), 1307-1313.

Massardier-Nageotte, V., Pestre, C., Cruard-Pradet, T., & Bayard, R. (2006). Aerobic and anaerobic biodegradability of polymer films and physico-chemical characterization. *Polymer Degradation and Stability, 91*(3), 620-627.

Mekonnen, T., Mussone, P., Khalil, H., & Bressler, D. (2013). Progress in bio-based plastics and plasticizing modifications. *Journal of Materials Chemistry A, 1*(43), 13379-13398.

Miao, C., & Hamad, W. Y. (2013). Cellulose reinforced polymer composites and nanocomposites: a critical review. *Cellulose, 20*(5), 2221-2262.

Mohanty, S., & Nayak, S. (2012). Biodegradable nanocomposites of poly (butylene adipate-co-terephthalate)(PBAT) and organically modified layered silicates. *Journal of Polymers and the Environment, 20*(1), 195-207.

Muenmee, S., Chiemchaisri, W., & Chiemchaisri, C. (2016). Enhancement of biodegradation of plastic wastes via methane oxidation in semi-aerobic landfill. *International Biodeterioration & Biodegradation, 113*, 244-255.

Neto, W. P. F., Mariano, M., da Silva, I. S. V., Silvério, H. A., Putaux, J.-L., Otaguro, H., . . . Dufresne, A. (2016). Mechanical properties of natural rubber nanocomposites reinforced with high aspect ratio cellulose nanocrystals isolated from soy hulls. *Carbohydrate polymers, 153*, 143-152.

Pathak, S., Sneha, C., & Mathew, B. B. (2014). Bioplastics: its timeline based scenario & challenges. *Journal of Polymer and Biopolymer Physics Chemistry, 2*(4), 84-90.

Patil, R., Dalev, P., Mark, J., Vassileva, E., & Fakirov, S. (2000). Biodegradation of chemically modified gelatin films in lake and river waters. *Journal of applied*

polymer science, 76(1), 29-37.

Paula, G. A., Benevides, N. M., Cunha, A. P., de Oliveira, A. V., Pinto, A. M., Morais, J. P. S., & Azeredo, H. M. (2015). Development and characterization of edible films from mixtures of κ-carrageenan, ι-carrageenan, and alginate. *Food hydrocolloids, 47*, 140-145.

Rhim, J.-W., & Kim, Y.-T. (2014). Biopolymer-based composite packaging materials with nanoparticles. In *Innovations in food packaging* (pp. 413-442): Elsevier.

Rosa, M., Medeiros, E., Malmonge, J., Gregorski, K., Wood, D., Mattoso, L., . . . Imam, S. (2010). Cellulose nanowhiskers from coconut husk fibers: Effect of preparation conditions on their thermal and morphological behavior. *Carbohydrate polymers, 81*(1), 83-92.

Sekiguchi, T., Saika, A., Nomura, K., Watanabe, T., Watanabe, T., Fujimoto, Y., . . . Kanehiro, H. (2011). Biodegradation of aliphatic polyesters soaked in deep seawaters and isolation of poly (ε-caprolactone)-degrading bacteria. *Polymer Degradation and Stability, 96*(7), 1397-1403.

Sirviö, J. A., Kolehmainen, A., Liimatainen, H., Niinimäki, J., & Hormi, O. E. (2014). Biocomposite cellulose-alginate films: Promising packaging materials. *Food chemistry, 151*, 343-351.

Son, H. N., & Seo, Y. B. (2015). Physical and bio-composite properties of nanocrystalline cellulose from wood, cotton linters, cattail, and red algae. *Cellulose, 22*(3), 1789-1798.

Sung, S. H., Chang, Y., & Han, J. (2017). Development of polylactic acid nanocomposite

films reinforced with cellulose nanocrystals derived from coffee silverskin. *Carbohydrate polymers, 169*, 495-503.

Tomasi, G., Scandola, M., Briese, B. H., & Jendrossek, D. (1996). Enzymatic degradation of bacterial poly (3-hydroxybutyrate) by a depolymerase from Pseudomonas lemoignei. *Macromolecules, 29*(2), 507-513.

Tran, T. T., Roach, P., Nguyen, M. H., Pristijono, P., & Vuong, Q. V. (2020). Development of biodegradable films based on seaweed polysaccharides and Gac pulp (Momordica cochinchinensis), the waste generated from Gac oil production. *Food hydrocolloids, 99*, 105322.

Volova, T., Boyandin, A., Vasiliev, A., Karpov, V., Prudnikova, S., Mishukova, O., . . . Xuân, B. B. (2010). Biodegradation of polyhydroxyalkanoates (PHAs) in tropical coastal waters and identification of PHA-degrading bacteria. *Polymer Degradation and Stability, 95*(12), 2350-2359.

Yamano, N., Kawasaki, N., Ida, S., & Nakayama, A. (2019). Biodegradation of polyamide 4 in seawater. *Polymer Degradation and Stability, 166*, 230-236.

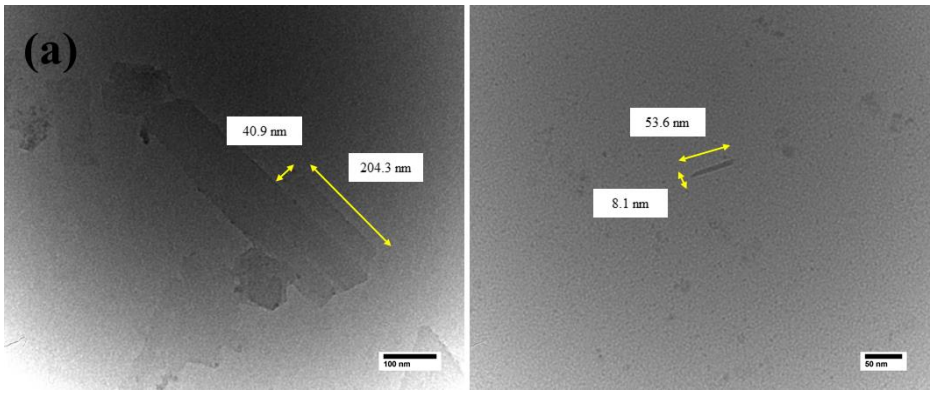
(a)
40.9 nm
204.3 nm
100 nm
53.6 nm
8.1 nm
50 nm

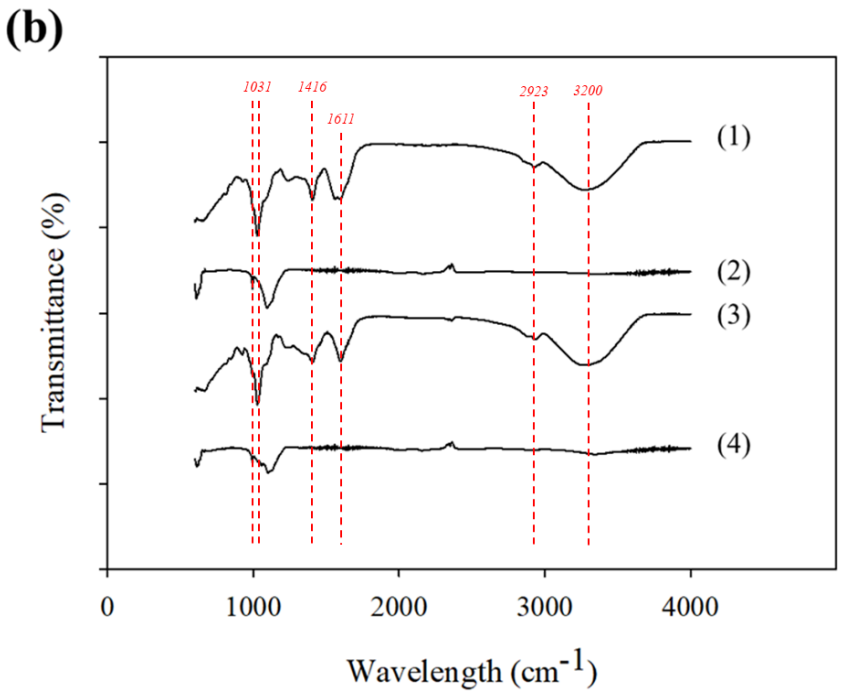
(b)
1031
1416
1611
2923
3200
(1)
(2)
(3)
(4)
Transmittance (%)
0
1000
2000
3000
4000
Wavelength (cm-1)

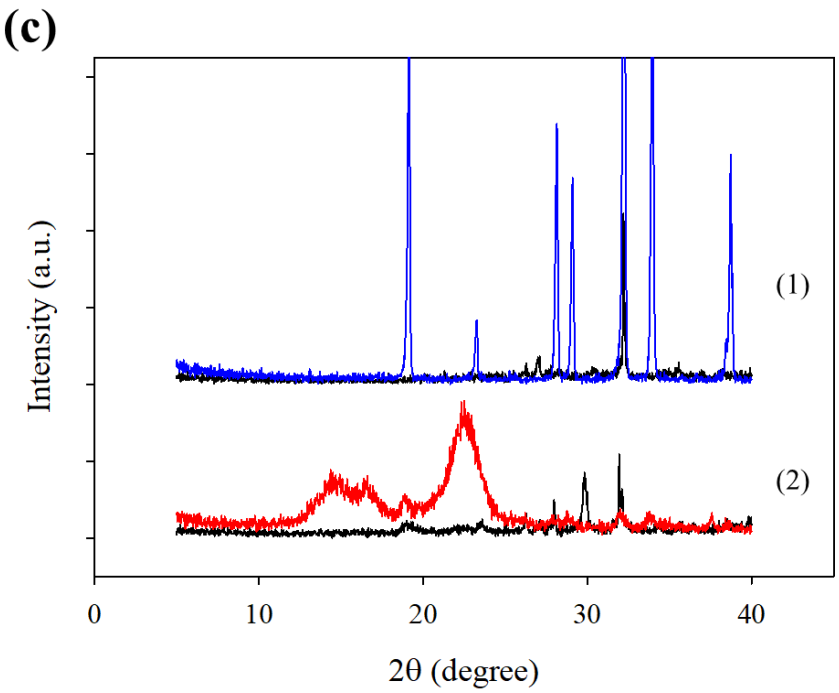

Figure 6.1. Characteristics of CNCs from seaweeds. (a), TEM images of CNCs from kombu (left) and sargassum (right); (b), Chemical structure of kombu (1), CNCs from kombu (2), sargassum (3), sargassum from CNCs (4); (c), XRD spectra of kombu (black) and CNCs from kombu (blue), (1), sargassum (black) and CNCs from sargassum (red).

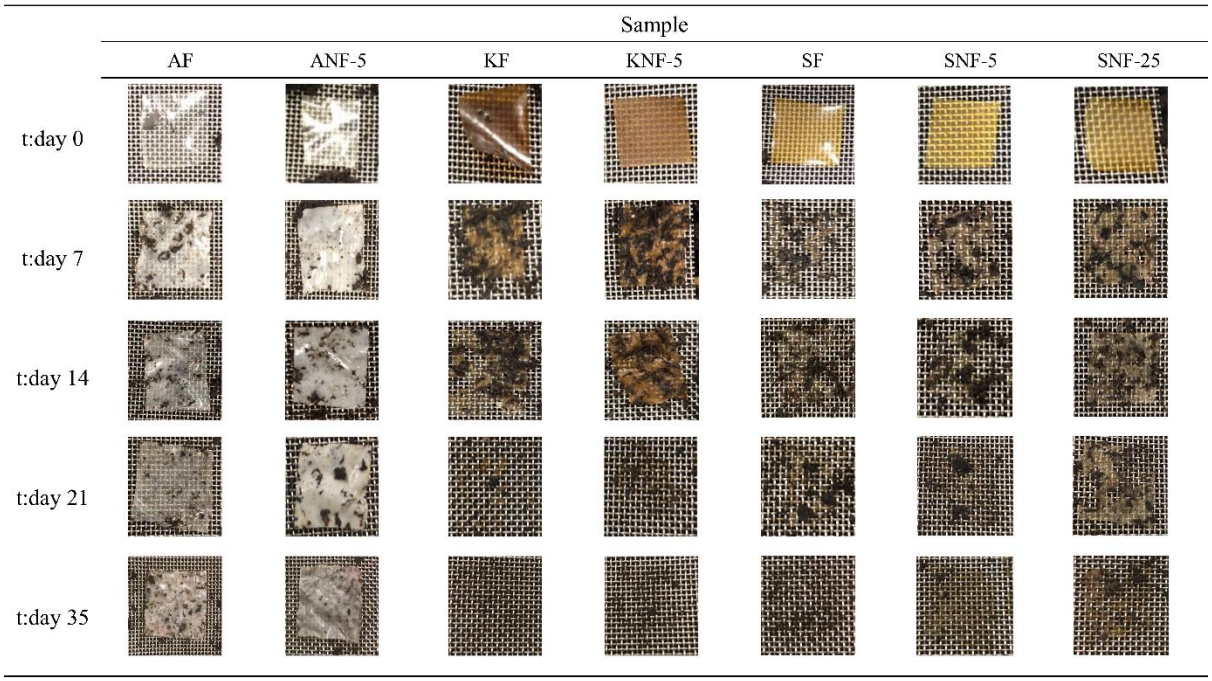

Figure 6.2. Bionanocomposite films after different exposure times in soil burial.

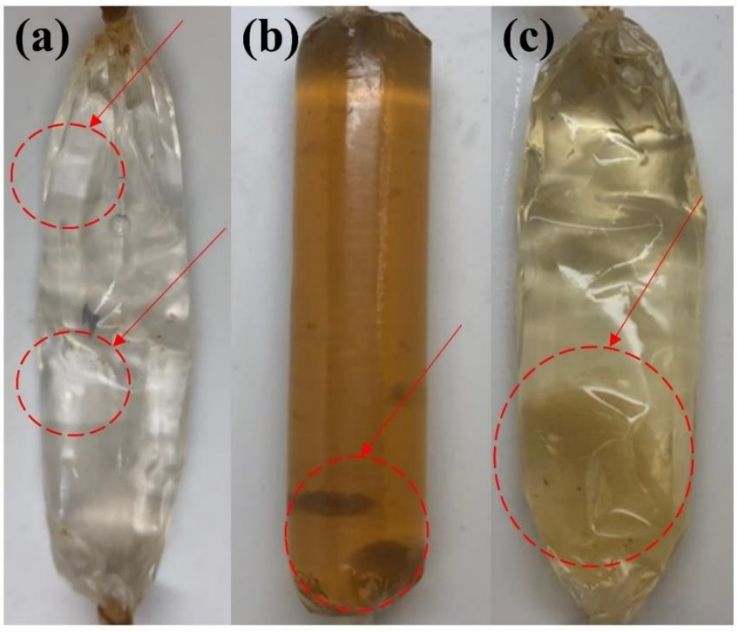

Figure 6.3. Bionanocomposite films after different exposure times in lake water immersion.

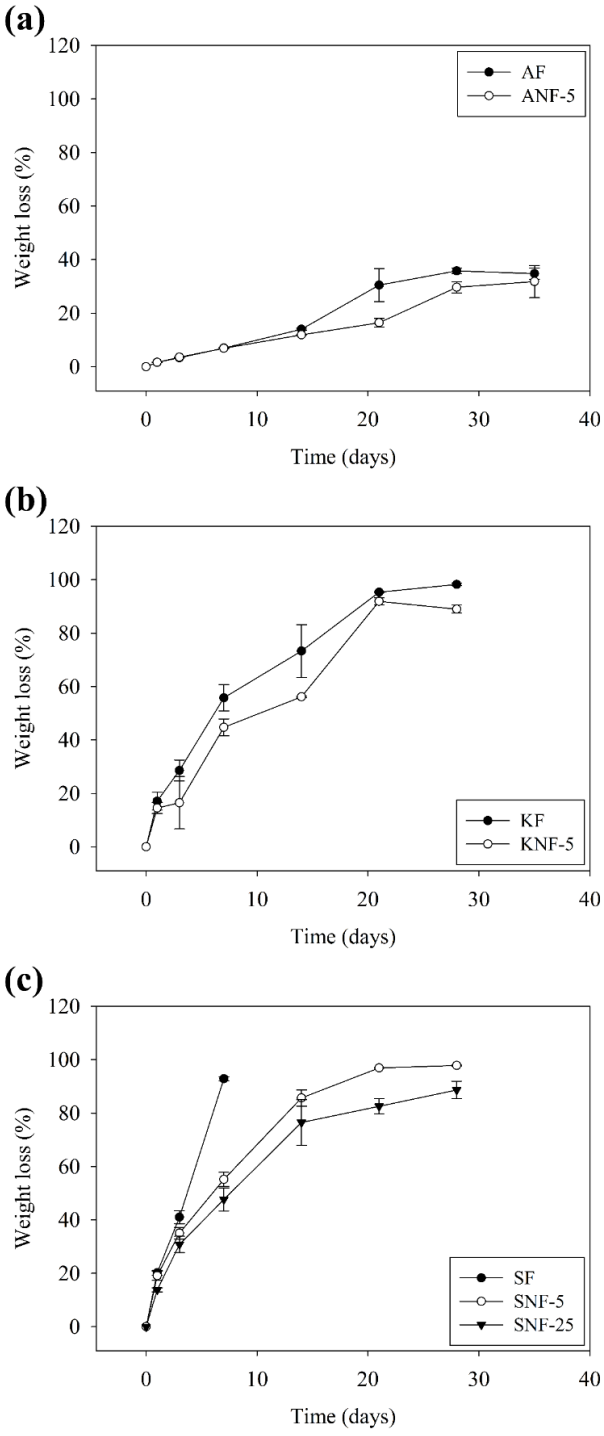

Figure 6.4. Weight loss curves during exposure time in soil burial. (a), AF and ANF-5; (b), KF and KNF-5; (c), SF, SNF-5, and SNF-25.

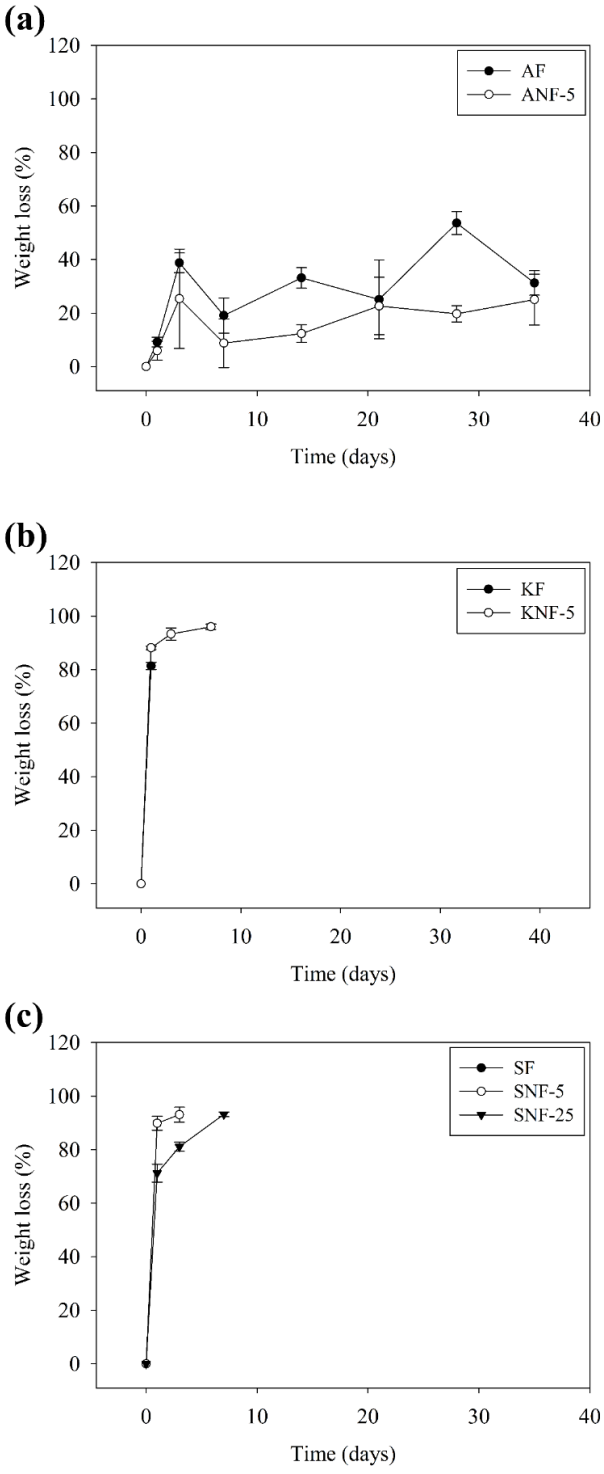

Figure 6.5. Weight loss curves during exposure time in lake water immersion. (a), AF and ANF-5; (b), KF and KNF-5; (c), SF, SNF-5, and SNF-25.

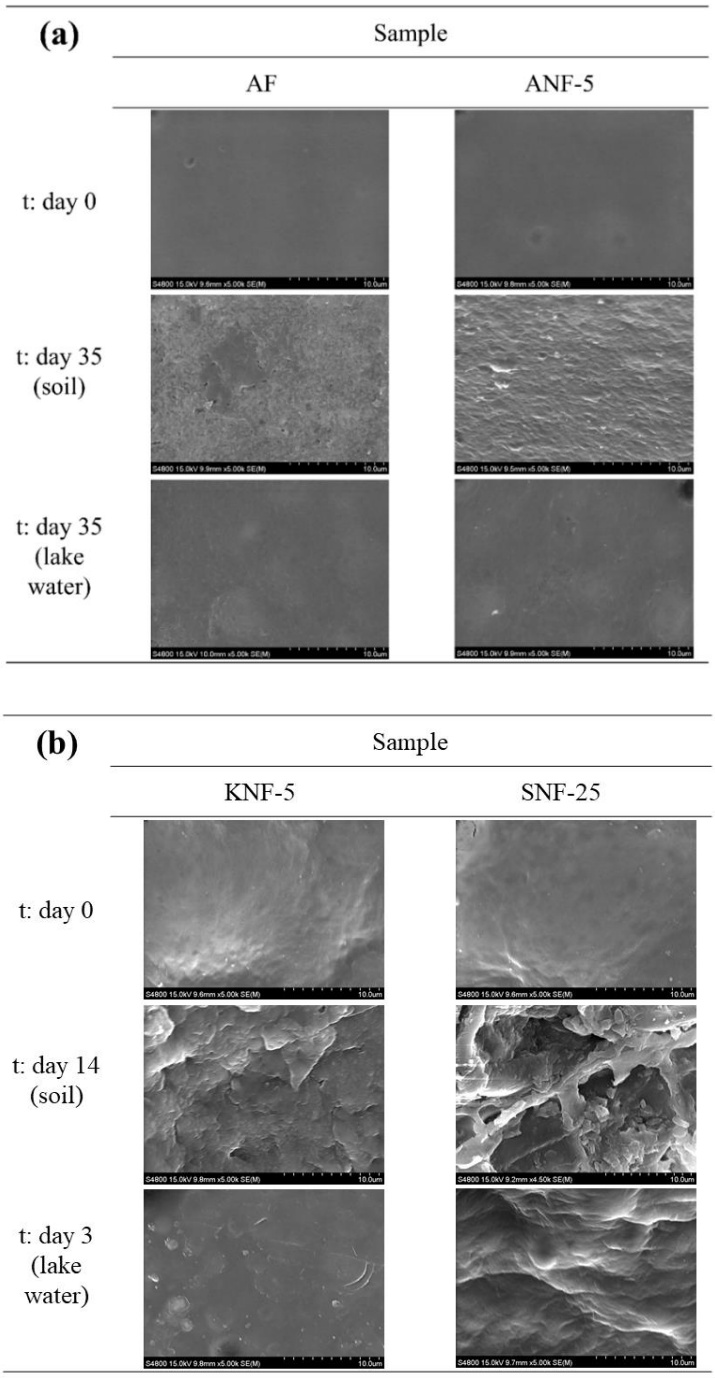

Figure 6.6. SEM images of the surfaces of bio-nanocomposite films before and after different exposure times in soil burial and lake water immersion. (a), AF and ANF-5; (b), KNF-5 and SNF-25.

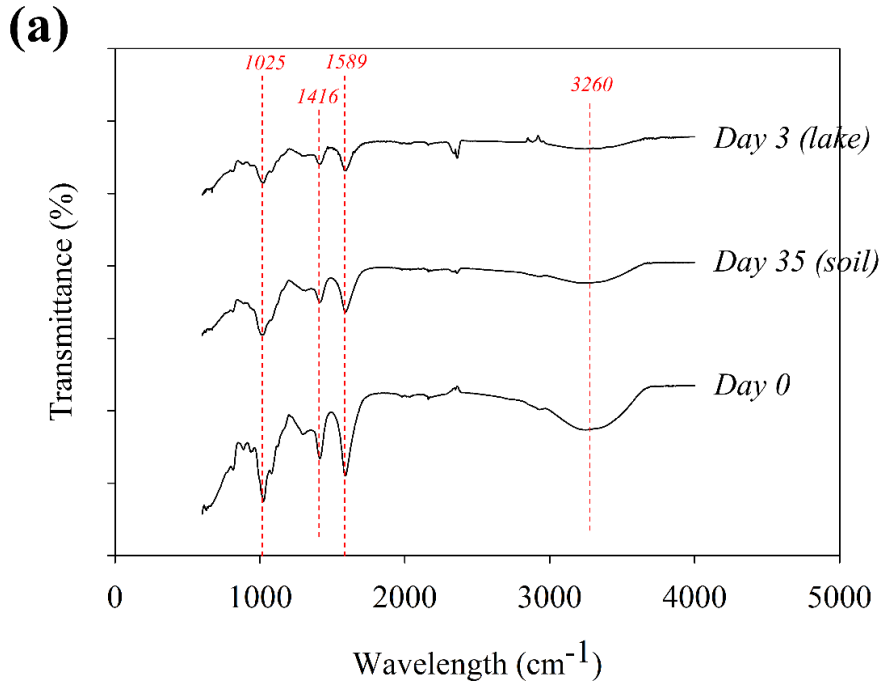
(a)
1025
1589
1416
3260
Day 3 (lake)
Day 35 (soil)
Day 0
Transmittance (%)
0
1000
2000
3000
4000
5000
Wavelength (cm-1)

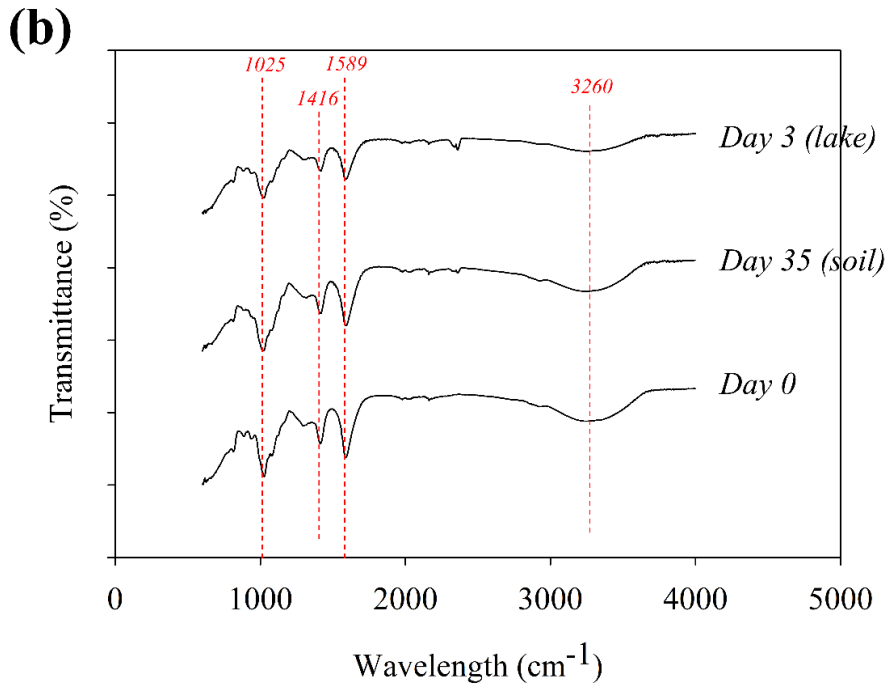
(b)
1025
1589
1416
3260
Day 3 (lake)
Day 35 (soil)
Day 0
Transmittance (%)
0
1000
2000
3000
4000
5000
Wavelength (cm-1)

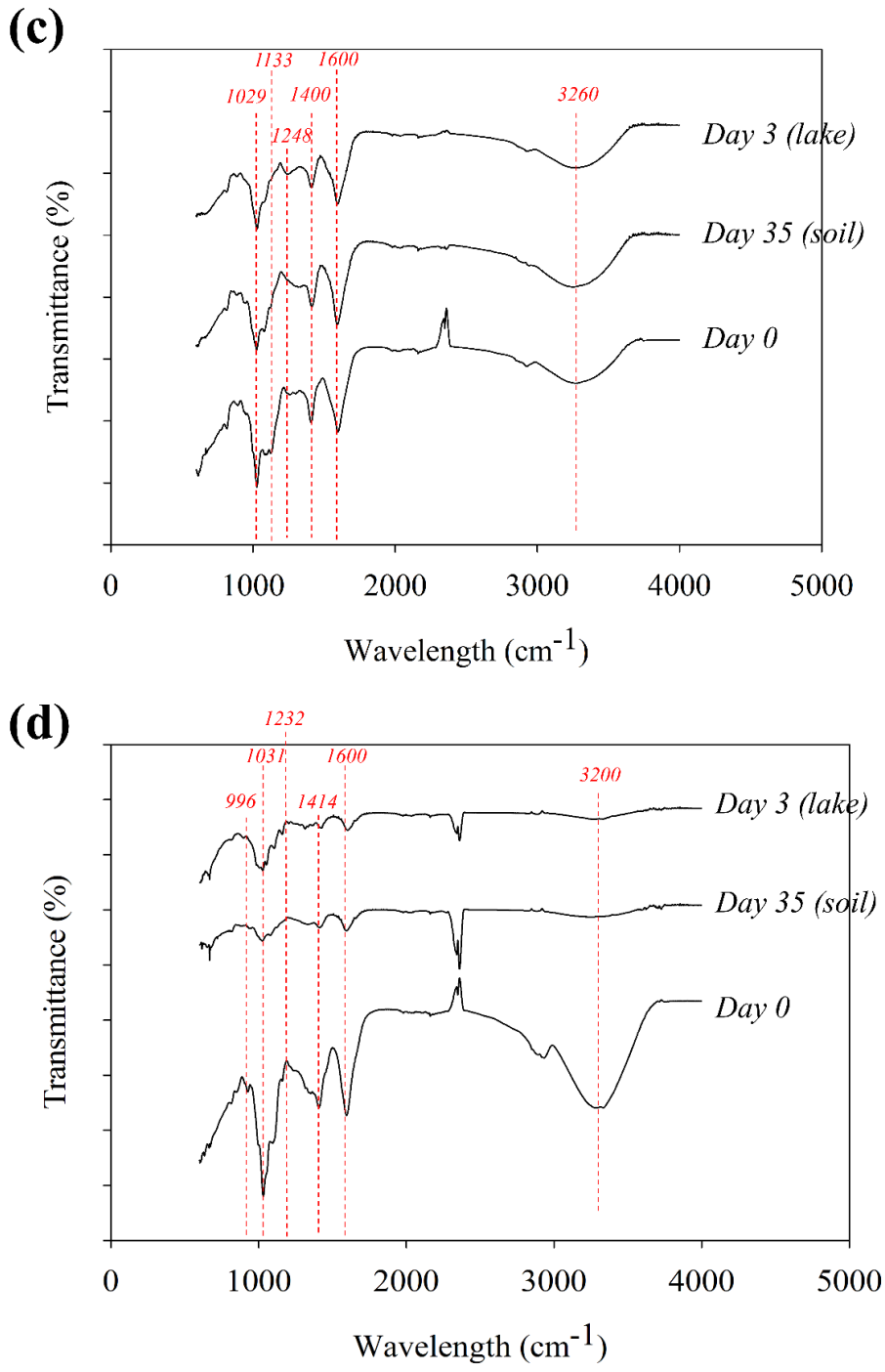

Figure 6.7. FTIR spectra of bionanocomposite films before and after different exposure times in soil burial and lake water immersion. (a), AF; (b), ANF-5; (c), KF-5; (d), SNF-25.

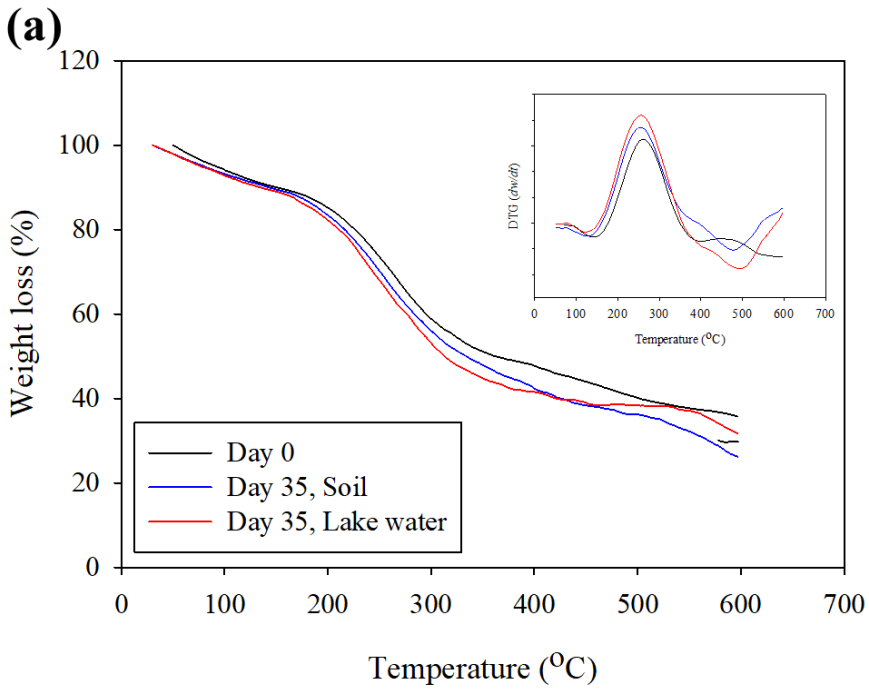
(a)
Weight loss (%)
Temperature (°C)
Day 0
Day 35, Soil
Day 35, Lake water
DTG (dw/dt)
Temperature (°C)

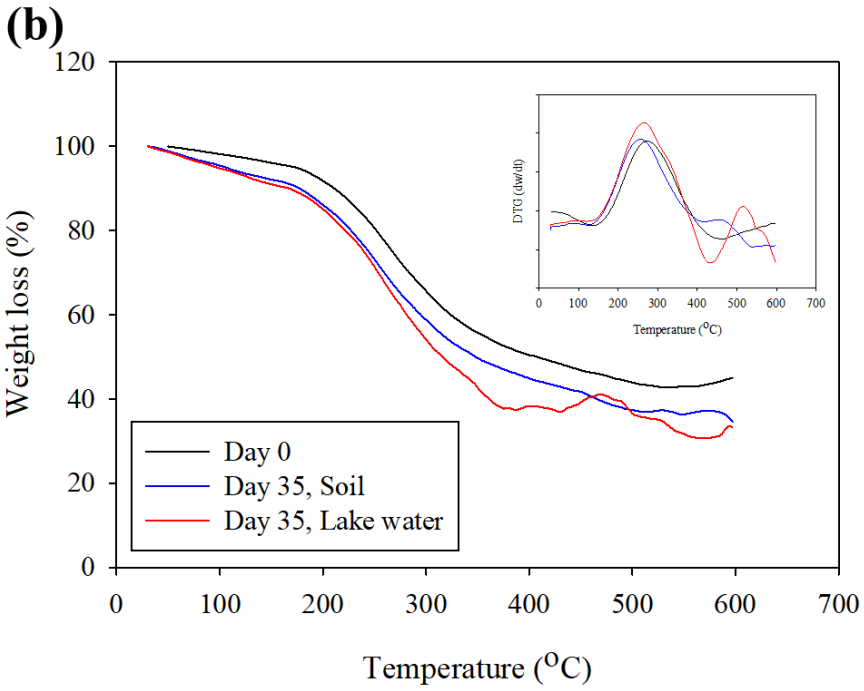
(b)
Weight loss (%)
Temperature (°C)
Day 0
Day 35, Soil
Day 35, Lake water
DTG (dw/dt)
Temperature (°C)

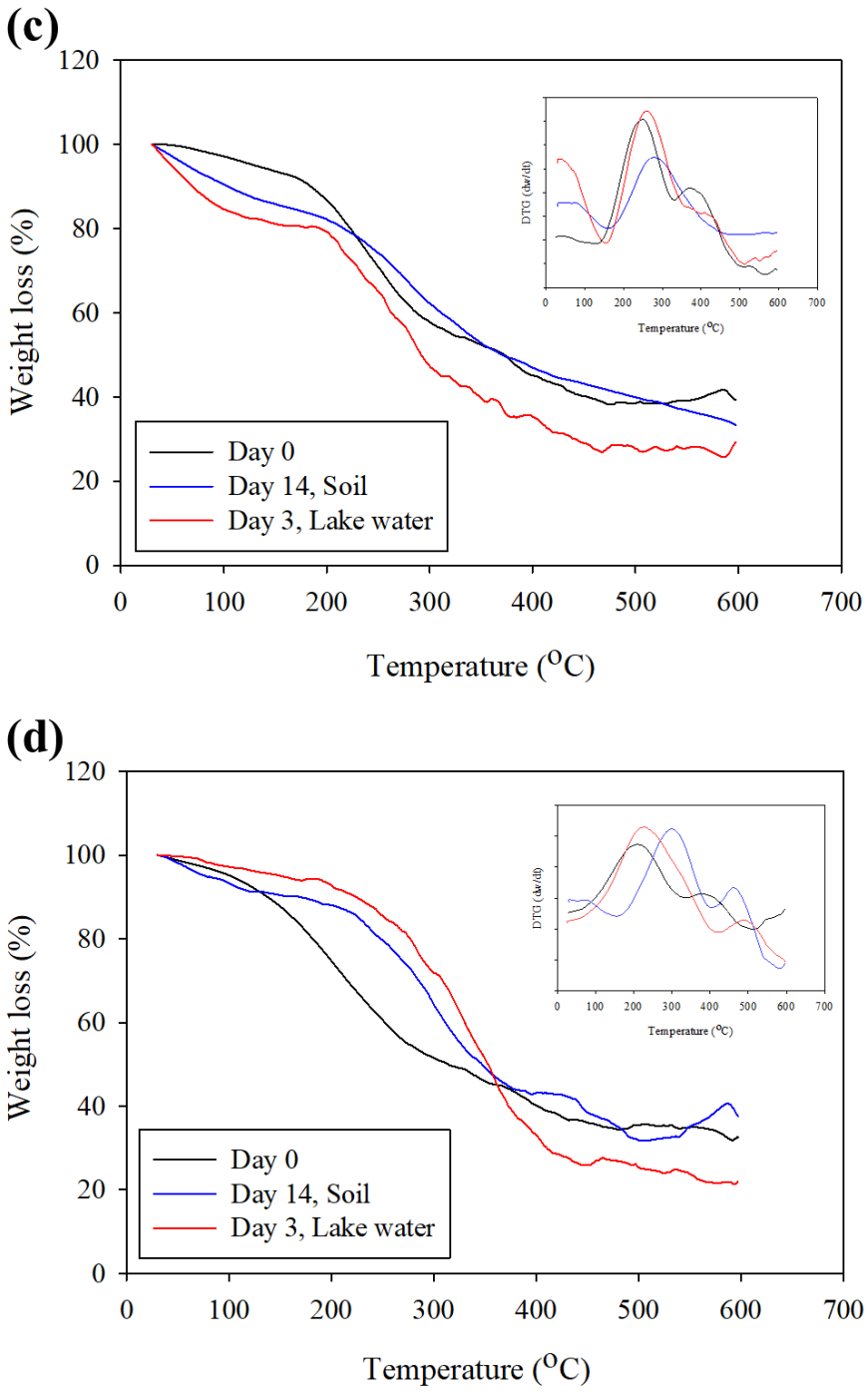

Figure 6.8. TGA and DTG curves prior to and after different exposure times in soil burial and lake water immersion. (a), AF; (b), ANF-5; (c), KF-5; (d), SNF-25.

CHAPTER SEVEN

CONCLUSION

In the present study, CNCs were successfully isolated from marine biomass of each seaweed group through de-polymerization, bleaching, acid hydrolysis, and mechanical dispersion processes. Aspect ratio varied from about 2.79 to 10.49 and FTIR analysis showed amorphous parts would decrease during the process, successfully. Crystalline index increased in all cases from extracted cellulose (about 61.01 – 75.76%) to CNCs (66.97 – 98.89%). Thermal stability of all seaweed samples increased through the processes.

Then, CNCs from *Sargassum fluitans* applied to the alginate nanocomposite films and characterized by physicochemical, mechanical, barrier, and thermal stability analysis. Morphological observations showed the structural modifications and improvements of the mechanical, barrier, and thermal properties when CNCs were incorporated in nanocomposite films. Generally, as CNCs concentration increased, mechanical, water vapor, oxygen, and light barrier properties were increased but an agglomeration of CNCs could disturb the reinforcing effect on the mechanical properties of the films at a very high percentage of addition. Through TGA and DSC tests, it was proven that adding CNCs could also increase thermal stability.

Also, *Laminaria japonica* and *Sargassum natans* crude extracts would be novel sources for biopolymer nanocomposite films with cellulose nanocrystals from residues of

these seaweeds. Physicochemical, mechanical, barrier and thermal properties were improved by adding CNCs and kombu biopolymer films showed better characteristics than that of sargassum films. Morphological observations showed that structural modifications with the CNC layer led to an improved mechanical, barrier, and thermal properties. Seaweed biopolymer films have been facing challenges of industry acceptance due to concerns of poor mechanical and barrier properties. However, these properties were improved by adding CNCs. Therefore, results from this study suggest support seaweed biopolymer nanocomposite films have shown the potential to be used as a novel biopolymer film for food packaging systems. Additionally, antioxidant properties investigated in this study proved seaweed biopolymer films could be used to improve food preservation or to design functional foods.

Effect of CNCs after biodegradation test with indoor soil burial and lake water immersion was performed with alginate and seaweed nanocomposite films. Weight loss test showed the addition of CNCs to the films rendered degradation rate slower than the films without the addition of the CNCs due to its reinforcement effect to molecular bonding strength in the polymer matrix, especially for the high crystallinity and small crystal size of CNCs from seaweeds. SEM images showed that wrinkles, holes, pores, and cracks were observed in the later stages of the degradation process. FTIR spectra showed the diminishing intensity of peaks after the degradation process. At last, TGA and DTG plots showed nanocomposite films presented higher thermal stabilities due to the nucleating effect of CNCs. Results reported in this study suggest that CNCs from seaweeds showed easy access, relatively higher crystallinity, and better thermal stability compared to

traditional CNCs sources. In addition, there were no significant differences in their characteristics between each seaweed because they had all good range in aspect ratio, crystallinity, and thermal stability for use as a filler in packaging system. Also, the degradation of biopolymer nanocomposite films with CNCs could be prolonged during the biodegradation process with enhanced molecular bonding strength by covering weak points of seaweed nanocomposite films. Thus, the results of this study suggest that alginate and seaweed nanocomposite film have the potential to be used for a novel biomaterial for packaging systems.